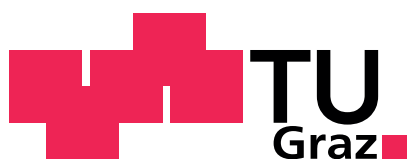# Masterthesis

Trace Oxygen Sensors

Philipp Lehner

Institute of Analytical Chemistry and Food Chemistry
University of Technology, Graz

Supervisor: Univ.-Prof. Dipl.-Chem. Dr.rer.nat. Ingo Klimant

Graz, August 2011

Abstract

In this thesis various matrices are tested for their suitability in trace oxygen sensors and a device to reliably calibrate sensors for trace level oxygen concentrations is built and presented. This device, named "Measurement Cube" relies on an absolute approach in oxygen metering to achieve concentrations inside the test chamber ranging from 0.05 hPa to 5 hPa pO_2. Even lower concentrations, however, may be achieved if 1 % oxygen test gas is used for metering instead of air. The device has also connectors for a thermostat, an internal Pt-1000 for direct temperature feedback and is capable of full automation if connected to a PC. It is further shown that modification of polymer matrices can reach considerable improvements in oxygen sensing sensitivity. For example, the repeated trimethylsilanization of polyphenylenoxide effectively doubled the K_{SV} value of this matrix, but further work still remains to be done on this subject. Of the various polymer matrices tested Teflon AF showed the best performance with K_{SV} values as high as 0.57 hPa^{-1} and 5.1 hPa^{-1} for platinum(II)- and palladium(II)benzoporphyrin dyes in Teflon AF 2400 respectively. Another presented approach was the covalent coupling of a pentafluorophenylporphyrin based dye to a silica gel matrix. The resulting sensor showed excellent linearity and sensitivity with K_{SV} values of 0.374 hPa^{-1} and 6.71 hPa^{-1} for the platinum(II)- and palladium(II) based dyes respectively. The developed sensors may be interesting for applications in food packaging, breweries or for marine biology.

Kurzfassung

Diese Arbeit beschäftigt sich mit verschiedenen Matrizes, die auf ihre Verwendbarkeit in Sauerstoff-Spurensensoren getestet werden. Außerdem wird ein neues Gerät, mit dem man solche Spurensensoren verlässlich kalibrieren kann, gebaut und getestet. Dieses Gerät, genannt der „Measurement Cube", verwendet eine Absolutmethode zur Einstellung von Sauerstoffkonzentrationen innerhalb der Testkammer von 0,05 hPa bis 5 hPa pO_2. Es ist jedoch möglich, sogar noch kleinere Sauerstoffkonzentrationen einzustellen, wenn als zudosiertes Gas 1% Sauerstoff-Testgas anstele von Luft verwendet wird. Zusätzlich hat das Gerät Anschlüsse für einen externen Thermostat, mit interner Temperaturverifizierung durch einen Pt-1000 Thermistor und ist komplett automatisierbar bei Steuerung durch einen verbundenen PC. Außerdem wird in dieser Arbeit gezeigt, wie die Modifizierung von Polymermatrizes einen deutlichen, positiven Einfluss auf deren Permeabilität für Sauerstoff haben kann. Zum Beispiel hat die wiederholte Trimethylsilanisierung von Polyphenylenoxid den K_{SV}-Wert dieser Matrix effektiv verdoppelt. Allerdings sind die Möglichkeiten in diesem Bereich noch nicht vollends ausgeschöpft. Von den vermessenen polymerbasierten Matrizes zeigte Teflon AF die beste Permeabilität mit hohen K_{SV}-Werten von 0,57 hPa^{-1} für den platin(II)-, und 5,1 hPa^{-1} für den palladium(II)basierten Farbstoff, jeweils in Teflon AF 2400. Eine andere demonstrierte Herangehensweise ist die kovalente Bindung von pentafluoroporphyrinbasierten Farbstoffen an eine Silica-Gel-Matrix. Die resultierenden Sensoren zeigen sehr gute Linearität und Sensitivität mit K_{SV}-Werten von 0,374 hPa^{-1} für den platin(II)-, und 6.71 hPa^{-1} für den palladium(II)basierten Farbstoff. Die in dieser Arbeit entwickelten Sensoren würden sich zum Beispiel beim Testen von Lebensmittelverpackungen, für Brauereien oder für Forschung in der Meeresbiologie anwenden lassen.

Dedication

I'd like to thank everybody in my working group (and the whole institute) for creating such a pleasant and motivating working environment. Special thanks go to Head of Institute Ingo Klimant. Without his constant stream of ideas and input there simply would be no thesis I could present. Further thanks go to Sergey Borisov whose expertise in everything dye and synthesis related spared me tedious literature search more than once. Finally I dedicate this thesis to my wife, her constant support made my work a pleasurable experience and she also managed to make me stay on track and in time during the finalization of this work.

Philipp Lehner

Graz, August 2011

Contents

1 Introduction

Oxygen as an analyte has been of continuous interest since its discovery 1771 due to its fundamental necessity both in most biological systems as well as in many technical processes. Because of its many appliances it is no surprise that oxygen analysis has made big improvements since the very first canary based sensors. Starting from mostly qualitative sensors used in mining to the quantitative lambda sensor being implemented in most modern automobiles, which is used to measure remaining oxygen in the combustion gas. For oxygen dissolved in water common quantitative methods include the Winkler titration, Clark electrode and optical sensors.

As the technological and scientific advance continues, increasingly lower concentrations of dissolved oxygen begin to be of significance and interest. Most common sensors are optimized for physiological concentrations of oxygen and rarely go below 400ng g^{-1}. However, detection of low oxygen concentrations may be important for safety (oxygen leaks) and food packaging and could be of interest in breweries where dissolved oxygen concentration in beer production is kept in the range of approximately 10 - 50 ng g^{-1} for quality assurance. Furthermore, water boilers should have oxygen concentrations of lower than 7 ng g^{-1} to prevent corrosion[1]. In addition the detection of bottle leaks might be an application for trace oxygen sensors[2]. Last but not least applications in marine science call for increasingly lower detectable concentrations of dissolved oxygen as so called "oxygen-minimum zones", and related marine ecosystems become the focus of current research where biologically relevant oxygen concentrations can be anywhere from 70 ng g^{-1} to as low as 0.06 ng g^{-1}.[3, 4]

Optical sensors are especially suited for protruding into the lower boundaries of trace oxygen analysis because, in contrast to other sensor types, they do not directly consume oxygen in the process. This consumption of the analyte is negligible at higher analyte concentration but gains significance if the analyte concentration becomes lower. An optical sensor generally consists of at least two components: a photoactive dye that is quenchable by the analyte and a surrounding matrix in which the dye is immobilised. Important dye parameters are luminescence brightness (which is proportional to the product of molar absorption coefficient and quantum yield), Stoke shift, decay time, quenching constant, photo- and chemostability. For low oxygen concentrations one usually relies on platinum(II) and especially palladium(II) porphyrin complexes. Other dyes with even longer decay times are known[5, 6], but they suffer from low luminescence brightness. Combined with the fact that these dyes show extraordinary sensitivity in common polymer matrices, a working sensor with some of the more permeable matrices in this work would be hard to calibrate with the available methods.

Although there is still much room for improvements relating to dyes, this work focuses on the second component of an optical sensor: the matrix. Important matrix properties are the permeability for the analyte and solubility of the dye as well as surface properties that decide in which environment the sensor can be used and also if the matrix is able to retain other possible quenchers from reaching the dye and generating cross talk.

Popular matrices that have shown high oxygen permeability include: poly(isobutyl methacrylate-co-tetrafluoropropylmethacrylate)[7], poly(styrene-co-pentafluorostyrene)[8] and poly(1-tri-methylsilyl-1-propine)[9]. Additionally some sensors based on silica gel[10] and ormosil

matrices[11] have also shown to display great oxygen permeability.

In this work matrices are characterised and modified to expand upon the available variety of sensors and reach further into the lower regions of trace oxygen sensors. A further focus of this thesis is the construction of a reliable measurement apparatus to characterise the trace oxygen sensors resulting from the combination of these matrices with porphyrin based dyes.

1.1 Background

1.1.1 Luminescence

Luminescence is the emission of electromagnetic radiation from any substance and occurs through the relaxation of electronically excited states. It is formally divided into two categories with different relaxation mechanisms: fluorescence and phosphorescence. In the case of fluorescence the return to the ground state is spin-allowed and occurs rapidly by emitting a photon. Typical lifetimes of singlet excited states are in the magnitude of 10^{-8} seconds or shorter. In contrast, in triplet excited states, the electron has the same spin orientation as the ground state electron so the return to the ground state is spin-forbidden and occurs much slower. Resulting phosphorescence lifetimes are in the range of 10^{-6} seconds to 10^{0} seconds, though much longer lifetimes can exist. The distinction between these two categories is not always sharp, several transition metal ligand complexes exist with mixed singlet-triplet states that can display intermediate lifetimes.[12, pp. 1-2]

1.1.2 Decay Time
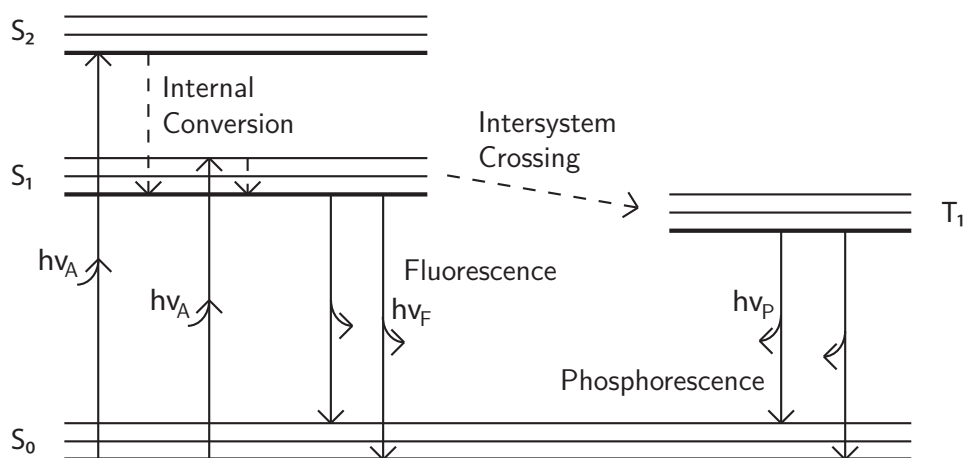
Figure 1.1: Typical Jabloński diagram showing the different possibilities for excitation and de-excitation.

The different states in which a luminophore can exist are typically displayed in a Jabloński diagram as seen in figure 1.1. The layers in the diagram represent the different singlet states, S_0 is the ground state and S_1 and S_2 are excited singlet states. T_1 represents the triplet state. There are different ways to excite a luminophore but the relevant method in this thesis is the absorption of photons of a specific energy, called photoluminescence. If a photon of discrete energy is absorbed by the luminophore, an electron is elevated in an excited state equalling the energy of the absorbed photon. Due to the speed of this process, according to the

Franck-Condon Principle, the electron can only reach vibrational excited states from which it has to reach a non-vibrational excited state through relaxation. Additionally if this state is higher than S_1 it can cross over to a vibrational state of S_1 of the same energy with subsequent relaxation, this is called internal conversion. This process can also take place from S_1 to S_0, but there is a competing process where energy is set free through emitting a photon of the corresponding energy called fluorescence. In the same way, an excited electron that reached a triplet state through inter system crossing, can also emit a photon to return to the ground state; this is called phosphorescence. Two important characteristics of every luminophore directly describe this last step. The first, the quantum yield which is given by equation 1.1, describes the percentage of photons emitted compared to photons absorbed and is given by the rate constants Γ and *k_nr* summarising the radiationless depopulation processes of the excited state.

$$Q = \frac{\Gamma}{\Gamma + k_{nr}} \tag{1.1}$$

The second characteristic, the lifetime or decay time, is the time after which the excited state depopulates and represents the stability of the excited state. It is given through equation 1.2.

$$\tau_n = \frac{1}{\Gamma + k_{nr}} \tag{1.2}$$

Since the depopulation is essentially random, this time only represents an average characteristic for a given substance. After an excitation pulse, luminescence brightness can in most cases be observed as a mono exponential decay with an average decay time τ. [12, pp. 4,10]

1.1.3 Quenching

Luminescence intensity as well as decay time can be decreased by various mechanisms which are called quenching. The most important of these for optical oxygen sensors are static and dynamic quenching. Static quenching is the formation of a complex between luminophore and quencher, that reduces or completely eliminates luminescence of the quenched luminophore. Decay times, however, remain unaffected because only the concentration of active luminophore is changed and not excited state stability. In contrast, dynamic quenching is the de-population of the excited state through energy transfer to the quencher molecule via collision. Therefore it decreases intensity as well as decay time. [12, p. 11]

1.1.4 Stern Volmer Plots

For dynamic or collisional quenching, the correlation between the lifetime- and intensity decay and the quencher concentration is given through the Stern Volmer equation for dynamic quenching:

$$\frac{I_0}{I} = \frac{\tau_0}{\tau} = 1 + k_q \tau_0 [Q] = 1 + K_{SV}[Q] \tag{1.3}$$

In this equation k_q is the bimolecular quenching constant, τ_0 is the decay time in absence of a quencher, $[Q]$ is the concentration of the quencher, and K_{SV} is the Stern Volmer constant. For interpreting this correlation for different quencher concentrations, a so-called Stern Volmer plot is often used. If τ_0/τ is plotted against the quencher concentration, the resulting curve will yield an intersect of 1 with the y-axis and the slope is $k_q \cdot \tau_0$ or K_{SV}.

1.1.5 Two Site Model

The above correlation is, however, only true for linear plots. In polymer films, Stern Volmer plots are often shown to deviate from linear behaviour. In addition to the deviation from purely dynamic quenching through static quenching there is another effect which causes a downward curvature of the resulting plot: the formation of multiple domains. These micro-heterogeneities cause a behaviour distinctly deviating from the linear plots expected from a homogeneous film. The Two Site Model accounts for these inhomogeneities by expanding the Stern Volmer equation so that it is determined by two domains with different quenchabilities. This modified Stern Volmer equation is:

$$\frac{I_0}{I} = \frac{\tau_0}{\tau} = \frac{1}{\frac{f_{01}}{1+K_{SV1}[Q]} + \frac{1-f_{01}}{1+K_{SV2}[Q]}} \tag{1.4}$$

f_{01} is the factor determining the influence of one domain to the observed lifetime, K_{SV1} and K_{SV2} are the Stern Volmer constants for the two domains. This is, of course, a simplified model. A real polymer is not expected to show exactly two distinctive domains, still this approach provides good fits for most sensors. A further simplification that is often used, is to set K_{SV2} as zero, so that the equation describes two domains with only one being quenchable.[13]

1.1.6 Permeability

The permeability of a given combination of matrix and diffusant is based on a summation of the influence of multiple effects. This circumstance makes the permeability of a given pair extremely difficult to predict. The permeability for thin films of polymer at equilibrium conditions is defined as

$$P = D \cdot S \tag{1.5}$$

With D being the diffusion coefficient and S being the solubility[14, p. 243]. These two parameters are easily accessible empirically, however, predicting values for a given polymer and quencher molecule is not trivial since a lot of factors are important to diffusion that require extensive knowledge of intrinsic properties that reaches far deeper than the structural formula.

Factors important to the diffusion coefficient include, but are not limited to:

- The size and state of the diffusant, its chemical functionality and charge[15]

- The morphology of the polymer including: intrinsic free volume, tacticity, rigidity, crystallinity and chain arrangement [16]

- The compatibility of the solute with the polymer matrix[17]

Because of this, there is no unified theory to predict permeability values for all possible combinations.There are a few approaches[18, 19, 20],but one has to fall back onto empiric determination for reliable results. However, knowledge of the above points enables one to at least make an educated guess in which direction permeability will be pushed by a specific change in polymer characteristics.

1.2 Measuring Decay Times

The decay times presented in this thesis were obtained using measurements in the frequency domain. In such frequency domain measurements a sinusoidally intensity modulated light source is used to excite the luminophore. The finite time response of the luminescence results in a demodulation that is observed as the phaseshift Φ. In figure 1.2 the intensities of excitation and emission are plotted against time to highlight the observed phaseshift.
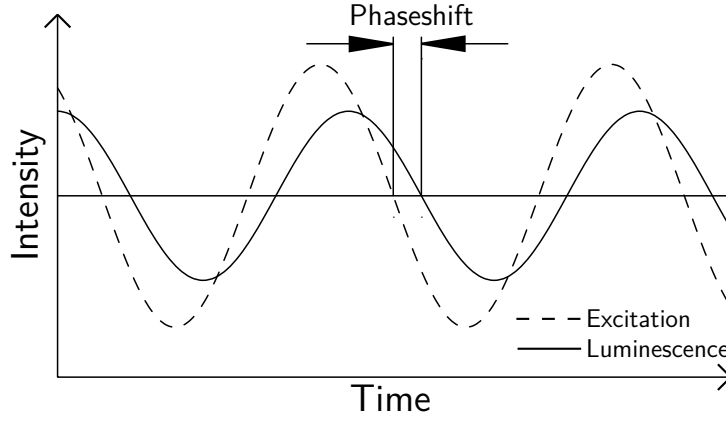

Figure 1.2: The observed phaseshift of the luminescence in frequency domain measurements.

Depending on the luminophore this phaseshift increases from $0°$ to $90°$ and, for a mono- or multi exponential decay, cannot exceed $90°$. For a luminophore showing mono exponential decay, the decay time has this simple relation to the phase shift:

$$\tan \Phi_{\omega} = \omega\tau \tag{1.6}$$

With ω being the circular modulation frequency given as

$$\omega[rad \cdot s^{-1}] = 2\pi \cdot f[Hz] \tag{1.7}$$

In this case f is the number in cycles per second. As a result the decay time of a luminophore can be calculated as

$$\tau = \frac{\tan \Phi_{\omega}}{2\pi \cdot f} \tag{1.8}$$

The obtained decay times can then be used for further analysis.[12, p. 143]

2 Methods and Materials

2.1 List of used chemicals

The tables in this section draw a complete list of all chemical compounds used in this thesis and where they were obtained from along with a CAS number if applicable. Table 2.1 holds all the used dyes, while table 2.2 contains a list of polymers, whereas table 2.3 lists all other materials used.

Full Name	Abbreviation	Obtained from
platinum(II)-5,10,15,20-meso-tetrakis(2,3,4,5,6-pentafluorophenyl)-porphyrin	Pt-TPFPP	Frontier Scientific
palladium (II)-5,10,15,20-meso-tetrakis(2,3,4,5,6-pentafluorophenyl)-porphyrin	Pd-TPFPP	TriPorTech
modified platinum(II)-5,10,15,20-meso-tetraphenyl-tetrabenzoporphyrin	Pt-TPTBP	TUGraz
modified palladium(II)-5,10,15,20-meso-tetraphenyl-tetrabenzoporphyrin	Pd-TPTBP	TUGraz

Table 2.1: The dyes used in this thesis.

Full Name	Abbreviation	Obtained	CAS
Ethyl-cellulose 50 % ethoxy content	EC	Aldrich	9004-57-3
polystyrene	PS	Scientific Polymer	9003-53-6
poly(tert-butylstyrene)	t-Bu PS		26009-55-2
polysulfone		Aldrich	25135-51-7
poly(perfluorobutylsulfon)		TU Graz	
poly(2,2,2-trifluoroethylmethacrylate)	PTFEMA	Scientific Polymer	54802-79-8
poly(2,6-dimethyl-p-phenylenoxide)	PPO	Scientific Polymer	25134-01-4
E4 Silikon	E4	Wacker	
Teflon AF 1600		DuPont	37626-13-4
Teflon AF 2400		DuPont	

Table 2.2: A list of polymers obtained for use and further modification in this thesis.

Full Name	Obtained from	CAS
t-butyl dimethylchlorosilane	Serva	60090-92-2
3-Phenoxypropyldimethylchlorosilane	ABCR	69733-73-9
nonafluorohexyldimethylchlorosilane	ABCR	119386-82-2
tridecafluoro-1,1,2,2-tetrahydrooctyldimethylchlorosilane	ABCR	102488-47-1
3-Aminopropylmethyldiethoxysilane	ABCR	919-30-2
(3,3,3-triflourpropyl)methyldimethoxysilane	ABCR	358-67-8
trimethylchlorosilane	Aldrich	75-77-4
tetrahydrofurane	Roth	109-9-9
toluene	Roth	108-88-3
chloroform	Roth	67-66-3
hexane fraction	Promochem	110-54-3
diphenylether	Aldrich	101-84-8
octafluorotoluene	ABCR	434-64-0
n-butyllithium 10M in Hexane	Aldrich	
sodiumhydroxide	Roth	1310-73-2
acetic acid	Roth	64-19-7
LiChroSorb Si60	Merck	
hydrogen peroxide		7722-84-1
perfluorobutyrylchloride	Aldrich	375-16-6
fluorinated FC-75	ABCR	335-36-4

Table 2.3: Other Materials used in the course of this thesis.

2.2 Luminescent Dyes

Because improvement of the luminescent dye itself was not an objective of this thesis, two of the currently most reliable dyes easily available were used. The structures of the chosen dyes can be seen in figure 2.1. Porphyrins are widely used as oxygen sensors[21, 22, 23] and various benzoporphyrins also have shown to be highly suited as oxygen sensor dyes[24]. In figure 2.1 only the more sensitive palladium(II) complexes are shown but also the platinum(II) complexes of both porphyrins were used in this thesis. In the rest of this thesis the porphyrins will be called TPFPP for the 5,10,15,20-meso-tetrakis-(2,3,4,5,6-pentafluorophenyl)-porphyrin and TPTBP for the modified 5,10,15,20-meso-tetraphenyl-tetrabenzoporphyrin respectively.
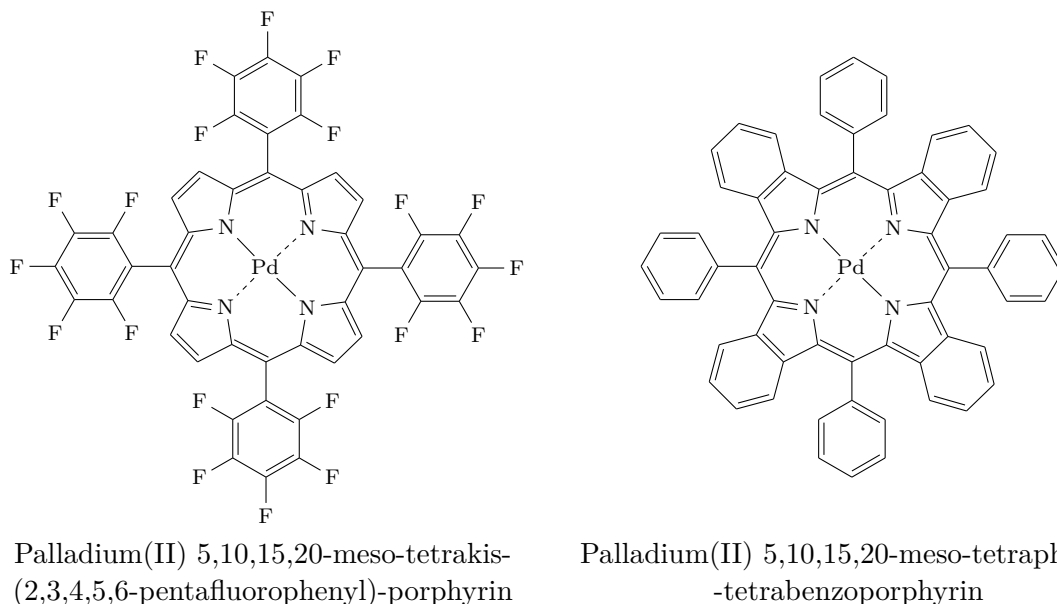

Palladium(II) 5,10,15,20-meso-tetrakis-(2,3,4,5,6-pentafluorophenyl)-porphyrin

Palladium(II) 5,10,15,20-meso-tetraphenyl-tetrabenzoporphyrin

Figure 2.1: The dyes used throughout this thesis. Please note that while the tetrapentaflourophenylporphyrin structure is correct, the structure given for the benzoporphyrin is only the generic structure. A further modified version obtained from the institute of analytical chemistry and food chemistry (University of Technology, Graz) was used as dye in the experiments conducted in this thesis.

2.3 Sensor preparation

A sensor as used in this thesis consists of a luminescent dye in a thin polymer film coated onto a substrate, usually Mylar® foil or glass. Mylar® foil (biaxially-oriented polyethylene terephthalate) is a good choice for common sensors. However, depending on the dye, migration into the substrate can be a substantial factor. Therefore all sensors that are measured in this thesis were cast onto a glass substrate. The notable exception is sensors which were measured with the massflow device described briefly in section 2.4. These were cast onto Mylar® foil, in the assumption that possible migration effects won't have a noticeable influence on the results because of lower sensitivity.

2.3.1 Sensor casting

To obtain a sensor — a dye-doped polymer film on a substrate with a defined thickness — a cocktail containing the dissolved dye and polymer in a suitable solvent is knife coated using either a $25\,\mu$m or $75\,\mu$m spacer. To make sure sufficient signal intensity is obtained the spacer has to be chosen according to the concentration of the dye. Afterwards the films are dried and stored under ambient conditions in darkness.

Obviously the used solvent and the ratio of solvent polymer and dye depend on an array of different factors like: solubility of dye and polymer in the solvent, luminescence brightness of the dye and solubility of the dye in the polymer. Table 2.4 gives a short overview of typical ratios of dye, polymer and solvent. Modified polymers use the same composition as its unmodified counterpart and if a cocktail with a different composition was used it is explicitly stated at that point in the thesis.

Polymer	Dye	Solvent	d/p / $wt\%$	p/s / $wt\%$	spacer / μm
ethylcellulose	Pt-TPTBP	80/20 EtOH/H_2O	1.5	10	25
perfluoroethylcellulose	Pt-TPTBP	80/20 EtOH/H_2O	1.5	10	25
poly trifluoroethylmethacrylate	Pt-TPTBP	THF	1.5	10	25
poly dimethylphenylenoxid	Pt-TPTBP	$CHCl_3$	1.5	10	25
poly styrol	Pd-TPTBP	$CHCl_3$	1.5	5	-
poly tert-butylstyrol	Pt-TPTBP	$CHCl_3$	1.5	10	25
polysulfon	Pt-TPTBP	$CHCl_3$	1.5	10	25
LiChroSorb particles	Pt-TPFPP	25/75 E4/Hexane	-	12	75
LiChroSorb particles	Pd-TPFPP	25/75 E4/Hexane	-	12	75
trimethylsilanisized PPO	Pt-TPTBP	$CHCl_3$	1.5	10	25
fluoroalkylsilansized PPOs	Pt-TPTBP	Fluorotoluene	1	10	25
Teflon AF 1600	Pt-TPTBP	C_7F_8	1	5	75
Teflon AF 1600	Pd-TPTBP	C_7F_8	1	5	75
Teflon AF 2400	Pt-TPTBP	C_7F_8	0.5	5	75
Teflon AF 2400	Pd-TPTBP	C_7F_8	0.5	5	75

Table 2.4: Different cocktail compositions used for the sensors in this thesis.

2.3.2 Spray-coating sensors

For the prototype device described in section 2.4.3 another special type of glass substrate was used. A first and promising approach for creating a low oxygen sensor was the use of Pd-TPFPP in polystyrene. Since the adhesion of polystyrene on glass is quite poor, a plan of spray-coating a sensor cocktail onto a roughened glass disc was formed. Further it was decided that, to minimize inhomogeneities resulting from edge effects, only a circle slightly smaller than the disc diameter should be spray-coated. Dimensions can be seen in Figure 2.2.

To achieve this the glass discs had to be properly masked, therefore a mask was cut from
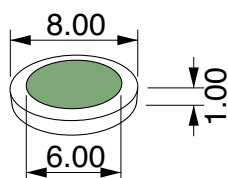
Figure 2.2: Dimensions of discs in millimetre, spray coated with a dye cocktail.

Mylar® foil using a cutting plotter and for correct alignment a disc holder was cut from cardstock using the same technique. In figure 2.3 the process of folding the cutting template to the finished masking device is presented.
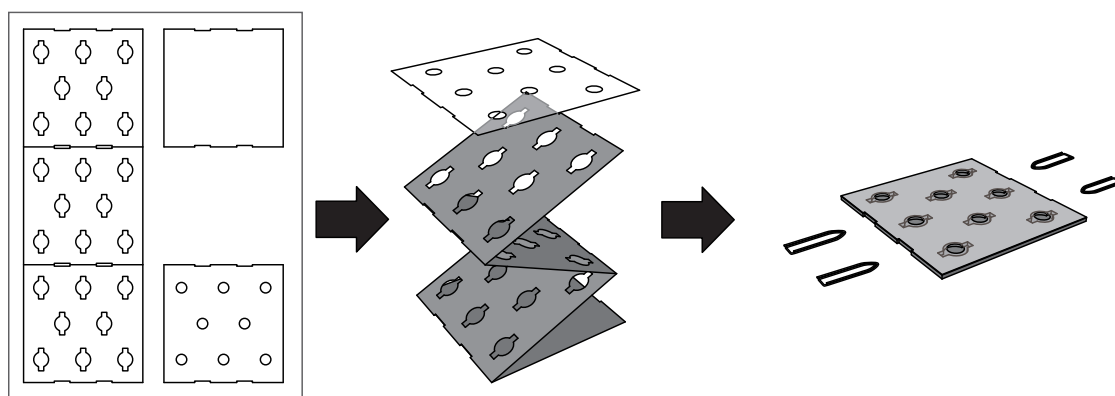

Figure 2.3: Assembly of a disc masking device from a plotted template. The finished device is glued and the polymer mask is fixated using paper clips.

The dye cocktails were mixed with $1.5\,wt\%$ Pd-TPFPP dye in relation to a polystyrene matrix, as a solution of $5\,wt\%$ matrix in $CHCl_3$. After stirring until a homogeneous solution was reached, the cocktail was loaded in a commercially available airbrush and applied from a distance of about $5\,cm$ onto the masked glass discs. After a short drying period the discs could be removed from the masking device and were ready for use.

2.4 Designing a Measurement Apparatus

In order to characterize different oxygen sensors one has to reliably provide a medium that can interact with the sensor and has a defined concentration of oxygen. A homemade mass flow controller unit has been used to get exact oxygen concentrations in the range of approximately $5\,hPa$ to oxygen saturation. It consists of massflow controllers which are dosing gases into a common outlet which in turn is connected to a sensor mounting chamber. This method was used for matrix characterization using the Pt-TPFPP dye. However, for measurement of the more sensitive trace oxygen sensors, where concentrations of $0.1\,hPa$ to $10\,hPa$ are required, this method is insufficient. Therefore a special device had to be constructed that can reliably regulate oxygen concentration in this range.

2.4.1 Measurement Types

The method of controlling oxygen partial pressure by mixing two component gases can be considered a relative method. Because only the difference between the two gas flows is important for the current oxygen concentration. The volume of the test-chamber has no influence although it should be small enough to propagate fast adjusting to equilibrium conditions. A problem with relative methods is, that once the mass flow of the two components differs by more than one power, otherwise negligible factors like the venturi effect start to influence the mixing, which in turn becomes unreliable.

Possibly better options are absolute methods, where there is a fixed amount of gas in a defined test-chamber volume and then a controlled fraction of analyte gas is deployed. The analyte partial pressure only depends on how small an amount one can dose. However, a few additional considerations have to be made. In relative methods the component gases generally have the same temperature, but in an absolute environment the inert gas in the test-chamber generally is of specific temperature due to the test-chamber being regulated by a thermostat and the analyte gas is of another temperature e.g. room temperature. As a result gas volumes are no longer directly comparable and one has to rely on mole fractions instead of volume fractions to calculate a correct partial analyte pressure. The test-chamber has also got to be sufficiently gas tight to prevent oxygen in the surrounding air from falsifying measurement results.

2.4.2 Preconsiderations

Before actually planning the physical appearance of such a device a few considerations have to be made:

- How can the device be made sufficiently gas tight including the inhibition of permeation?

- How can the internal temperature of the device be controlled?

- How should the sensor be mounted in the device to be optically readable from the outside?

- What is a reproducible method of introducing small quantities of analyte gas into the device?

Elimination of Permeation

Since an absolute method relies on analyte gas to be only brought into the system via intentional metering, it is very prone to permeation from the outside medium, especially if the analyte is as abundant in the surrounding medium as oxygen. Oxygen permeability differs widely with various material types and even within specific subgroups. Silicate glass, ceramics and metals are usually impermeable with the exception of a few specifically crafted alloys. Polymers have the biggest spread in permeabilities ranging from very good (used as matrices for trace scale sensors) to practically non existent (used as insulation for space crafts).

Temperature Control

The next issue approached is that of temperature control. Options include submerging the whole device in a thermostat or having water of a specific temperature pumped through the outer walls of the device. While silicate glass has a low gas permeability, its equally low thermal conductivity makes it a less than ideal choice as hull material. From a temperature control point of view metals are preferable and they are easier to handle than glass.

Sensor Mounting

The sensor has to be optically accessible from the outside during measurement and there has to be some way to exchange sensors between measurements. This necessity leads to two major weak points in the hull of such a device. If one uses glass as hull material optical access is self evident and standard taper joints provide an adequate albeit not perfect permeation barrier. A metal housing has to have a window for optical access and some means of opening it, possibly introducing a seal, which is also a certain weak point for permeation.

Analyte Metering

The point most important to understand the scale of such an apparatus is the last one. If one assumes that, as an upper bound, typical step sizes should increase the oxygen partial pressure by 0.1 hPa. Then, if one uses the relation between partial pressure and mole fraction

$$x_i = \frac{p_i}{p} = \frac{n_i}{n} \tag{2.1}$$

and inserts the ideal gas law solved for n and also takes into account that the the total number of moles n_t is the sum of initial amount and added amount

$$n = \frac{pV}{RT}$$
$$n_t = n_{Dose} + n_{Device} \tag{2.2}$$

then the resulting equation describes the correlation of dosed volume and resulting partial pressure:

$$p_i = \frac{n_{Dose}}{n_{Dose} + n_{Device}} = \frac{\dfrac{pV_{Dose}}{RT_{outside}}}{\dfrac{pV_{Dose}}{RT_{outside}} + \dfrac{pV_{Device}}{RT_{inside}}} \tag{2.3}$$

In case that all gases are at room temperature and atmospheric pressure and V_{Dose} is much smaller than V_{Device}, the equation can be simplified and rearranged:

$$p_i = \frac{V_{Dose}}{V_{Device}} \cdot p$$
$$V_{Dose} = \frac{V_{Device} p_i}{p} \tag{2.4}$$

Then the required amount of air to be injected for a 0.1 hPa step into an arbitrarily set measurement volume of 0.5 L is:

$$\frac{0.5\,\text{L} \cdot 0.1\,\text{hPa}}{1013.25\,\text{hPa}} \cdot \frac{100}{21} = 236\,\mu\text{L} \tag{2.5}$$

There are quite a few manual and automated metering devices available to dispense gases in this scale. A simple example being microlitre syringes.

2.4.3 First Prototype

Based on those early considerations a first prototype was constructed. Since this was supposed to work as a proof of concept, only materials already available in the laboratory were used. The

device itself consisted of a three-neck round bottom flask with a septum over one neck which acts as a seal through which air could be injected with a microlitre syringe. An inert gas valve connected to a nitrogen gas cylinder serves as gas inlet and a glass taper plug with its head cut off serves as sensor mount and optical fibre guide. This glass plug can also be slightly pulled out to serve as an inert gas outlet while flushing. To provide means of faster mixing a polymer foil was fixed to a magnetic stir bar and held in place by an outside rare earth magnet. In Figure 2.4 a schematic of this prototype is seen with its parts labelled.
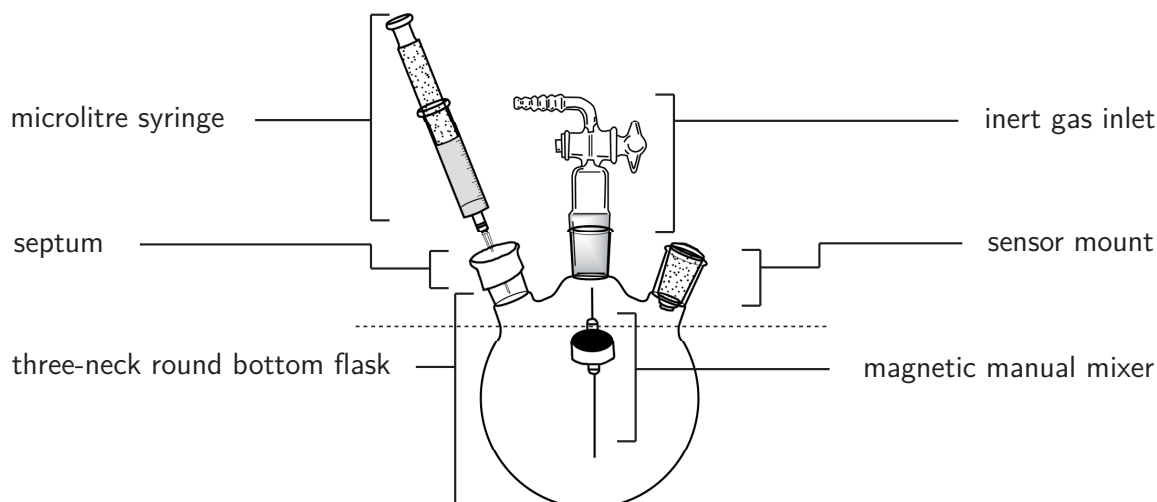
Figure 2.4: A prototype measurement device built with equipment commonly found in a laboratory environment.

During a typical measurement the device got submersed in the water basin of a thermostat up to the dotted line in figure 2.4 and flushed with inert gas for a duration of five minutes before closing the valve and starting the measurement. The syringe was filled with air which was injected through the septum, and after the syringe was removed, manipulation of the magnet moved the polymer foil and therefore mixed the gases until equilibrium was reached. When a stable sensor readout was obtained, the syringe got inserted again and the process was repeated as often as necessary. The results of these measurements, as well as reasons for ultimately choosing to build a specific device of our own are presented in the experimental part in section 4.2.

2.5 Measurement Cube

Once the decision was made to build our own sophisticated measurement device for low oxygen concentrations, a few additional design parameters in addition to the ones listed in section 2.4.2 were established.

- The device should be able to perform measurements on its own, in order to minimize human influence on reproducibility and frankly to make life of scientists who use it, especially the author's, easier.

- The device should be largely self contained and be able to stand on a bench without additional tripods or stands.

- The device should be flexible as to what kinf of analyte gas is injected, e.g. test gas with 1 % analyte or synthetic air instead of surrounding air.

- Its raw material cost should not greatly exceed 500 €.

2.5.1 Planning

With all required parameters in place, planning of the physical appearance could begin. As reliable temperature regulation was a problem with the prototype device, the new apparatus should be made of metal. The entry point for planning was how to fit all required connections onto a metal body and make the number of seams as few as possible.

Form Factor

The metal alloy of choice was brass because it is rather cheap and easy to process. Brass is available commercially in sheets of various thickness and as a variety of tubes with different wall strengths and inside diameters. This left two obvious choices for the final shape, either a cube made of sheets or a tube capped with two sheets. Drafts of how such devices would look like are seen in figure 2.5.
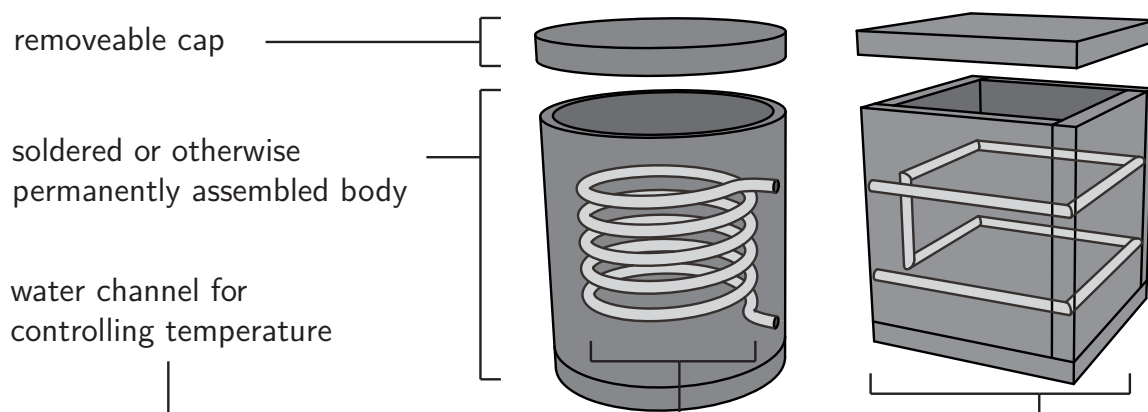
Figure 2.5: Two possible form factors for an automated absolute measurement device.

Tube shape has the advantage of minimizing metal-metal joints and therefore reducing the risk of leaks, since soldering the parts was not an option and another possibly less effective method had to be searched for. However, because water channels cannot be implemented directly into the device walls, two additional boreholes are required. The sealing between cap and body is the weak point in both designs. The final decision was to use a box design solely based on the fact that it was easier to manufacture and the confidence that there would be means available to seal joints effectively, even without soldering. Due to its shape and purpose the device was fittingly named the "Measurement Cube".

Minimizing Permeation Influence

As already discussed, a major error source is the permeation of oxygen through seals or joints that are inevitably required for the final functionality. Because there is little to be done against these effects beside minimizing the exposed area of seals and maximizing their thickness, an additional precaution had to be taken: The measurement device must be placed inside another

compartment that is continuously flushed with nitrogen gas thereby reducing the outside concentration of oxygen and minimizing the effect of permeation. One has to be careful, though, to allow enough time of flushing the inside and outside compartment prior to a measurement, in order to allow the parts prone to permeation to reach equilibrium with the surrounding medium, thereby eliminating dissolved oxygen in these parts.

Automating

Automation was a prime construction concern and in order to understand what type and quantity of components would be incorporated, one has to first decide on a list of tasks that the device would have to perform during a typical measurement:

1. Flood the inner and outer compartment until equilibrium is reached.

2. Close all valves, effectively sealing the inner compartment.

3. Dose a specific amount of oxygen into the compartment.

4. Create turbulence inside the compartment to speed up mixing.

5. Wait until a stable readout is obtained.

6. Repeat steps 3. - 5. until enough data are collected.

While this work flow could be realized in a number of ways the minimum components required are:

- Two valves that control the entry and exit of inert gas.

- A metering pump for dosing the oxygen containing gas, or air.

- Something to facilitate mixing, for example a fan.

- An interface that enables remote control of the other components through a computer running specific software.

The valves had to be reasonably gas tight when closed, but if one takes into account that the gas on the outside of the valves is either inert gas from a pressure source or the inert gas in the outer compartment, for inlet and outlet valve respectively, then it seems that even common solenoid valves are in fact reasonably gas tight. Therefore two solenoid gas valves (BMV 604) were obtained from Bavaria FluidTec, Germany (www.bavariafluidtec.de). A metering pump (FMM 20) was purchased from KNF, also Germany (www.knf.de). And as a fan a standard CPU fan was used. Additionally a Pt-1000 thermistor was added for temperature verification inside the measuring compartment. As interface an Arduino Duemilanove board was obtained (www.arduino.cc). This board combines an ATmega micro controller and USB controller with open source firmware and makes controlling simple digital outputs via software on an attached PC straightforward and easy.

2.5.2 Building

The first step in building was the machining of 1 cm thick brass plates into the parts that would make up the measuring compartment of the device. While soldering was unfortunately not an option, the desire to minimize permeation led to the use of metal-metal joints glued together with a two component epoxy resin (301-2) that shows exceptionally low permeation, obtained from EPOTEK, USA (www.epotek.com). In figure 2.6 the dimensions of the machined parts are displayed.
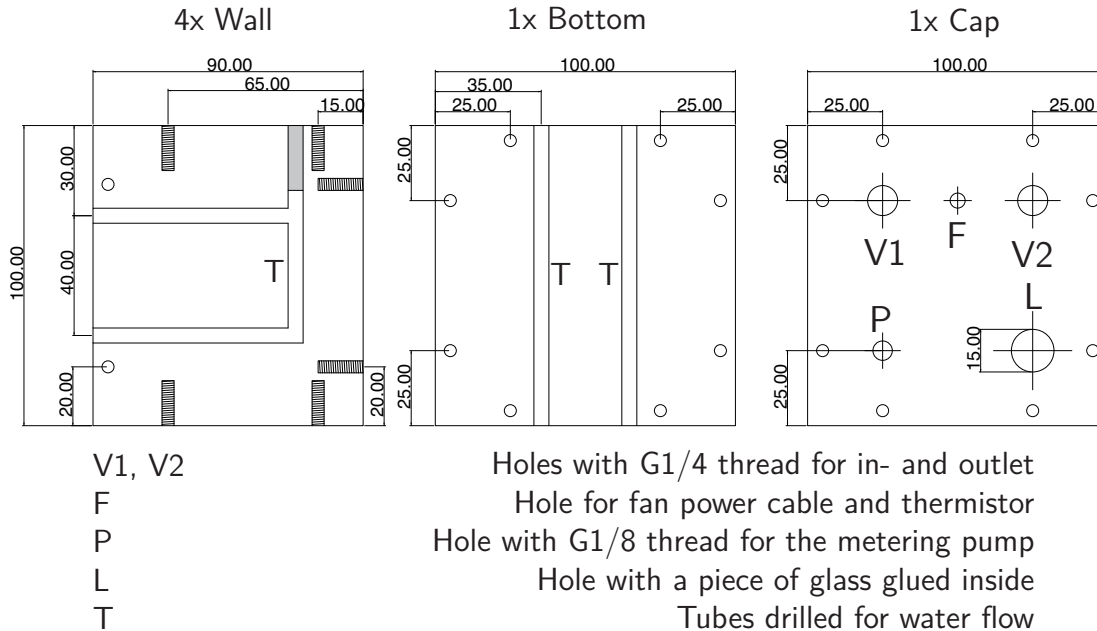

V1, V2	Holes with G1/4 thread for in- and outlet
F	Hole for fan power cable and thermistor
P	Hole with G1/8 thread for the metering pump
L	Hole with a piece of glass glued inside
T	Tubes drilled for water flow

Figure 2.6: Dimensions of parts machined from 1 cm thick brass sheets that make up the compartment walls of the Measurement Cube. All sizes are in millimetres.

As you can also see in the figure the tubing for the water from an external thermostat is drilled into the sides and one drill hole is closed to create a circuit. For a better understanding of how the waterflow through the walls is routed see the right hand side of figure 2.7. After the parts had been constructed, assembly of the cube could begin. The body of the cube (its four sides and the bottom) were joined and 301-2 epoxy resin was applied to the joints which were then screwed together. Resin was also generously applied to all inner edges and cured for two hours at 80 °C. Due to the very low viscosity of the uncured resin the cube was rotated twice during curing. Also, using the same resin, a glass piece was glued to the cap. Figure 2.7 shows a rendering of the cube before and after these steps with additional hollow bolts to facilitate the instalment of tubes for thermostat water.

2.5.3 Automation

With the mechanical components constructed the last missing feature is automation. As discussed in section 2.5.1 an Arduino board was chosen to establish connection between software and electronic actors. All electronic components used in the construction, with the exception of the Arduino Board itself, were obtained from Conrad Electronics in Austria (www.conrad.at).
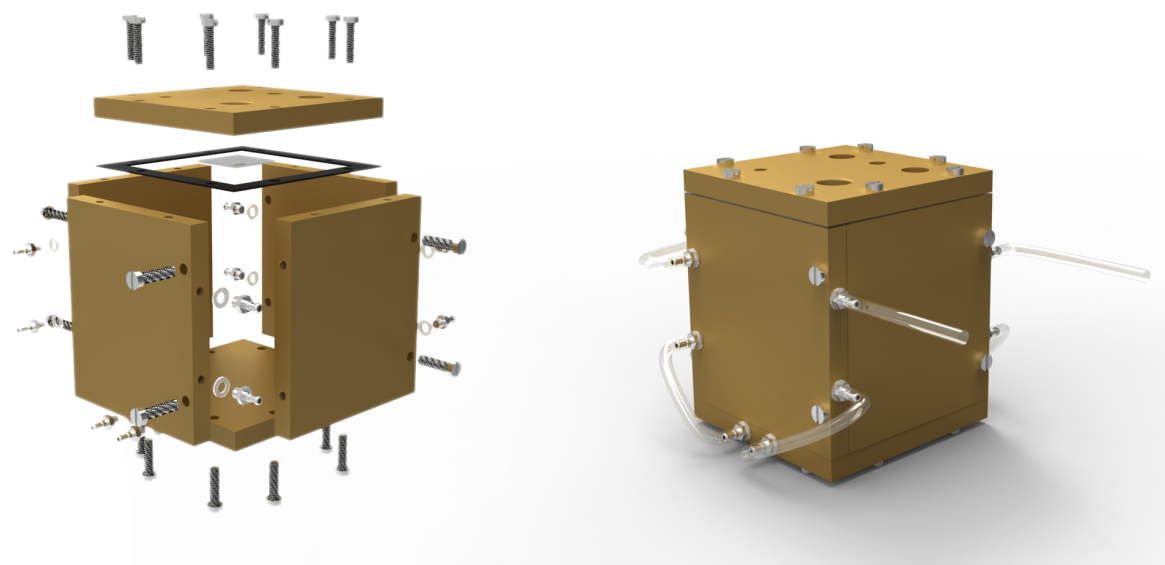
Figure 2.7: A rendering of the measurement cubes parts before and after assembly and glueing of the parts.

The Arduino Board

The Arduino Duemilanove board as pictured in figure 2.8, is equipped with an ATmega328 microcontroller and has 14 of its digital input- and output pins as well as six analog input pins accessible. Power can be supplied either via USB or via an external power source. Its output pins supply 5 V and 40 mA when switched to high. This of course isn't enough to directly supply a solenoid or electric motor. The analog input signals are divided into 1024 steps from 0 - 5 V. If an external power source is used it should supply between 7 V and 12 V for the internal voltage regulator to work properly.[1] Therefore the various other components had to be adapted to work within these limitations.

Solenoids and Fan

The obtained solenoids as well as the fan accept 12 V as input voltage. Therefore a matching external power supply was obtained, providing 12 V and up to 3 A of current. This is because solenoids can have a load of around 0.75 A when opened[2]. In figure 2.9 the circuit for connecting either a solenoid valve, the solenoid metering pump or a fan to a digital output pin of the Arduino board is depicted. An IRF640N MOSFET transistor was used to switch the load based on the state of the digital output and a schottky diode was used to protect the circuit board from inductive current generated by the solenoid being forced shut by a spring.

The Temperature Sensor

The Arduino analog input is rather limited in its resolution. As a result, to maximize the resolution in a sensible temperature range from 0 °C - 80 °C, these temperatures should be mapped to 0 V and 5 V input voltage respectively. To accomplish this goal a wheatstone bridge

---

[1] see "Arduino Duemilanove" retrieved June 2011, from http://arduino.cc/en/Main/ArduinoBoardDuemilanove
[2] See BMV604 Datasheet, retrieved June 2011, from http://www.bavariafluidtec.de
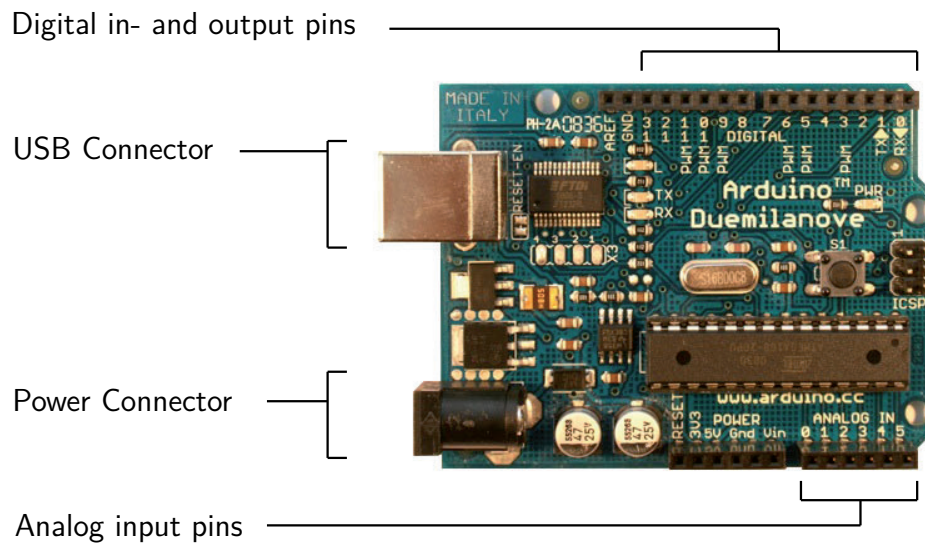
Figure 2.8: A picture of the arduino duemilanove board with its connections highlighted. (Original image retrieved from http://arduino.cc)
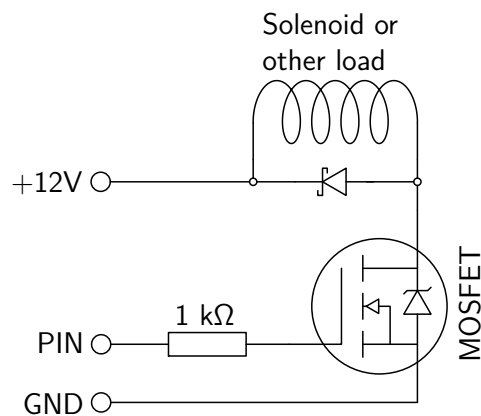

Figure 2.9: The circuitry used to connect e.g. a solenoid to one of the digital output pins of the Arduino Duemilanove board.

in combination with a rail to rail amplifier was used. The resulting circuit is depicted in figure 2.10, an LT1368 dual precision rail to rail OP amplifier was used. The values for resistors R1, R2, R3 were calculated using LTSpice[3]. The calculated values are presented in table 2.5. The simulated curve shown in figure 2.11 shows the linear dependence of thermistor resistance and resulting voltage.
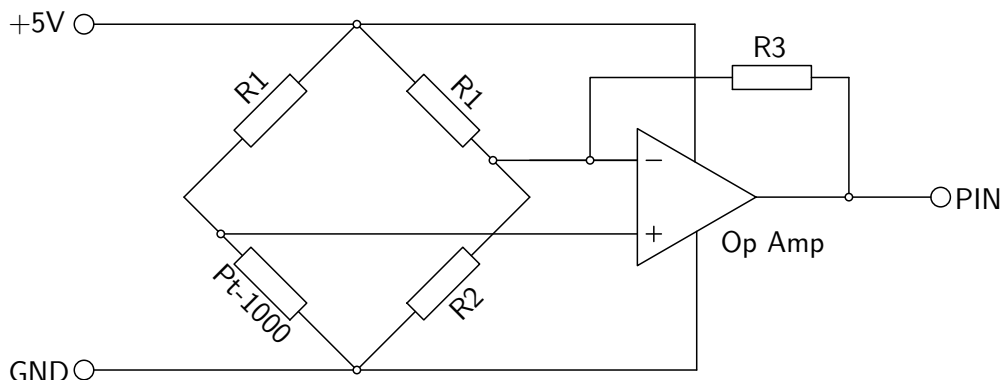
Figure 2.10: The circuitry used to connect a Pt-1000 thermistor to the analog input pin of the Arduino Duemilanove board with a wheatstone bridge and operation amplifier.

Resistor	Value / Ω
R1	10K
R2	1K
R3	27K

Table 2.5: The values of resistors used to construct a Wheatstone bridge for thermistor readout.

A so called prototype board was used to solder the components according to the presented circuit layouts. This board is specifically made to be mounted on top of the Arduino board to provide fast exchangeability. Once everything was in place only the software component remained to be built.

Firmware

For a computer based software to issue commands, some kind of interface has to be provided by the Arduino firmware via USB. The complete firmware source code can be seen in appendix 9.2. Table 2.6 provides a list of commands understood by the firmware, as well as a short explanation of what each command does. These commands have to be issued via a serial communication interface and must be terminated with a line feed character. The Arduino returns an "OK" whenever a command is finished, and does not accept inputs until it is finished with executing the previous command.

2.5.4 Software

All a computer program has to do is send commands to the measurement cube with correct timing, usually taken from a list or array that was somehow generated by user input. It does so

---

[3]downloaded from http://www.linear.com
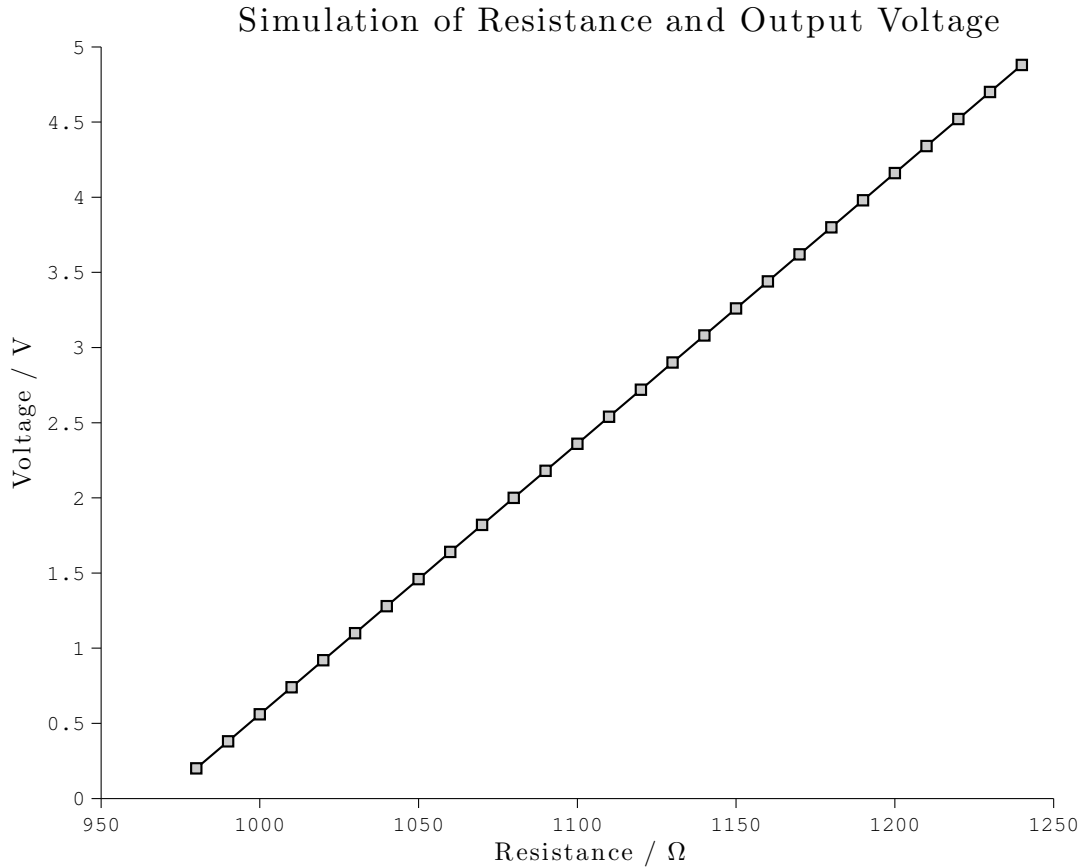
Figure 2.11: The curve given by LTSpice after optimized simulation, linearity over the whole range should make calibration fairly straightforward.

Command		Description
vin	<state>	Switches the inert gas inlet valve to the desired state, 'on' corresponds to open, 'off' means closed
vex	<state>	Does the same for the inert gas outlet valve
pum	<value>	executes a number of pump strokes equivalent to (<value> / 20)
fan	<state>	Switches the mixing fan on or off corresponding to <state>
rte		Returns the current temperature in °C as a float instead of "OK"
tsr		Returns the value of the current temperature slope constant used for calibration of the temperature sensor
tsw	<value>	Sets the value of the current temperature slope constant to <value>
tdr		Returns the current value of the temperature drift constant
tdw	<value>	Sets the temperature drift to <value>

Table 2.6: A list of commands understood by the Arduino firmware, <state> can be either "on" or "off" without quotation marks, each command has to be terminated by a line feed character.

either directly or with some kind of automation, e.g. an algorithm that determines the correct command sequence based on the users requirements. A variety of programs was written for this purpose. The first was called "Measurecube Control" and was used for debugging purposes, merely sending a command corresponding to a pressed button. The second program which was used for all measurements throughout this thesis was called "Measurecube Automator".It added features to control the timing and it sends commands listed in a table with the corresponding delays between them. A Microsoft Windows version was also created in LabView to allow other institute members to use the Measurement Cube. It was called "The very very rudimentary measurecube control". Also a more sophisticated LabView program for the same purpose was created, supporting advanced functions like saveing and loading of work-flows and algorithmic command array generation as well as integrated thermostat and lock-in amplifier control. This program, however, was not finished in time to be included in this thesis. In figure 2.12 the user interfaces of these programs are displayed.

(a) Measurebox Control

(b) Measurebox Automator

(c) Very Very Rudimentary Measurecube Control Program

(d) Master Control Program (not finished)
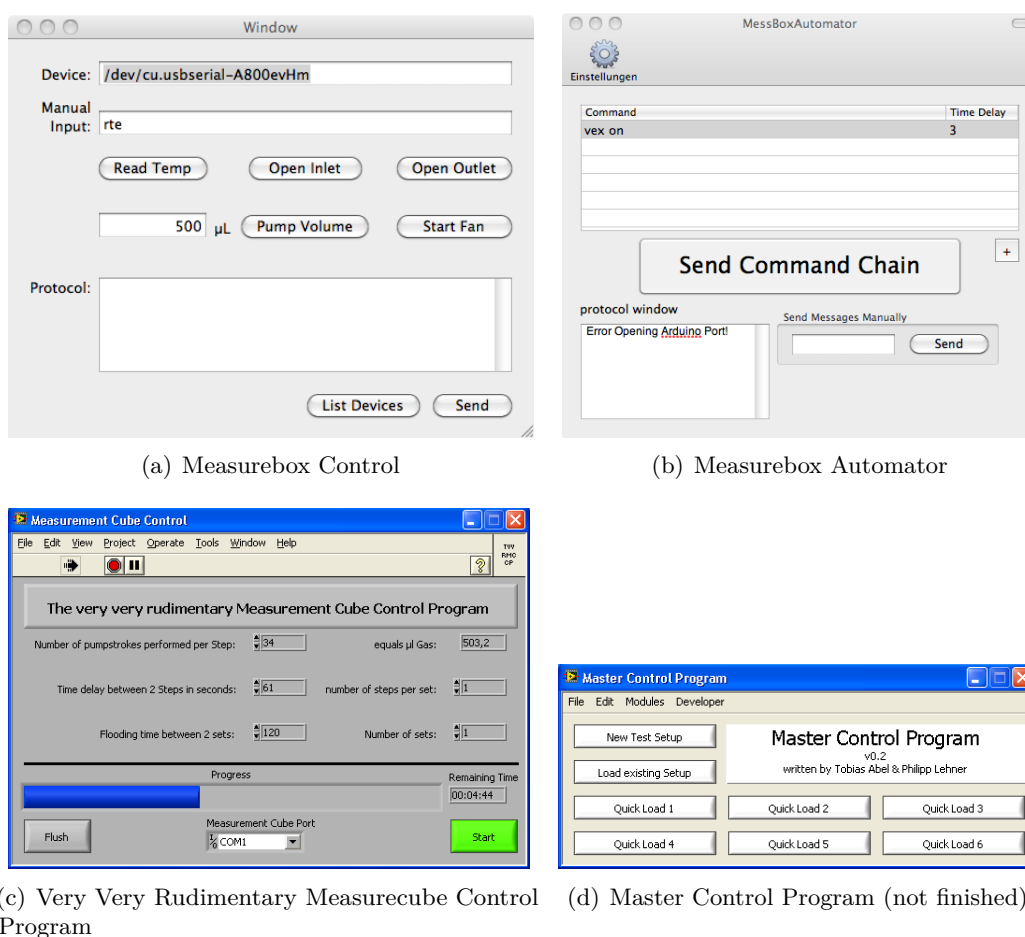
Figure 2.12: User interfaces of the various control programs written in the course of this thesis.

2.5.5 Outer Hull

A final consideration was adding a second hull to surround the whole device. This hull is constantly flushed with inert gas and it was hoped that this would significantly decrease the effects of diffusion through the few remaining seals. In a final version this outer hull should be reasonably gas tight with feedthroughs for the various connections of the inner hull. However, all measurements in this thesis were made with an improvised hull made of a standard PET container with part of its lid cut off to allow tubing and wires to pass. While this solution makes handling of the cube impractical when changing sensors, it still serves its intended purpose well.

2.5.6 Calibration and Testing

The now finished cube had yet to be calibrated and characterized. In equation 2.3 all the necessary variables are included. So in order to obtain a correct result for the partial pressure the Measurement Cube's inner volume, inner temperature and the exact dosage volume of the metering pump have to be known.

Metering Pump Calibration

The metering pumps data sheet claims that it is shipped with adjustable volume from $10\,\mu\text{L}$ to $20\,\mu\text{L}$. However no exact factory setting was given. As a result a testing assembly for the metering pump was devised. This can be seen in figure 2.13. A burette was turned upside down and its graduation used for volume determination. The volume inside is of course only valid if the pressures inside and outside are equal. As one can see this led to the outer container being raised until water levels match for obtaining the zero point. This was followed by lowering it again and letting the metering pump dose until the water levels meet, in which case the volume read from the burette's graduation equals the total dosed volume.

$$V_{Dose} = \frac{V_{Total}}{n_{Strokes}} \tag{2.6}$$

After repeated calibration the dosage volume of one stroke was determined to be $14.8\,\mu\text{L}$. While an adjuster bolt would have allowed to change this volume, it was decided that, since all calculations would be done by software anyway, the metering pump would be used in its current state in the measurement cube.

Device Volume

The device's inner volume is harder to determine. There are three possible approaches to the problem:

1. Determine the volume via some liquid filling the compartment

2. Calculate the volume based on its components

3. Measure the oxygen pressure with a calibrated sensor and known dosage volume and use these data to calculate the volume

The first point wasn't easy to accomplish, because some components must not be brought into contact with water (e.g. the fan). Therefore a non conducting liquid would have to be used. It wasn't clear either, how remaining bubbles would be removed from the cube's interior. Therefore a combination of approach 2 and 3 was used. At first the volume should be calculated
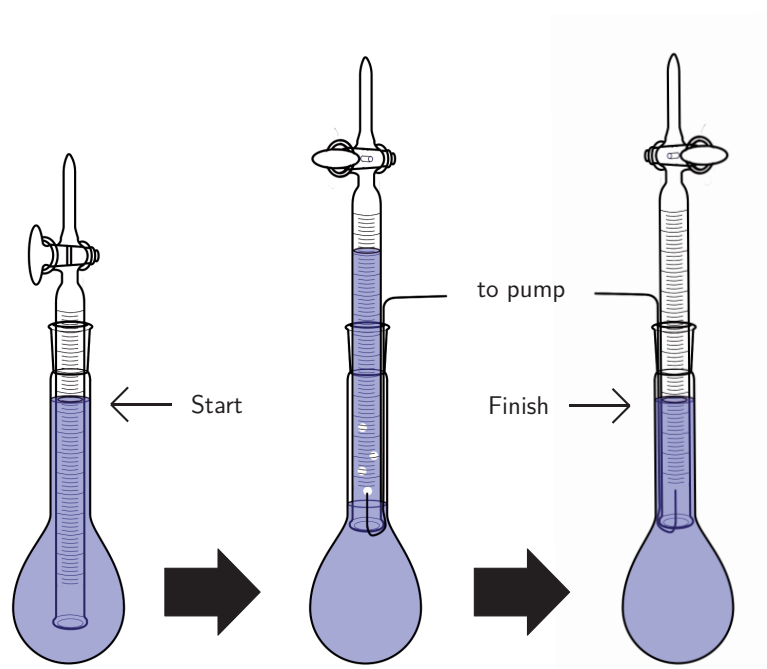
Figure 2.13: Test assembly used to calibrate the metering pump. Since readings are only valid if inside and outside pressure are equal, the water reservoir had to be raised and lowered accordingly.

Name	Volume / mL
inner cube volume	$640,0$
looking glass	$-0,7$
sensor mount	$-0,9$
valves	$0,5$
wire feedthrough	$-0,5$
thermistor	$-0,1$
elongation because of seal	$6,4$
pump	$0,1$
epoxy resin	$-2,0$
fan mounting	$-2,3$
fan	$-11,5$
	≈ 630

Table 2.7: A list of free and excluded volumes that in total give the volume of the inner cube compartment.

as exactly as possible and the result then verified through a measurement. In table 2.7 the volume is calculated as a sum of partial free- and excluded volumes. One can be confident that the error of this approach is below 1 %. Still a measurement was made to verify the result.

For this measurement the cube was attached to the outlet of the homemade massflow device mentioned in 2.4 and its in- and outlet valves opened so that the measured oxygen concentration depends only on the concentration output by the massflow device. After various concentrations had been run and measured, the device was disconnected and replaced with inert gas. The measurement cube's software was then used to inject the required amount of air to achieve the same concentration, according to our calculations. The resulting measurement data are described in figure 2.14.
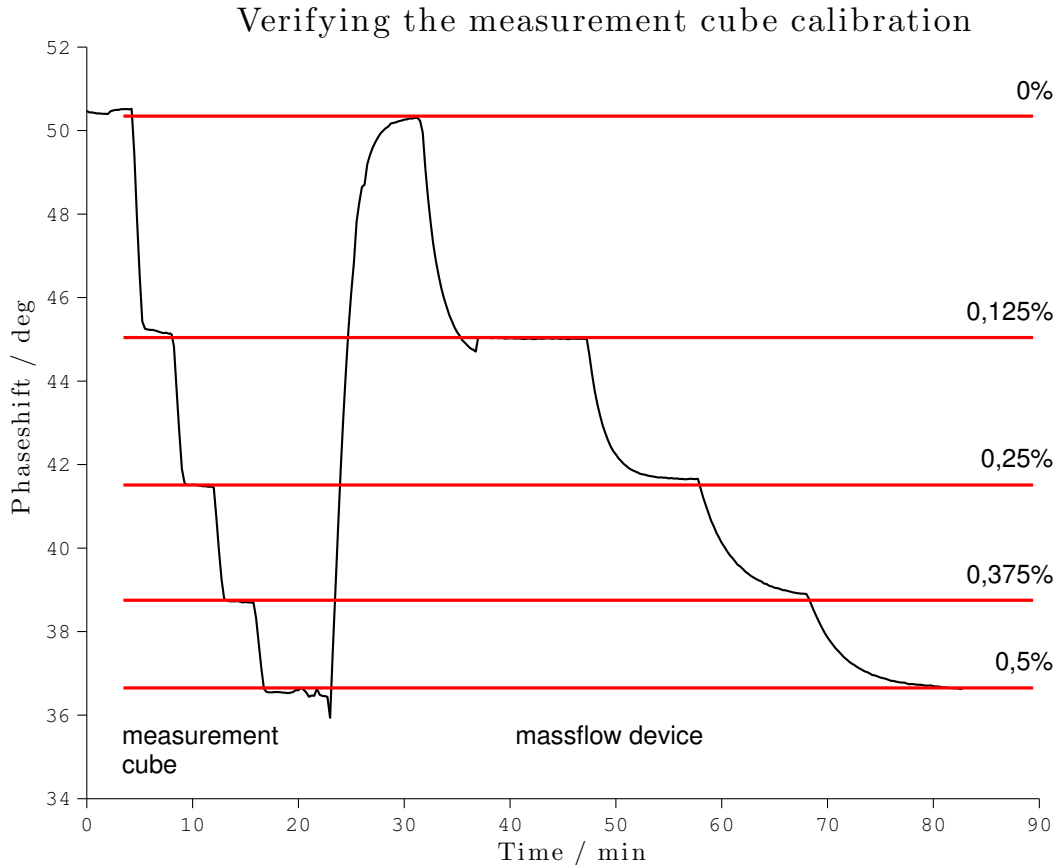
Figure 2.14: Data obtained after trying to reach specific concentrations also deployable by the massflow device. This was used to verify that the calculated volume and pump calibration were indeed correct.

Temperature Sensor

Due to the high linearity shown in figure 2.11, a two point calibration is sufficient for the temperature sensor. This calibration was executed by submerging the thermistor in the basin of a thermostat at 5 °C and 40 °C and calculating the slope and y-intercept of the corresponding linear equation. This constants where then embedded into the measurement cube's firmware source code, but they are remain changeable with the commands already listed in table 2.6.

3 Experimental

Although synthesis was not the major part of this thesis, a few polymer modifications were conducted. The procedures for these modifications are explained in this section and will only be referred to later on.

3.1 Perfluorination with trifluoroacetic anhydride

Et-Cellulose was modified using the method described by F. Z. Khan et al.[25]. This synthesis was performed at TU Graz by Sergey M. Borisov. In order to obtain the product, first $1.5\,\mathrm{g}$ ethylcellulose with 49 percent ethoxy-content is placed in a round bottom flask with two equivalents of imidazole and the flask is then evacuated and flushed with nitrogen. After that 50 ml of THF are added and the ethylcellulose is dissolved at room temperature. Trifluoroacetic anhydride is added dropwise and the solution is stirred for 24 hours before being precipitated with methanol, filtered, washed and dried under vacuum.

$$R_1 = H, CH_2CH_3$$
$$R_2 = H, CH_2CH_3, CHOCF_3$$
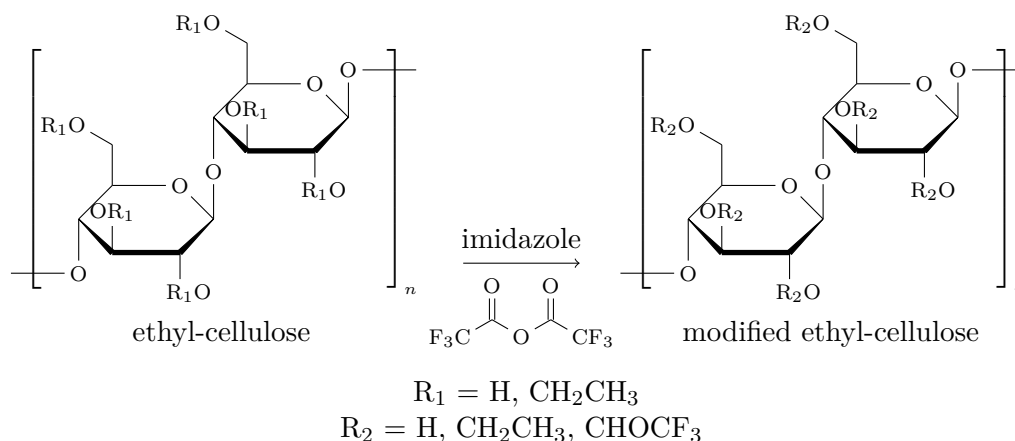
Figure 3.1: Reaction equation for modifying Et-Cellulose with trifluoroacetic anhydride

3.2 Perfluorination with perfluorobutyryl chloride

It was hoped that perfluoroalkylating polymers would enhance or at least alter the oxygen permeability of aromatic polymers. Perfluoroalkylation of polysulfon, polystyrol and polyphenylenoxide was also kindly performed by Sergey M. Borisov (University of Technology Graz), who used perflourobutyrylchloride and hydrogenperoxide to perfluorobutylate the aromatic polymers. In a reaction based on the work of A. Bravo et al.[26] the desired polymer is dissolved in $50\,\mathrm{g}$ of chloroform. Meanwhile a mixture of $2\,\mathrm{mmol}$ H_2O_2 and $4\,\mathrm{mmol}$ NaOH in FC-75 is stirred and $4\,\mathrm{mmol}$ perfluorobutyrylchloride is added to the inhomogeneous mixture. The polymer solution and the mixture are then combined and left to react at room temperature. The modified polymer is then precipitated with methanol and filtered, washed and dried.
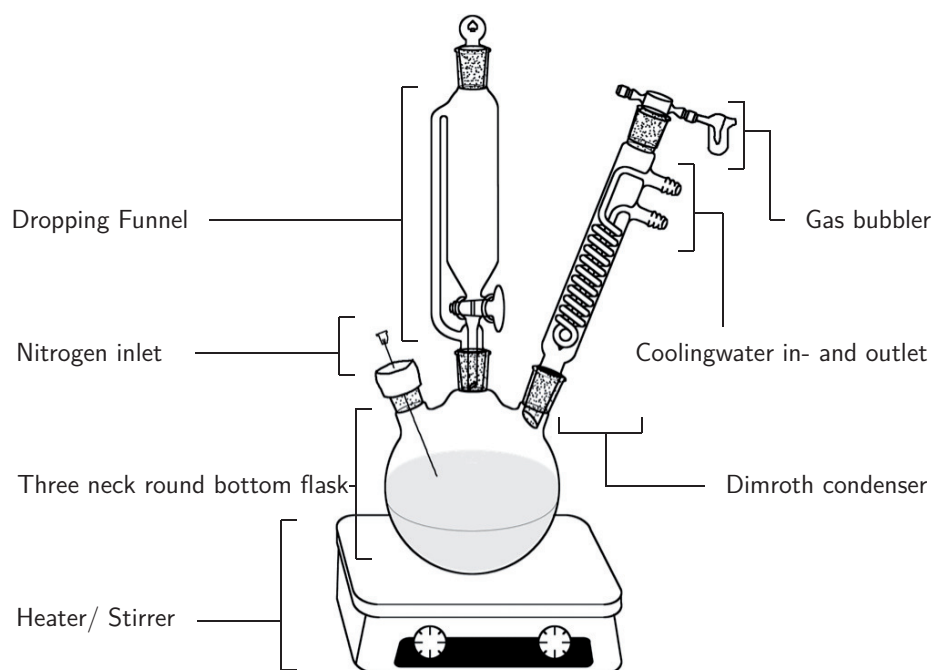
Figure 3.2: Assembly used to silanize polyphenylenoxide under inert gas flow.

3.3 Silanisation with chlorosilanes

Silanization of polyphenylenoxide showed a noticeable increase in oxygen permeability in the work of J. Zhang et al.[27]. Therefore it was promising to also try this modification and expand on it since there is a wide array of substituted chlorosilanes available. For preparation of the various alkylsilane modified polyphenylenoxide based polymers an assembly like the one seen in figure 3.2 was used.

To perform the reaction the required amount of PPO is weighed into a three neck round bottom flask and for each gram of PPO 50 mL water free THF and 150 mL toluene are added. Then septum, dropping funnel and condenser with affixed bubbler are added. The solution is heated to 50 °C and stirred until the polymer is dissolved. Nitrogen should also be bubbled through the solution from now on. Next the flask is cooled with ice to about 0 °C and 2 equivalents 10M butyllithium in hexane are added through the septum. Now the solution will turn orange and then yellow, presumably indicating mono- and disubstituted states, though this observations weren't verified. While this reaction step occurs, 2.5 equivalents of the chosen chlorosilane are added to the dropping funnel with 10 mL of toluene and left there for deoxygenation. After about 30 mins the solution has completely turned a bright yellow and the dropping funnel is opened to slowly add the chlorosilane. The solution becomes turbid in the process and is then filtered and washed. The filtrate is precipitated with methanol and then centrifuged. The sediment is repeatedly washed with methanol, redissolved in CH_2Cl_2 and precipitated and washed again (this step can be omitted if the resulting polymer does not dissolve in CH_2Cl_2). The polymer is then dried and stored under ambient conditions.
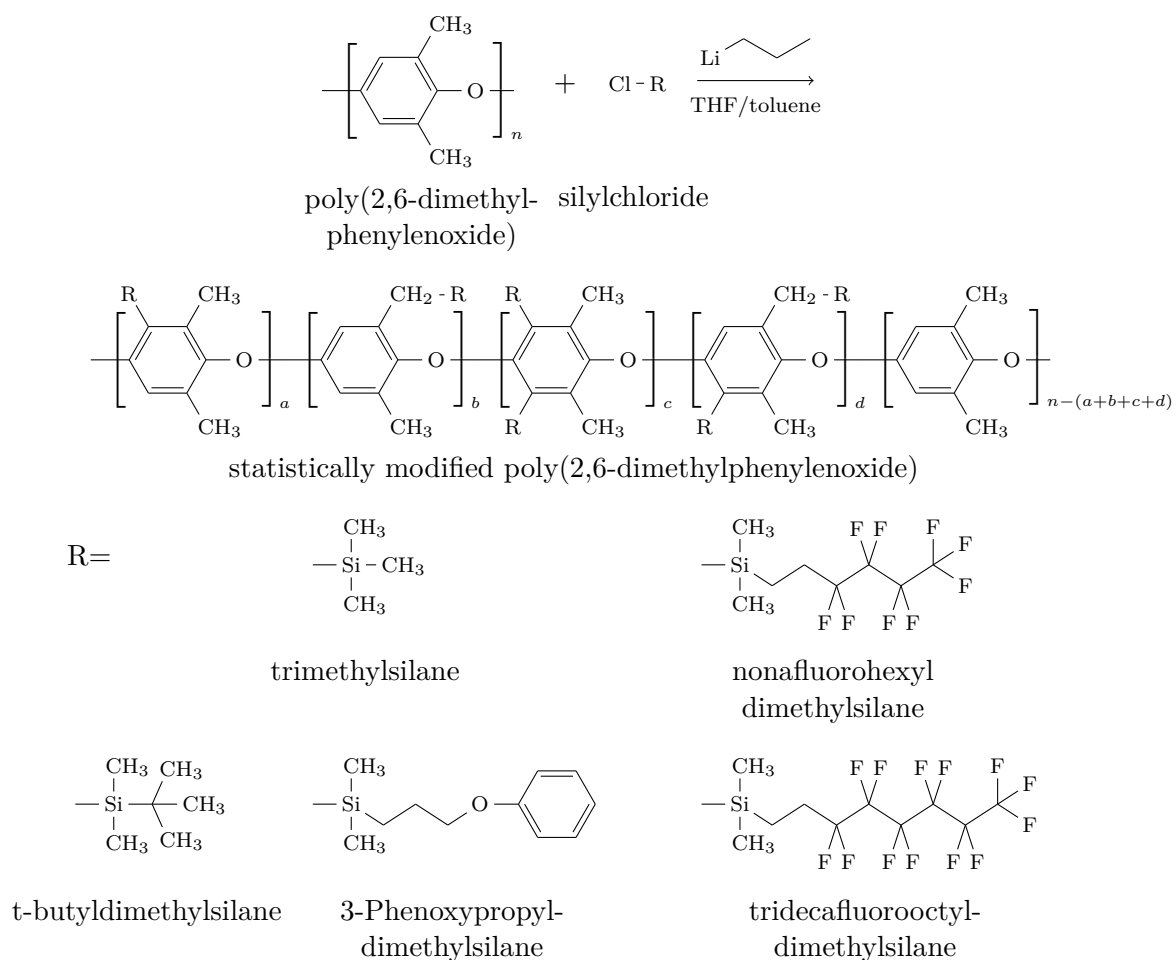
Figure 3.3: The assumed reaction for the PPO modification. Also shown are the different substituents attached to gain a range of products with hopefully varying properties. Note that polymer parts with the subscript c and d are only valid if multiple substitution per monomer is possible.

The supposed reaction is shown in figure 3.3, where one can also see the different alkylsilyl-substituents that should be attached to the final polymer. It has to be said, though, that none of these compounds were verified through structure analysis in the course of this thesis. Therefore it is quite possible that products actually have a different composition.

3.4 Covalent Dye Bonding

Silica gel like other porous materials, displays a very good oxygen permeability, however, due to its polarity it has only a very low affinity to lipophilic dyes like those based on porphyrins. Therefore the idea of covalently coupling porphyrin based dyes to a silica gel matrix was born. Previous works have shown that this can be a viable approach to sensors with highly linear calibration curves[10]. An approach for substitution of TPFPP is the nucleophilic substitution of amines on the pentafluorophenyl moiety. So in theory one has to provide a silica gel matrix surface modified with amines, and covalent coupling should be possible. The first step in this approach is to amino-modify silica gel particles. The scheme in figure 3.4 shows how an

aminosilane can be attached to the surface as a linker. These reactions were performed in 50 ml Falcon® tubes, in 20 ml of a 95/5 (v/v) mixture of EtOH and H_2O with 2 g of LiChroSorb particles. The particles are then washed with EtOH and dried.
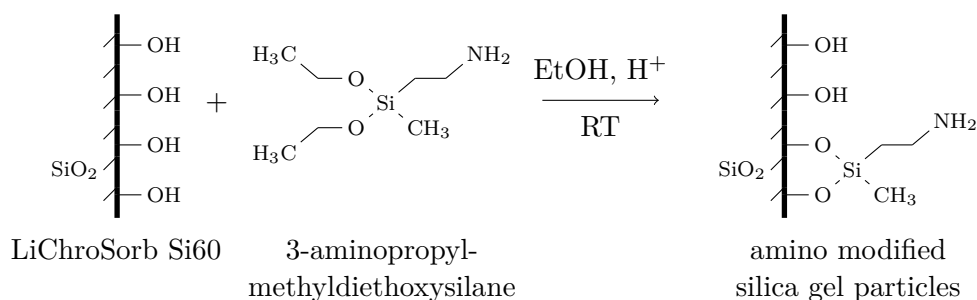
Figure 3.4: Modification of the surface of silica gel particles with an amino substituted ethoxysilane.

In figure 3.5 the followup reaction of covalently linking the pentafluorophenylporphyrin dyes to these modified particle surfaces is shown. In a round bottom flask with attached dimroth condenser, 0.9 g of the surface modified particles and 18 mg of either the platinum or palladium based dye are dispersed in diphenyl ether and stirred at 230 °C for three hours. After cooling, the dye-doped particles are centrifuged and washed five times until the supernatant is clear, so that only covalently bound dye remains on the particle surface. The particles are then dried and stored under ambient conditions until used. The easy separation and handling of the particles is a huge advantage over other sensor preparation techniques and highly convenient.

M = Pt, Pd
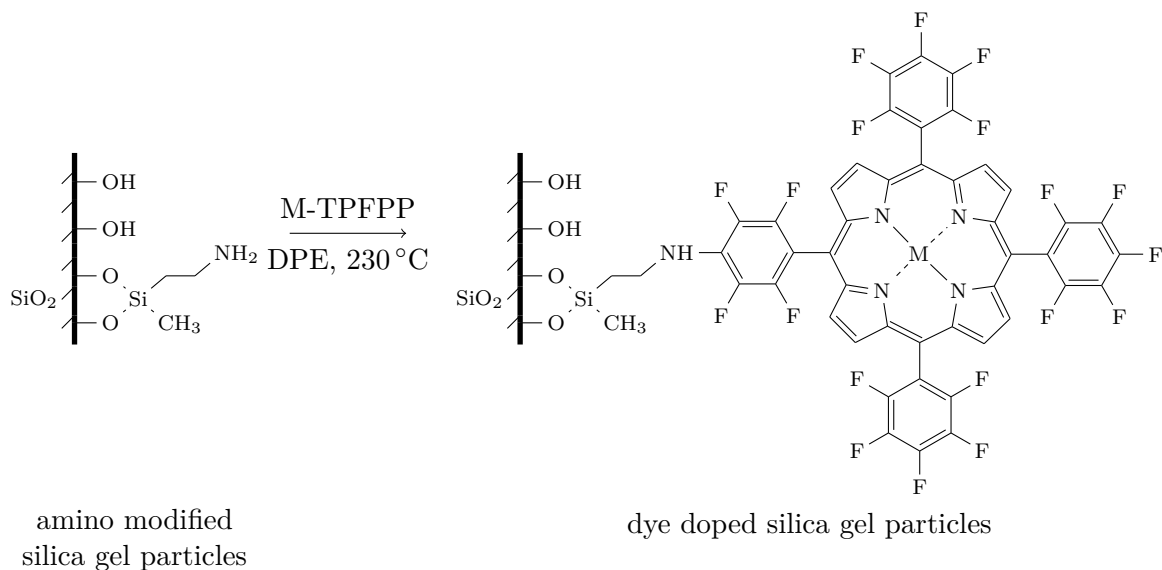
Figure 3.5: Scheme of the reaction used to covalently bond dyes to the surface of silica gel particles using an aminoalkylsilane linker.

Finally, on some of the dye-doped particles an additional fluoroalkyl silanization step was performed in the assumption that this would increase hydrophobicity and therefore make the sensors better suited for applications in water. For this reaction 400 mg of the dried dye-doped

particles were dispersed in 10ml of a 95/5 (v/v) mixture of EtOH and H_2O and $600\,\mu L$ of (3,3,3-trifluoropropyl)-methyldimethoxysilane were added after five minutes. The dispersion was then stirred for one hour and after addition of $2\,mL$ acetic acid the reaction was stirred overnight. The schematic for this reaction can be seen in figure 3.6 The particles were then washed five times with EtOH and dried under vacuum at $60\,°C$.

dye doped
silica gel particles

3,3,3-trifluoropropyl-
methyldiethoxysilane

end capped
silica gel particles

R = Pt-TPFPP, Pd-TPFPP
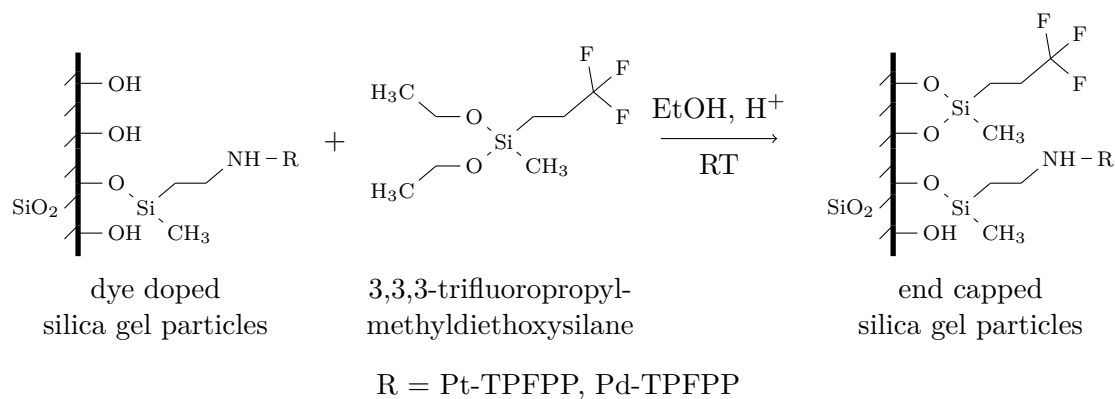
Figure 3.6: Scheme of the optional reaction performed to end-cap the silica gel surface with trifluoropropyl methylsilane.

Analysis of these particles with ICP OES revealed that they contained 0.303 mg/g of Pt and 0.12 mg/g of Pd, respectively. Which corresponds to 0.18 $wt\%$ of PtTFPP and 0.12 $wt\%$ of PdTFPP.

4 Results and Discussion

4.1 Data Acquisition

The luminescent decay times displayed throughout this section were obtained in frequency domain measurements. For most sensors excitation was performed using an LED of specific wavelength depending on the excitation spectrum of the dye obtained from Roithner, Austria (www.roithner-laser.com). This excitation light was sinusoidally modulated and filtered through a BG 12 glass filter from Schott, Germany (www.schott.com) and guided through a bifurcated fibre bundle to the sensor. The same bundle was used to guide the emission light back to a photomultiplier tube (H5701-02) obtained from Hamamatsu, Japan (www.hamamatsu.com) after passing through another filter from Schott. This time the type of the filter depended on the emission spectrum of the dye. Table 4.1 shows which LEDs and filters were used for different dyes, as well as the frequencies at which the excitation light was modulated. The resulting phase shifts were measured with an SR830 two phase lock-in amplifier from Stanford Research Inc., USA (www.thinksrs.com).

Dye	LED / nm	Emission filter	Modulation frequency / Hz
Pt-TPFPP	405	RG 630	3500
Pd-TPFPP	405	RG 630	302
Pt-TPTBP	450	RG 9	5000
Pd-TPTBP	450	RG 9	502

Table 4.1: The different setups applied for the dyes used in this thesis. Both filters were always used in conjunction with a plastic filter foil to completely eliminate excitation light.

It is important to mention that not all measurements were conducted using this setup, towards the end of this thesis another option became available. A purpose built phase shift measurement device that combines all the above parts into a single device, however, with a photodiode instead of a photomultiplier tube, called the Firepad. This device was built by Christoph Larndorfer as part of his master thesis in cooperation with Pyroscience, Germany (www.pyro-science.com) and was used for measuring Pd-TPTBP in Teflon AF. This is because a photomultiplier tube's quantum efficiency starts to drop drastically starting at approximately 800 - 900 nm. Which, of course, has a negative impact on the signal to noise ratio of dyes with a big part of their emission spectrum in the near IR range. In sensor coatings with high dye concentrations this is not observed to be a problem, however, in the special case of the low dye concentrations in Teflon AF (see table 2.4) this influence becomes noticeable and therefore the sensors couldn't be measured reliably until this new device was available.

4.1.1 Dynamic Range and Limit of Detection

The limit of detection is defined as three times the average noise of a blind measurement. Its value is greatly dependent on the measurement device used and is therefore not applicable if only sensors are considered. For sensors in this thesis an interesting characteristic that enables comparison is the lower boundary of the dynamic range. This also enables the assignment of possible applications for the different sensors.The bounds can be calculated from K_{SV} using the formula given in equation 4.1. There is no standardized way to obtain these bounds, and since they are meant to provide means for comparing the different sensors, they are not necessarily comparable with ranges given by other sources. While the limit of detection or even the limit of quantification may be lower than the bounds given (they should, however, closely resemble the limit of quantification for the measurement devices used in this thesis), they give a good approximation of what a specific sensor can accomplish.

$$P_{LowBound} \approx 0.003/K_{SV} \tag{4.1}$$

This is a somewhat crude approximation mathematically speaking. But under the assumption that the frequency is chosen so that the unquenched sensor shows a phase shift of roughly 50 degrees(which is true for all sensors in this thesis) the resulting smallest change quantifiable is very close to 0.003 $\tau_0\tau^{-1}$ for all sensors.

4.2 Prototype Measuring

4.2.1 *t*-butylstyrene

The first conducted measurements were performed with a spraycoated *t*-butylstyrol matrix with a Pd-TPTBP dye on a glass substrate. This was a preliminary measurement to assert two facts:

1. Is our prototype device capable of reliably measuring and metering small quantities of oxygen in the μL L^{-1} range?

2. How good is this first sensor , how big will our improvements have to be to reach our goals?

The prototype device used in this preliminary measurements is explained in detail in section 2.4.3, for each data point 500 μL of air was injected using a syringe of that volume. Then the magnet was moved until equilibrium was reached and a stable phase shift could be obtained. The results of these measurements can be seen in figure 4.1.

The results show that the device is certainly capable of measuring in the desired oxygen range (0.1 hPa to 5 hPa), however, a lot of improvements could be made. They are listed in the following subsection. Regarding the sensor it was shown that this preliminary test already yielded a promising sensor with a lower bound of approximately 1 Pa. This corresponds to an oxygen concentration of 0.4 ppb (ng g^{-1}) in water (at 25 °C). Since this is the lower boundary it is fair to assume that this sensor would deliver results in the range desired for application in e.g. breweries. Albeit being not quite sensitive enough for applications in marine and microbiological applications.

This early success induced confidence that sensors for even lower concentrations could be obtained just by finding better polymer matrices without the need for further dye improvement. At least not in the course of this thesis.

4.2.2 Next Steps

Measurement of these early data proved to be somewhat difficult though. As it turned out the low sensitivity of the photomultiplier tube towards the Pd-TPTBP yielded a bad signal to noise ratio and small shifts of the fibre would result in a noticeable change in signal due to background intensity variation. This is not a fault of the prototype device, though, and similar results were to be expected in any other device. This is why Pd-TPTBP was not used again until the very end of this thesis where the frequency domain device by Christoph Larndorfer mentioned in section 4.1 became available. It could, however, be expected that results obtained with Pt-TPTBP are proportional and that a sensor that shows higher sensitivity with Pt-TPTBP also does the same with Pd-TPTBP.

Pd-TPTBP in a t-butylstyrene matrix
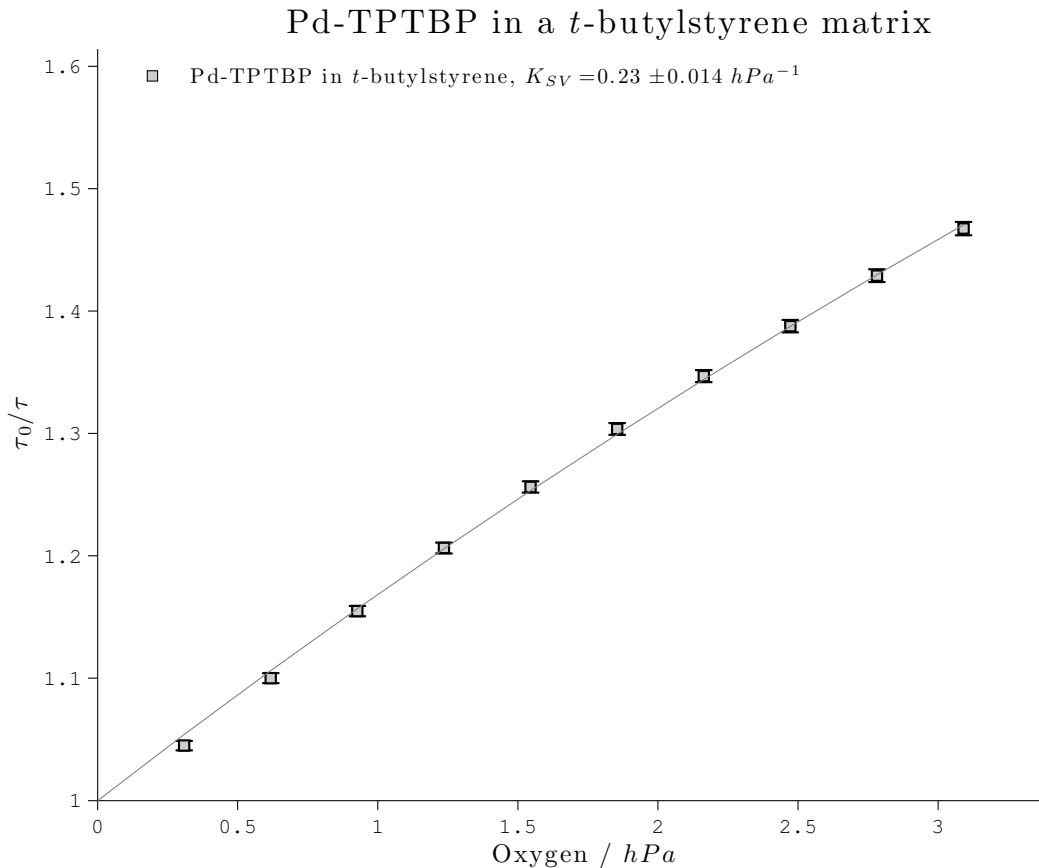
Figure 4.1: Stern Volmer plot of Pd-TPTBP in t-butylstyrene measured with the prototype device.

There were also a number of points in need of improvement that were directly related to the measurement prototype. These would have to be considered in the final measurement device already described in section 2.5.

1. Temperature regulation is supposedly a problem due to the sensor being situated in the neck of the flask and glass being a poor thermal conductor.

2. The drift is rather high although glass does not allow permeation of oxygen because of the comparably large surface of the rubber septum.

3. While the oxygen partial pressure region covered with this measurement is acceptably low, there is little room for improvement should future sensors be sensitive to even lower concentrations of oxygen. One solution would be to dose 1 % oxygen test gas instead of air, but this would require a fixed metering pump instead of a syringe.

4. The device requires someone to be constantly operating it, a factor that is anything but necessary with todays possibilities.

All of these points were addressed in the afore mentioned section 2.5 where the construction of the follow-up device, the measurement cube, is described. After this device was finished, Pd-TPTBP in *t*-butylstyrene was again measured, this time with the Measurement Cube, a comparison between the results obtained with the two methods can be seen in figure 4.2.
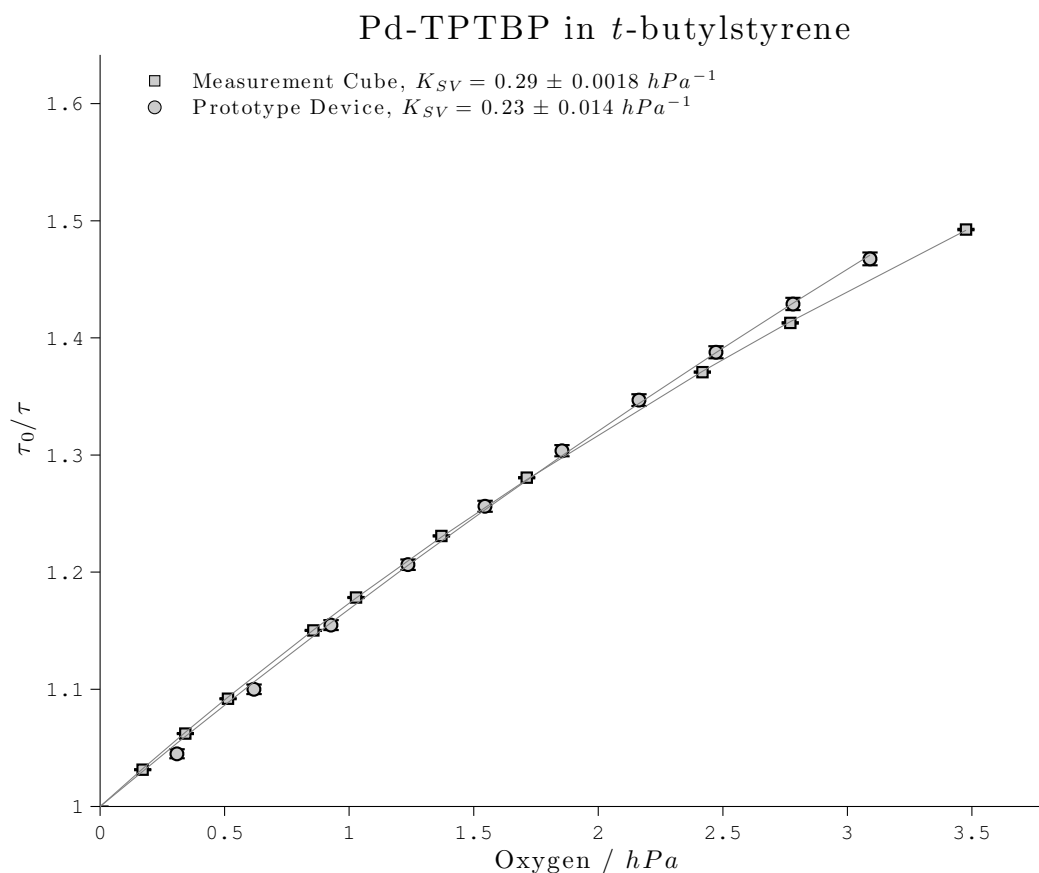
Figure 4.2: The results of Pd-TPTBP in *t*-butylstyrene measurement in the prototype device and the finished measurement cube compared.

As one can see the two methods are actually giving almost the same result, which in a way validates both methods as their results are reproducible with different equipment. It is also apparent that the error bars of the cube measurement are far smaller than those of the prototype device, proof that the time of building a sophisticated device was well invested. Additionally the two site model fit for the curve obtained by the measurement cube is better, which makes the K_{SV} value obtained through the measurement cube the more reliable one.

4.3 Preliminary Polymer Characterization

While the measurement cube was being designed and built, the available time was used to make a few preliminary characterizations of different promising polymers. All measurements in this section were performed with the massflow device mentioned briefly in section 2.4 unless otherwise stated. The dye used was exclusively Pt-TPTBP since it was expected to show acceptable solubility in all polymers and because it is sensitive in a range that does not require as low concentrations of oxygen as the Pd-TPTBP dye.

The sensors were cast from cocktails as described in section 2.3f. The interesting aspects of this characterization were foremost the attainable K_{SV} values, but also linearity and temperature dependence. First, five matrices that were readily available in the laboratory and already known to show good oxygen permeability were characterized to be able to compare their performance. These were: ethylcellulose, ormosil, PTFEMA, polystyrol and polyphenylenoxide. For interest and completeness all decay time plots for the sensors in this chapter can be seen in the appendix in section 9.1.

4.3.1 Ethylcellulose

ethyl-cellulose

R = H, CH$_2$CH$_3$
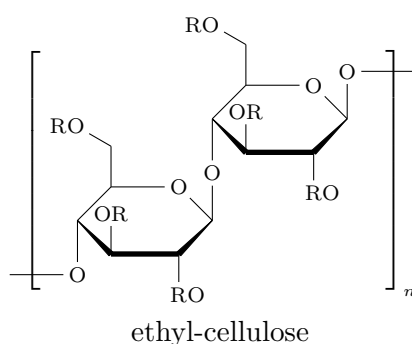
Figure 4.3: The structure of ethylcellulose. Ethylcellulose is available commercially with varying ethoxy content, the polymer used for this sensor had 50 % ethoxy content.

Ehtylcellulose is commonly used as oxygen sensing material[28] and it is often incorporated for CO$_2$ sensors [29] because it is permeable for carbon dioxide but not for protons, eliminating the cross sensitivity to pH. The results obtained for ethylcellulose can be seen in figure 4.4. As one can see, temperature dependence is very small for ethyl cellulose. The sensor is deviating from linear behaviour, which can be expected for all sensors with immobilised dye due to heterogeneities in dye surroundings. These obviously increase with decreasing dye solubility due to dye agglomeration. Also observable from the figure is the slight step towards the last data point at approximately 200 hPa. Since this data point is most certainly correct—it is pure synthetic air without any gases added in the massflow controller—it seems that the other points may experience minor deviations from the correct values due to slightly bad mixing. This effect can also be observed on most other plots obtained with the massflow device.

Ethyl-Cellulose at different temperatures
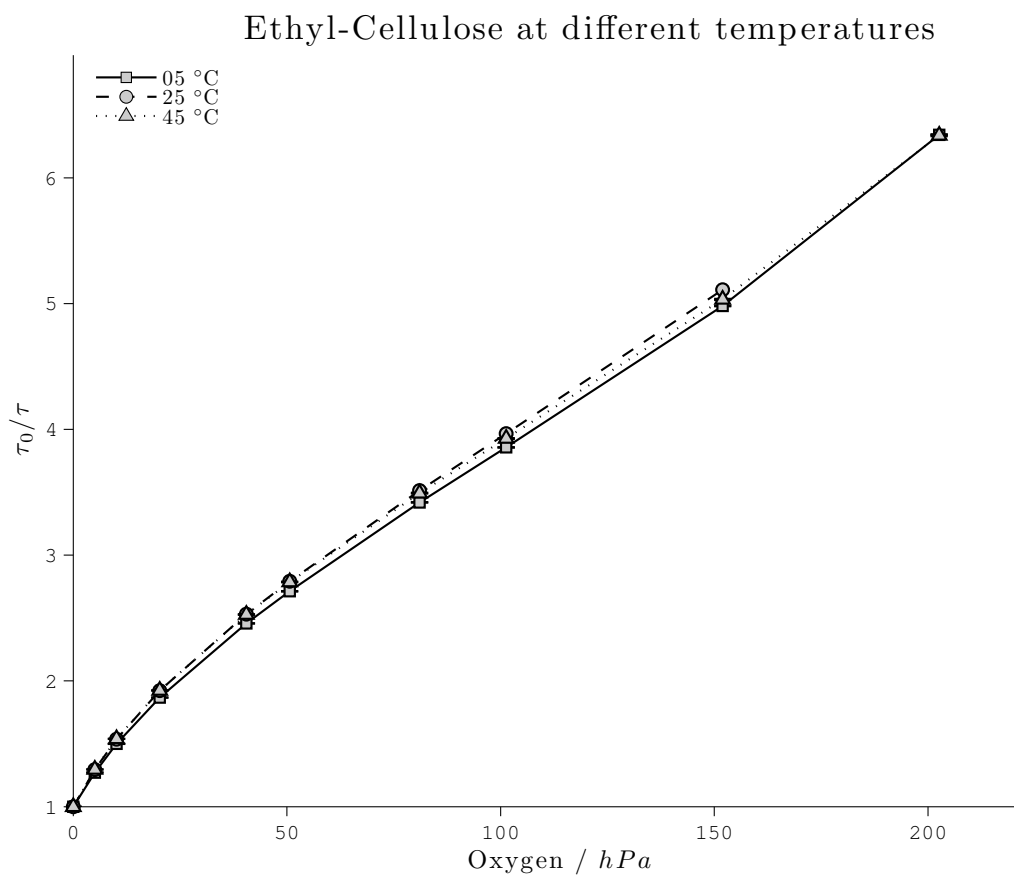
Figure 4.4: Stern Volmer plot of a Pt-TPTBP sensor with ethylcellulose matrix
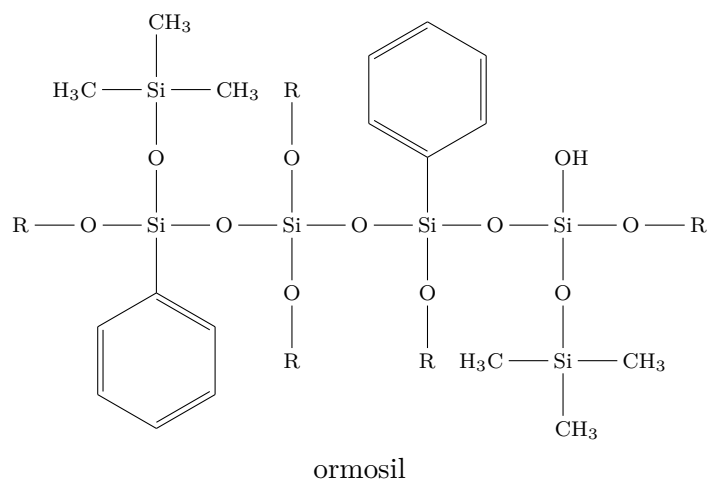
ormosil

R = cross linking to another part of the chain

Figure 4.5: Implied structure of an soluble ormosil glass, structure is not to be taken literally.

4.3.2 Ormosil

Ormosils are organically modified silica sol-gels that have proven to be highly suitable for oxygen sensing[11, 30]. Therefore an ormosil prepared at TU Graz was chosen to be also compared with the other promising matrices. The Stern Volmer plot for this ormosil can be seen in figure 4.6. Surprisingly, while the sensor shows good sensitivity for oxygen, it is strongly non-linear, which is contrary to results obtained in previous works by other authors[11, figure 7, 31, figure 6, compare] and suggests that something might have gone wrong in sensor film preparation resulting in film inhomogeneities or that the used dye has very bad compatibility with this matrix. It can also be seen that the temperature dependence is rather significant.
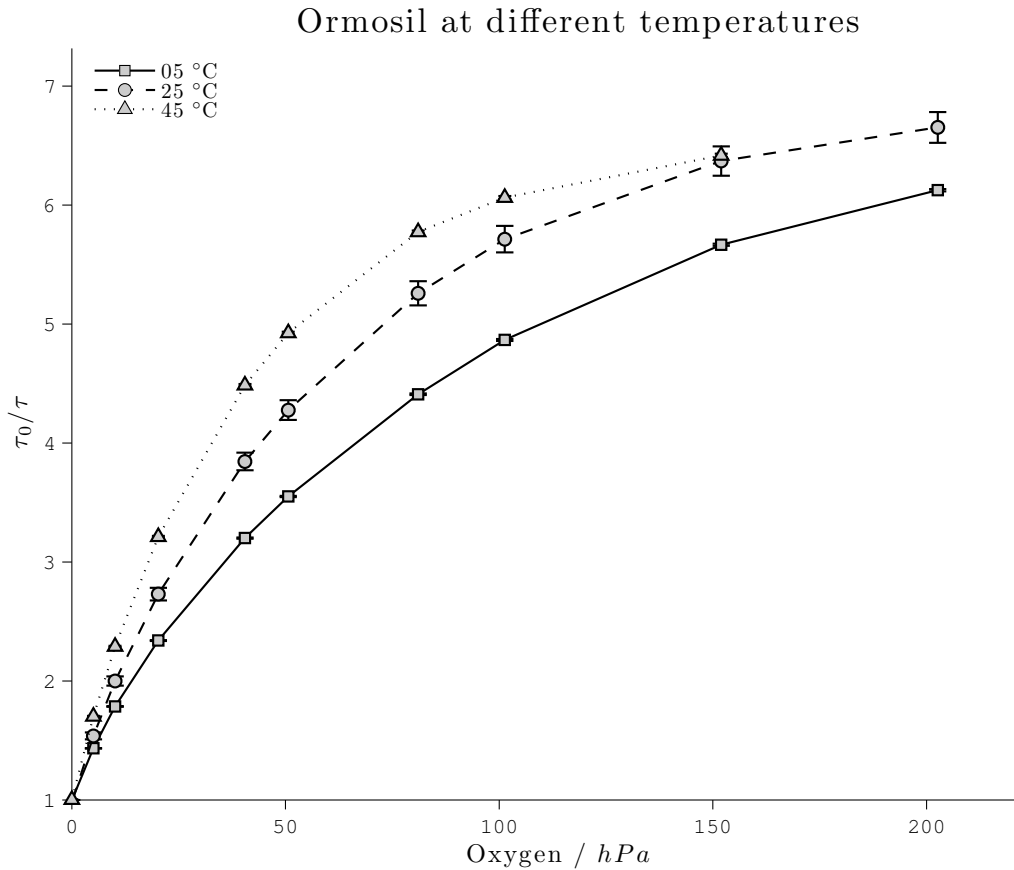
Figure 4.6: Stern Volmer plot of a Pt-TPTBP sensor with ormosil matrix.

4.3.3 PTFEMA

The next polymer characterized is poly trifluoroethyl methacrylate, the results are shown in figure 4.8. Its suitability as oxygen sensor accompanied by a high photo stability has already been shown elsewhere[32], and other methacrylates have also shown to be viable as sensors[7]. It was characterized to be able to compare it to other matrices in this section and while it is an adequate matrix it is neither extremely sensitive nor linear.
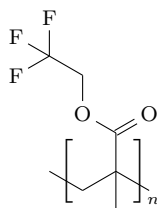
poly (2,2,2-trifluoroethyl methacrylate)

Figure 4.7: The structure of PTFEMA.

PTFEMA at different temperatures
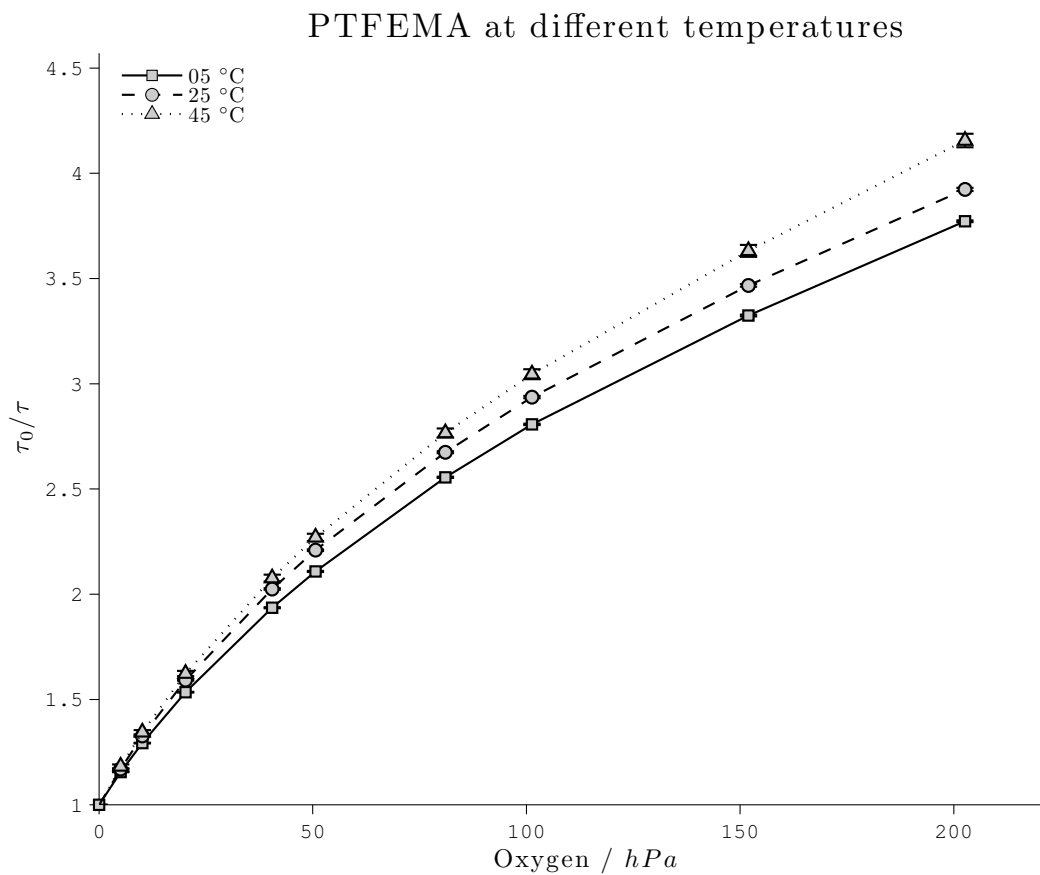
Figure 4.8: Stern Volmer plot of a Pt-TPTBP sensor with PTFEMA matrix
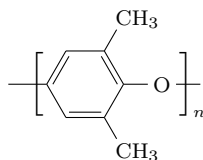
poly (oxy-2,6-dimethyl-1,4-phenylen)

Figure 4.9: The structure of PPO.

4.3.4 PPO

PPO was known to have good oxygen permeability, possibly due to its backbone rigidity and general steric demand. As with all the previous polymers a sensor was prepared and characterized at different temperatures, the results of which can be seen in figure 4.10. PPO shows very small temperature cross talk which would make it ideal for sensors easy to calibrate, and while the plot shows distinctive non linearity, the better sensitivity of the sensor compared to e.g. polystyrene makes more than up for it.
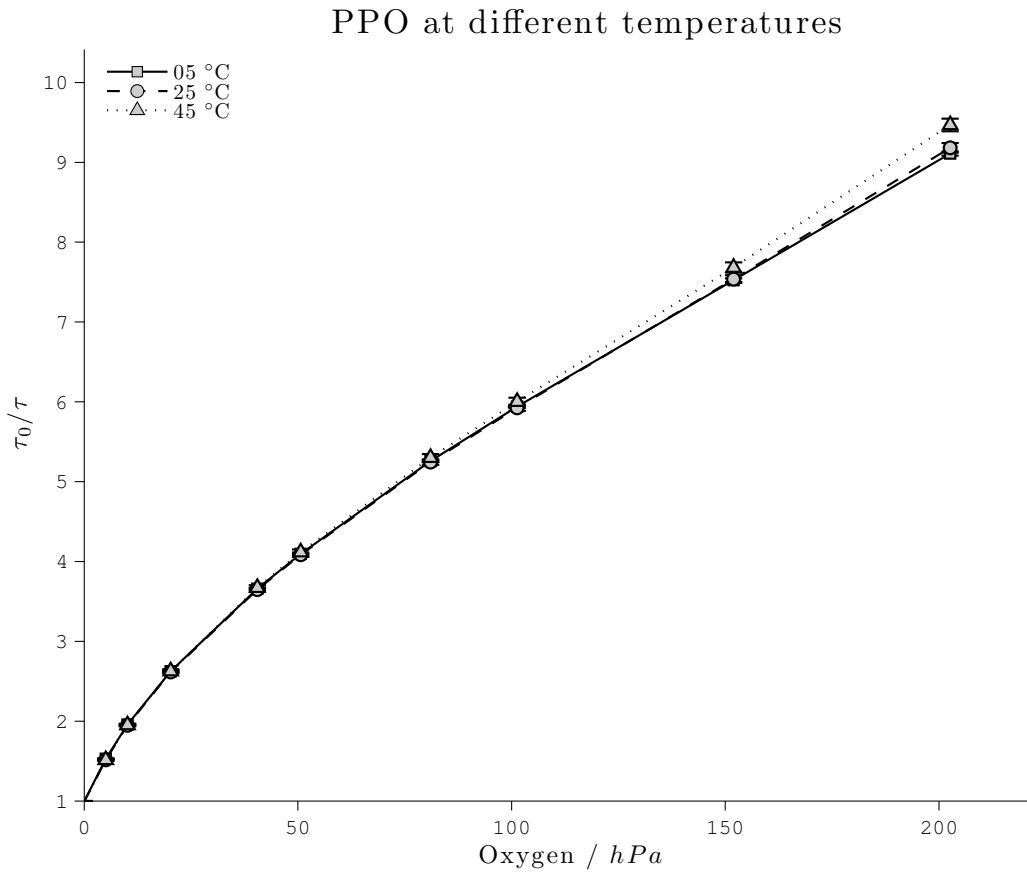
Figure 4.10: Stern Volmer plot of a Pt-TPTBP sensor with PPO matrix

4.3.5 Polystyrene
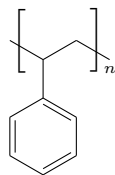
poly styrene

Figure 4.11: The structure of polystyrene.

Polystyrene and its copolymers have a wide array of applications in sensor films. Some of these sensors have proven to show good sensitivity[8]. While comparable results cannot be expected of unmodified polystyrene, it does make a good point of reference by showing "standard" behaviour: It is moderately non-linear, has a positive and quite linear temperature dependence and moderate sensitivity. Because of that it is going to represent a baseline that the performance of other polymers in this thesis can be compared to. The results for this measurement are displayed in figure 4.12.
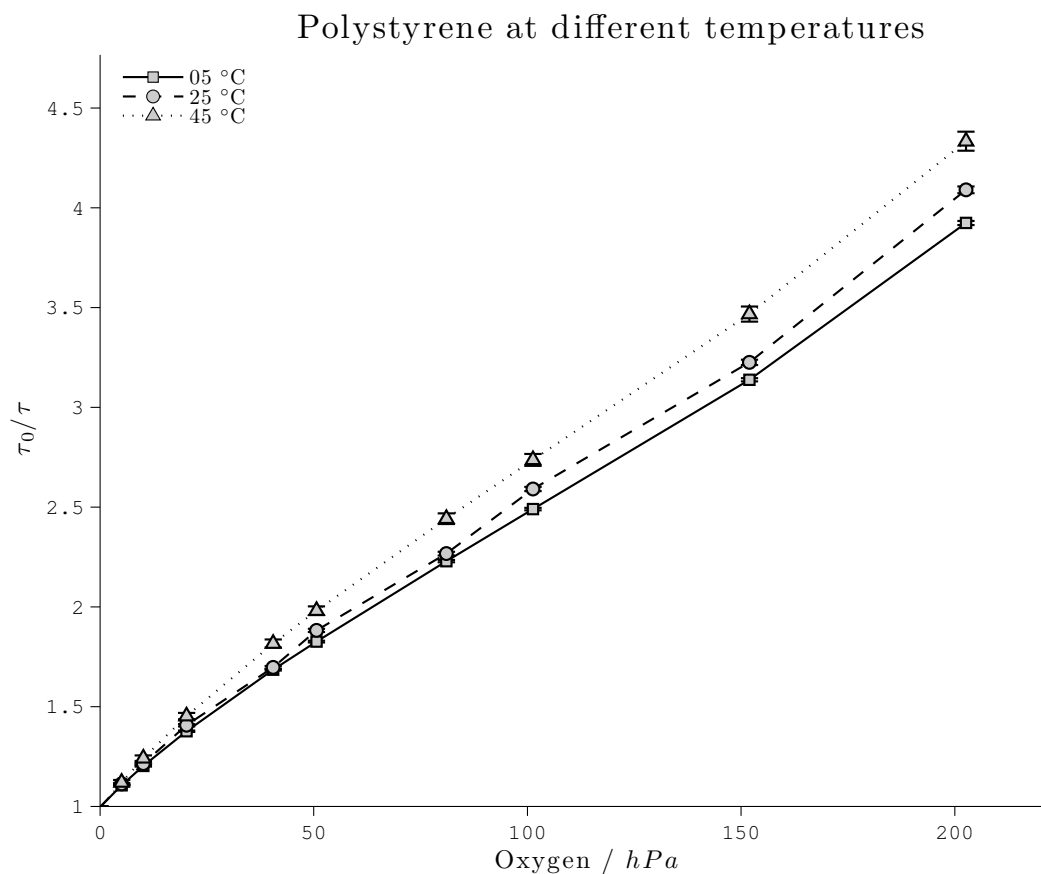
Figure 4.12: Stern Volmer plot of a sensor Pt-TPTBP with polystyrene matrix.

4.4 Initial Modifications

Now that these preliminary results are available, the next interesting step has to be how far, if at all, the permeability of these polymers could be altered by modification.

To see what impact fluorination of a polymer has, ethyl cellulose is compared to the performance of trifluoroethyl cellulose. The plots of these two polymers are compared in figure 4.13. A clear improvement can be seen and this implies that fluorination may have a positive influence on other polymers as well. The methods used are described in section 3, in the next subsections each of the modified polymers is compared to the original characterisation.But as was shown by other authors[27] also silanization can have a beneficial effect on oxygen permeability. Therefore the effects of silanization and perfluoroalkylation are compared later in this section, when both methods are used on the same polymer, namely polyphenylenoxide.
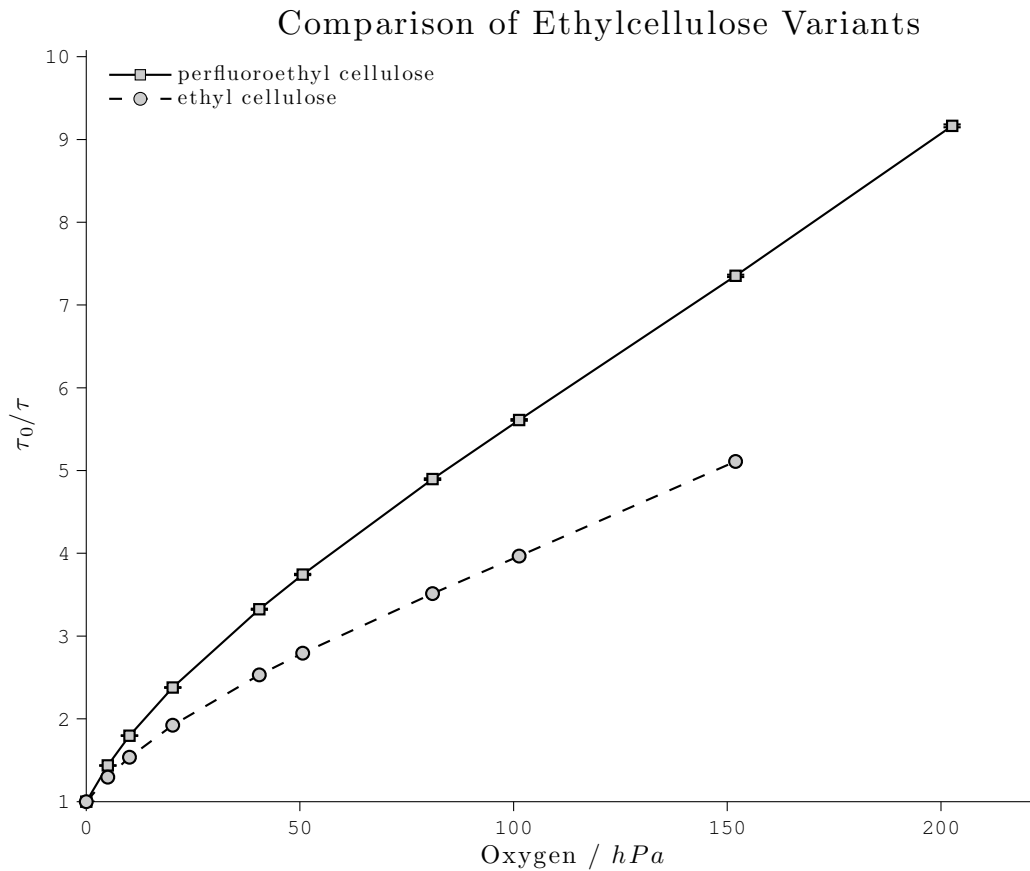
Figure 4.13: Comparison of an ethyl cellulose and trifluoroethyl cellulose sensor based on Pt-TPTBP.

4.4.1 Polystyrene

Polystyrene was modified as described in section 3. As hoped modification yielded a considerable increase in sensor sensitivity, bringing it even close to unmodified PPO. In figure 4.14 this modified version is compared to unaltered polystyrene, showing how the modified version is almost twice as sensitive.
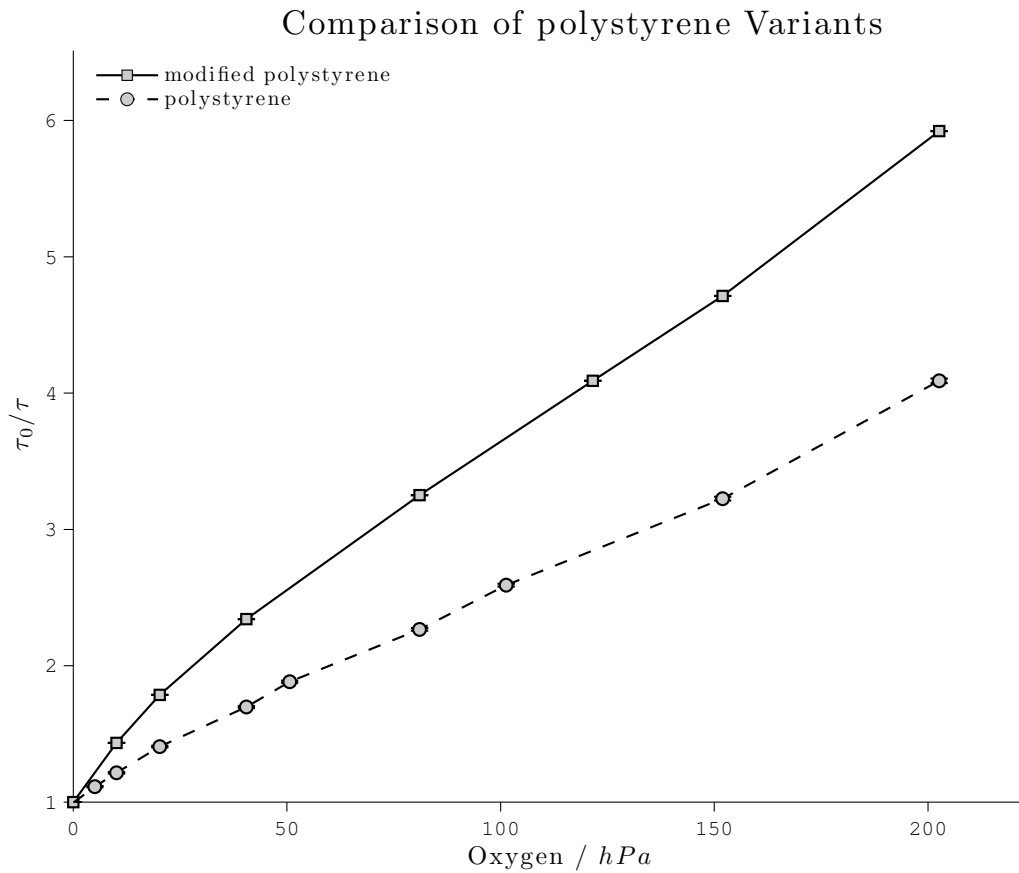
Figure 4.14: Comparison of a polystyrene and poly (perfluorobutylstyrene) sensor based on Pt-TPTBP.

4.4.2 PPO

PPO was modified using both methods independently, in order to gain further insight into the observable increase in sensor sensitivity. The results are depicted in figure 4.15. Both methods show a considerable increase, although not as drastic as with polystyrene. Even more surprising, though, both methods seem to have the almost same effect on permeability. Considering that the actual attached groups are quite different chemically this seems to indicate the permeability increase is mostly due to the steric demand of the above groups. Probably resulting from reduction of chain mobility and the subsequent disturbance of tight polymer folding. If this hypothesis is indeed correct then the introduction of even bigger substituents might further increase the permeability of the initial polymer.
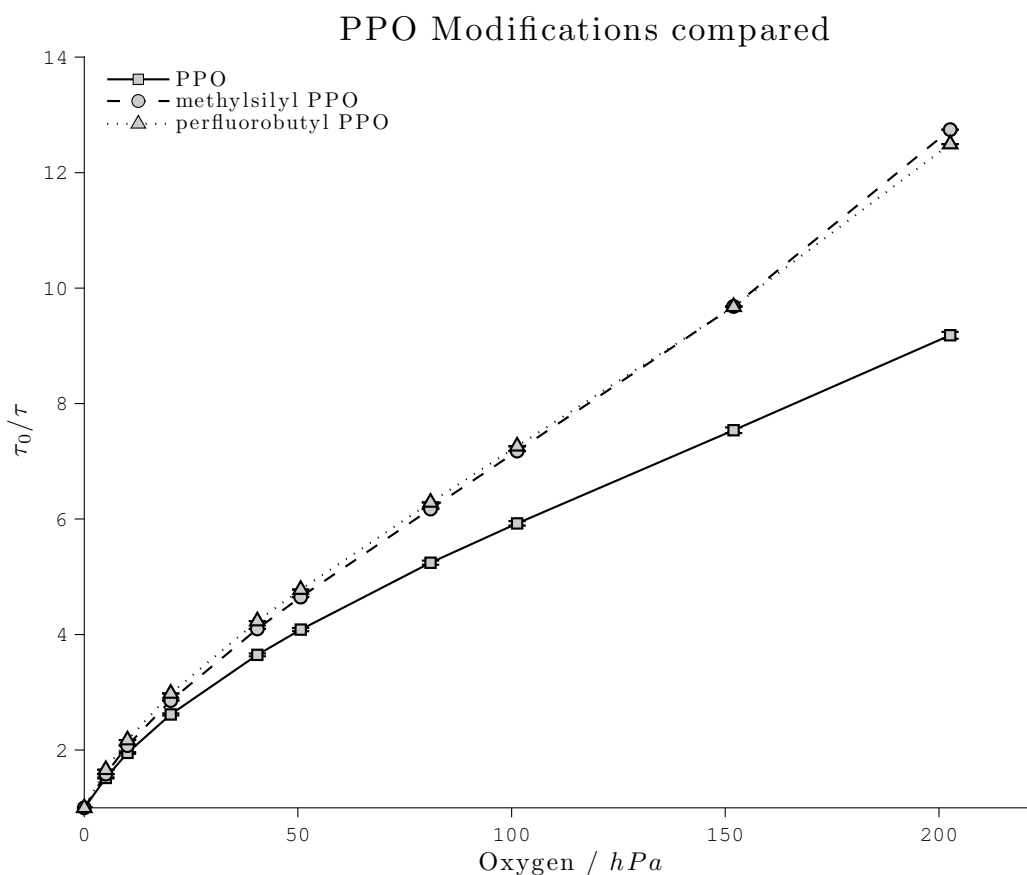
Figure 4.15: Comparison of unmodified PPO and a perfluorobutyl modified variant and a methylsilyl modified variant.

This also makes the implicit assumption that both methods have a comparable degree of substitution, which is not necessarily given and hard to prove without structure analysis - which wasn't performed in the course of this thesis. However, assuming that both methods give close to 100% substitution (meaning one substituent for each benzene) then it should still be possible to add a second substituent to a considerable amount of already modified rings in the polymer backbone. Though probably not all of them, since steric demand will invariably become a hindrance once the polymer chain gets increasingly crowded with substituents.

To find out what the reachable limits for each of the methods could be, follow-up experiments

were conducted. In the case of the perfluoroalkylation method the excess of perflourobutyrylchloride was increased and a sensor with the resulting polymer was crafted and compared to the original. As observable in figure 4.16 the increase to two equivalents did not result in a further improvement of permeability, however, an increase to four equivalents did improve the obtained results albeit only slightly suggesting that the initial modification was already close to the achieve able limit.
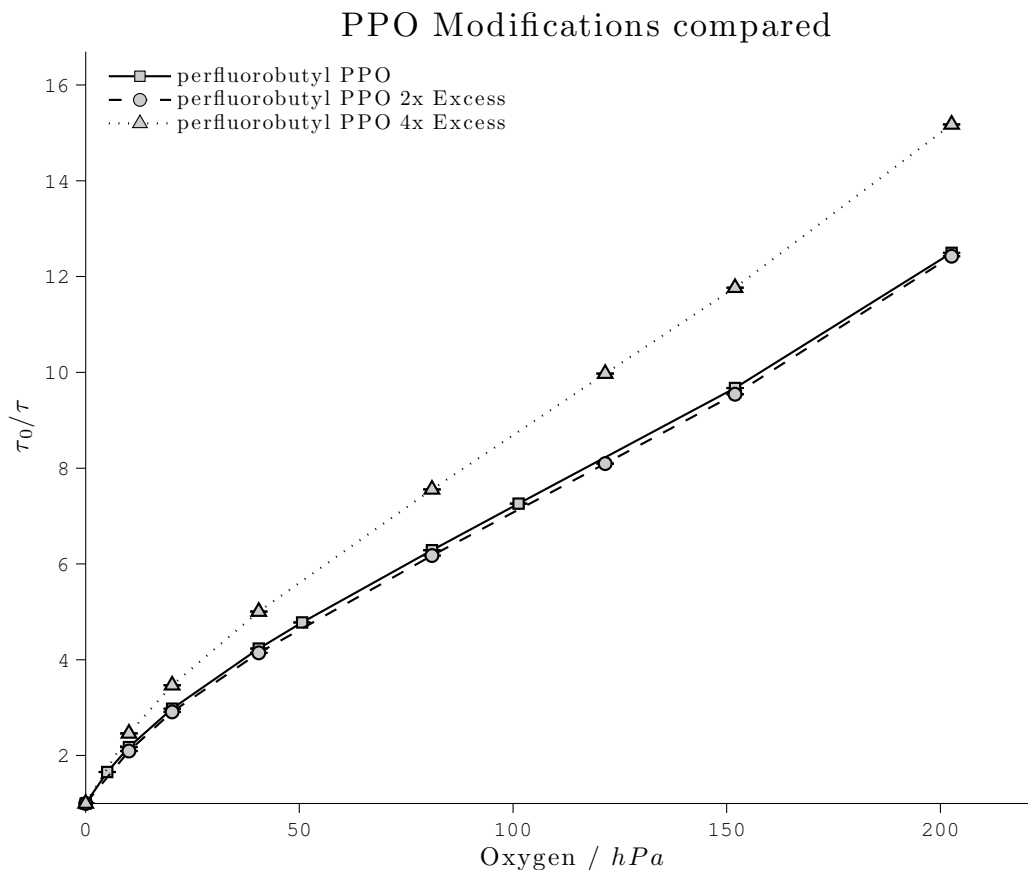
Figure 4.16: The effect of a bigger excess in the perfluorobutyl modification of PPO

In case of the methylsilanization method the reaction was performed two times in sequence with a high excess of both buthyllithium and thrimethylsilylchloride in the second reaction to achieve the same result. Figure 4.17 shows how this further modified polymer compares to the initial modified polymer with only one step of silanization. The resulting increase in sensor sensitivity is noticeably bigger compared to the perfluoroalkyl method and promises interesting results if repeated with differently substituted silanes.

PPO compared for multiple silanization
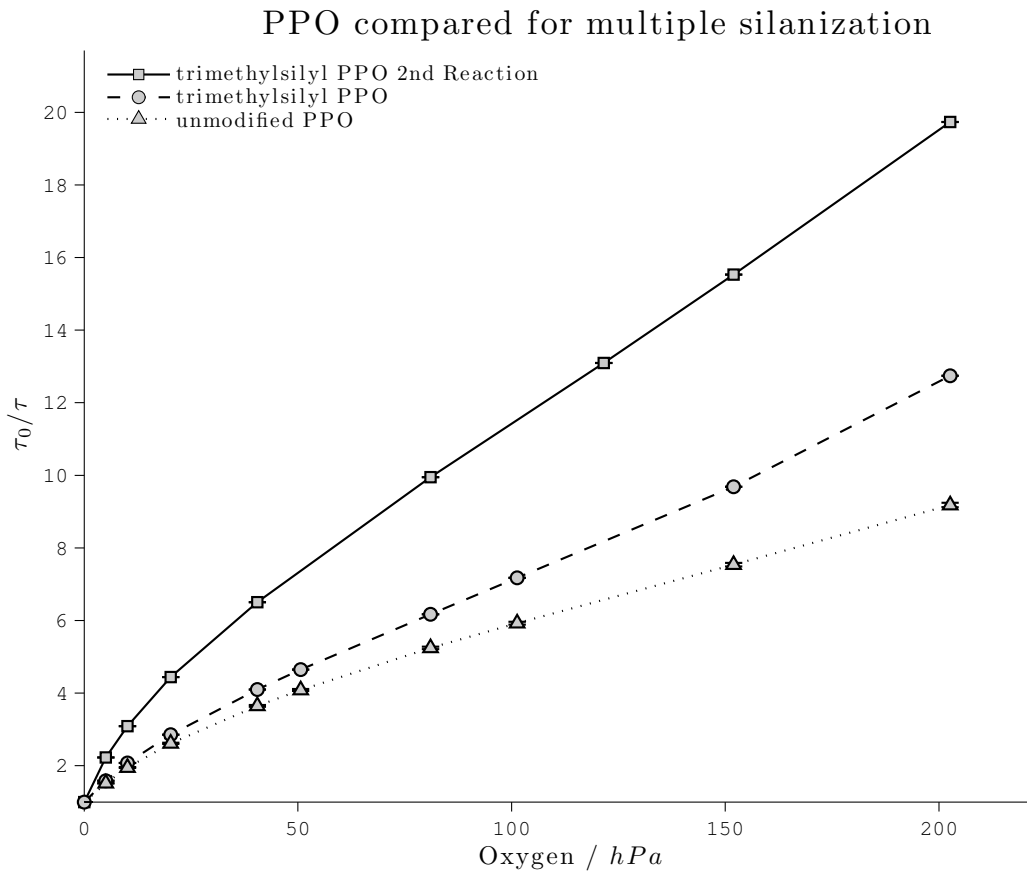
Figure 4.17: The effect of 2 sequential methylsilyl modifications on the sensitivity of the PPO matrix, the second one with a high excess of both silane and BuLi.

4.4.3 Polysulfon
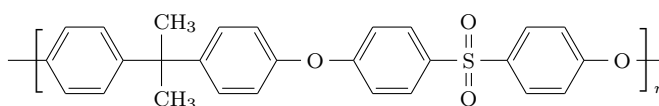
poly oxy-1,4-penylenesulfonyl-1,4-penyleneoxy-1,4-phenyleneisopropylidene-1,4-phenylene

Figure 4.18: The structure of polysulfone.

In a subsequent test polysulfone was also modified using the perfluoroalkination method to see if the effect would also be observeable in the same magnitude on a different aromatic main chain polymer. Indeed as figure 4.19 shows, though sensitivities are not comparable to those of PPO, the effect of increased permeability is still observable with polysulfone.
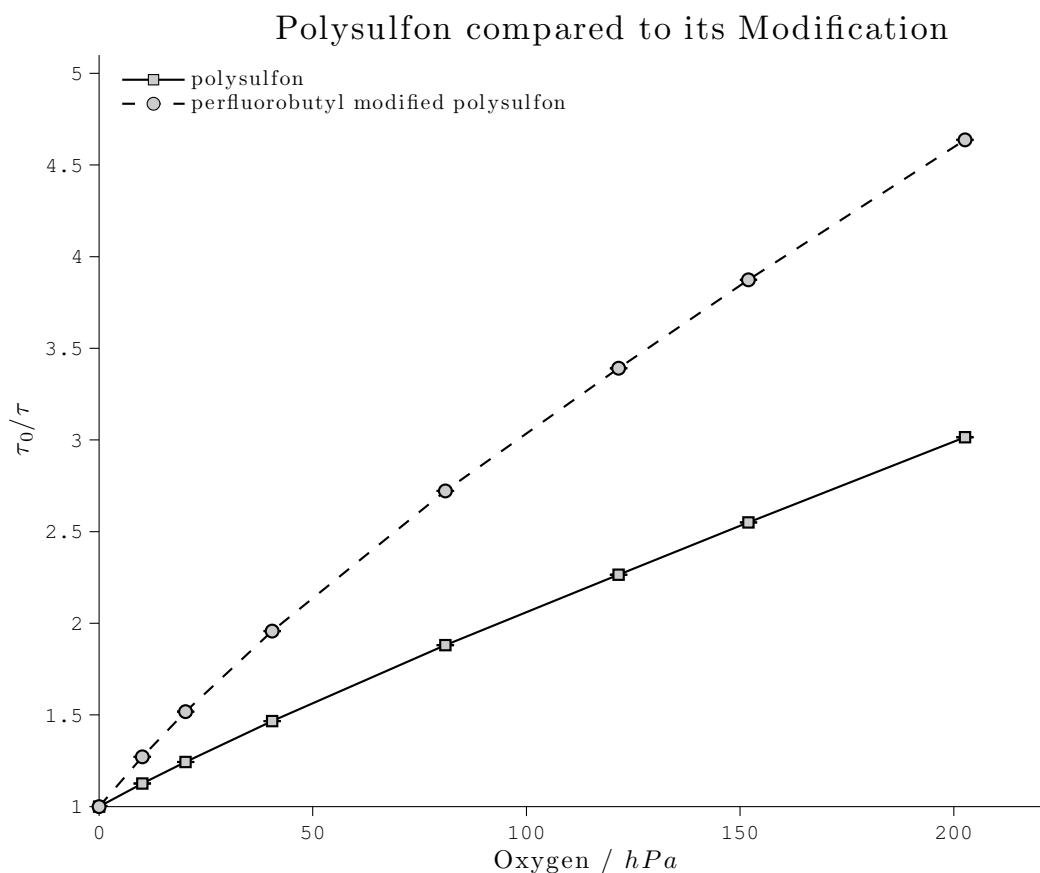
Figure 4.19: Results of a subsequent test using the perfluoroalkyl method on polysulfone to see if the same effects would be observable.

4.5 PPO Modification with bigger Substituents

After the initial positive results of PPO modifications with trimethlysilylchloride the possibility of further permeability increase through the use of bigger substituents was investigated. In

theory bigger substituents might further disturb tight packing of polymer chains and thus increase intrinsic microporosity. Four silanes with different substituents where chosen for this task, these were pictured in figure 3.3. However synthesis of the corresponding modified polymers proved to be complicated. The resulting products show extremely poor solubility and therefore separation and cleaning produced only a minimal yield. Solubility in a medium that also dissolves the dye is also mandatory in order to coat homogeneous sensor films. In the end only two of the four products could be used to obtain working sensor coatings. In the case of the nonafluorohexylsilyl modified PPO octafluorotuloene had to be used as solvent instead of chloroform to dissolve the polymer. In contrast to the results presented up to this point these two polymers were characterized using the measurement cube in anticipation of a drastic permeability increase. The actual results are presented in figure 4.20 with the first two points of unmodified PPO added for comparison. Interestingly not only was there no increase observed, but the resulting polymers both show a slight decrease in permeability. It is difficult to draw a definite conclusion, but assuming the resulting polymer was at least partially modified, which is likely, considering the changed solubility, the apparent effect would be that bigger side chains actually decrease free volume instead of creating it. If this is the case, then in future publications better results could possibly be obtained by using more rigid substituents.
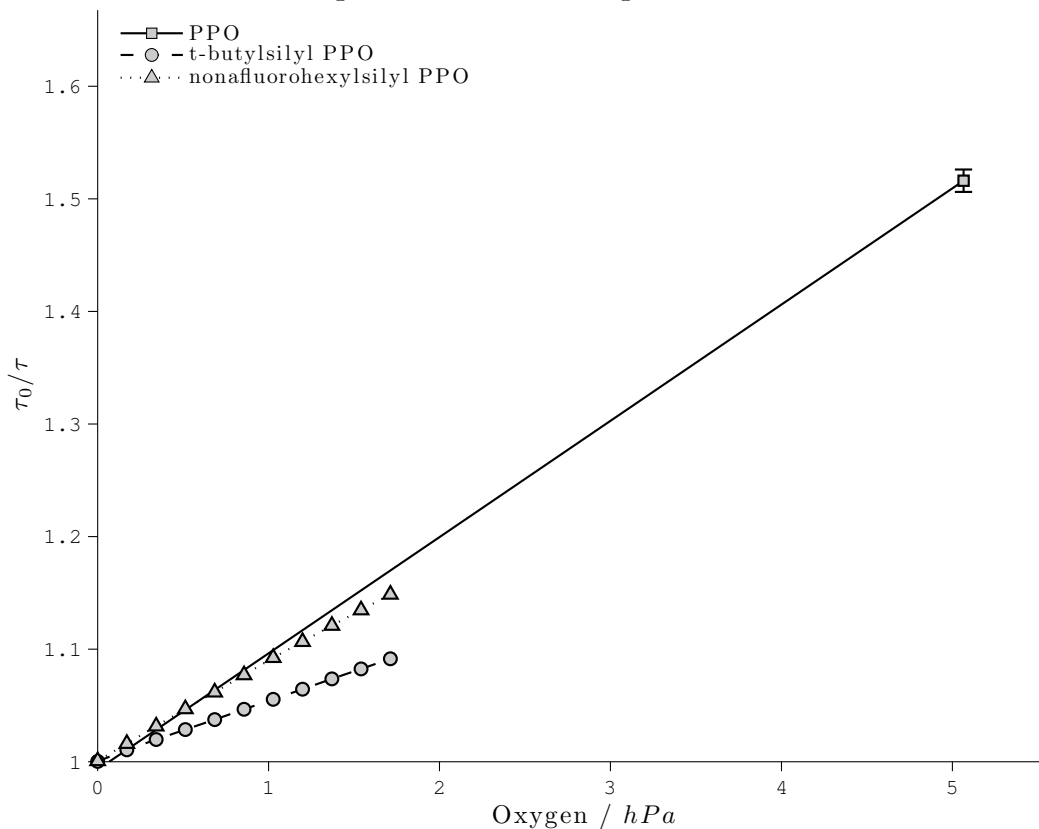
Figure 4.20: Comparing differently substituted silyl modifications with unaltered PPO.

4.6 Teflon AF
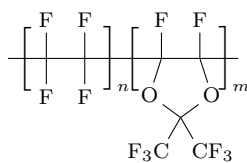
poly(tetrafluoroethene-*co*-4,5-difluoro-2,2-bis(trifluoromethyl)-1,3-dioxole

Figure 4.21: The structure of Teflon AF
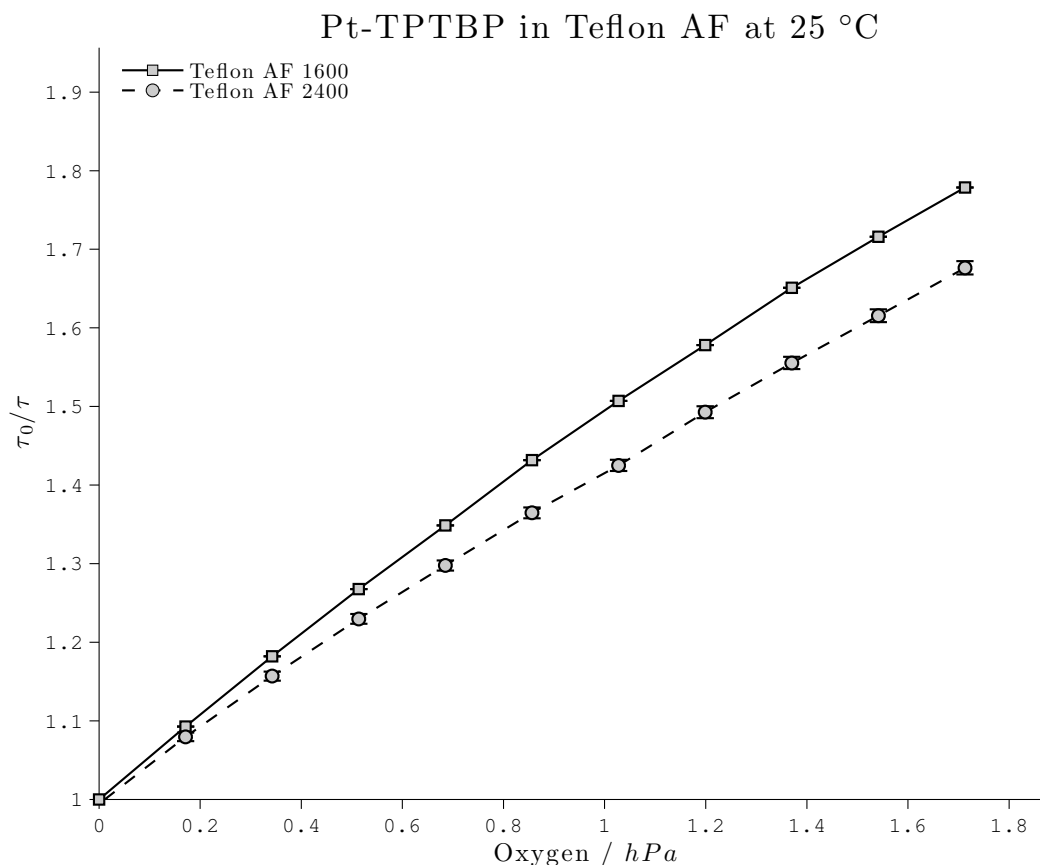
Figure 4.22: Characterization of Pt-TPTBP in Teflon AF matrices.

Teflon AF has in the past been demonstrated to display excellent oxygen permeability as well as excellent transmission in the whole visible spectrum and high chemical resistance and stability[33, p.57f]. Therefore a sensor combining a state of the art dye and this matrix is expected to perform well. The relatively low solubility even in fluorinated solvents and the low solubility for this specific dye makes creating these sensors a challenge, though.

This is the reason for the comparably low dye concentration compared to other sensors in table 2.4. The result is thicker sensor layers to achieve a somewhat acceptable signal to noise ratio. In figure 4.22 the obtained results for Pt-TPTBP in both Teflon AF 1600 and Teflon AF 2400 are shown. While the oxygen permeability of Teflon AF 2400 is approximately three

times as high as that of Teflon AF 1600, the results fail to convey that difference to actual sensor sensitivity. The same can be said about the Pd-TPTBP sensor shown in figure 4.23. Both sensors suffer from bad dye solubility, especially in Teflon AF 2400. Both sensors are comparable in sensitivity magnitude to the corresponding Silica Gel sensors presented in the next section (see table 4.3 for comparison).
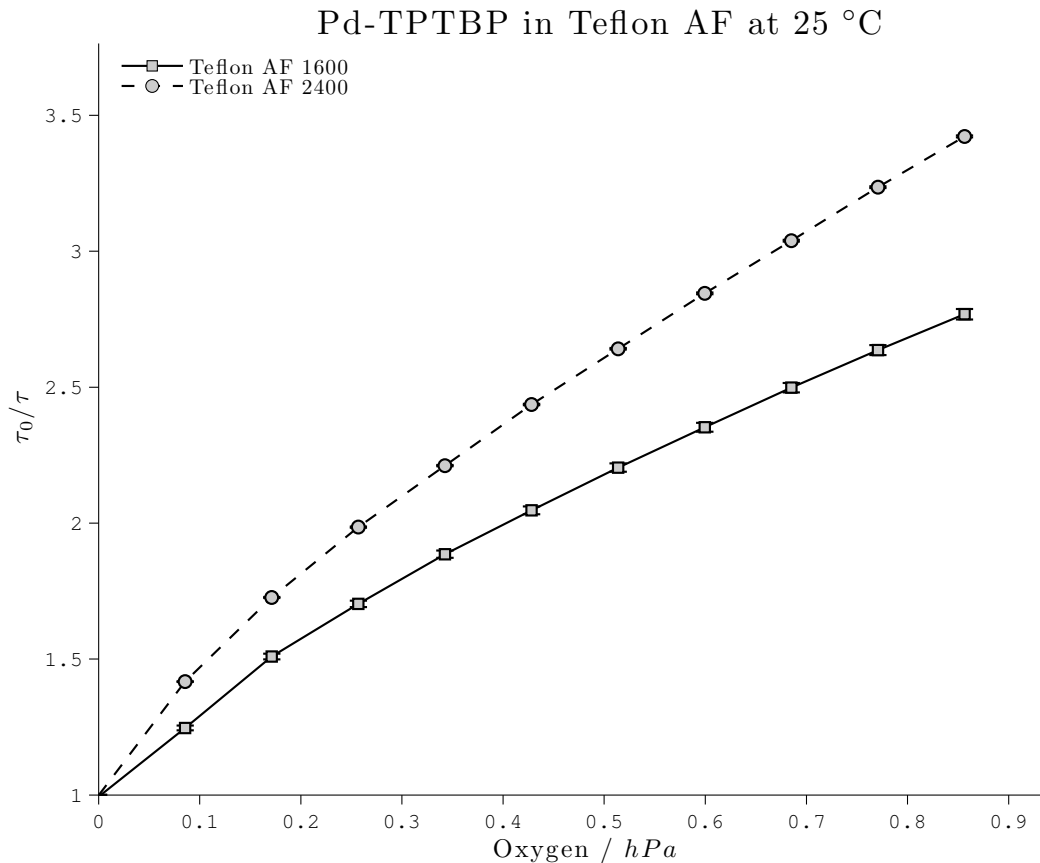
Figure 4.23: Characterization of Pd-TPTBP in Teflon AF matrices.

4.7 Silica Gel Sensors

The results presented in this section have also been published in Analytica Chimica Acta 2011 vol. 690[34]. A novel and interesting approach for designing tracescale oxygen sensors is the covalent immobilisation of the oxygen quenchable dye on the surface of silica gel particles. These dye doped particles where obtained as described in section 3.4.

4.7.1 Oxygen Consumption Effect

One argument often quoted in favour of optical sensors is that they do not consume the analyte. This need not always be true though, if approaching trace values of oxygen the normally negligible consumption of oxygen due to the photochemical reaction starts to gain significance. Under ideal circumstances the singlet oxygen species return to their ground state in the millisecond time domain. The exact time may depend largely on the surrounding medium and if physical transfer of energy is easily possible. However, there is a second mechanism of deactivation: through chemical reaction. Singlet oxygen is known for its high reactivity and readily oxidises dye, matrix molecules or impurities if they are prone to oxidation.
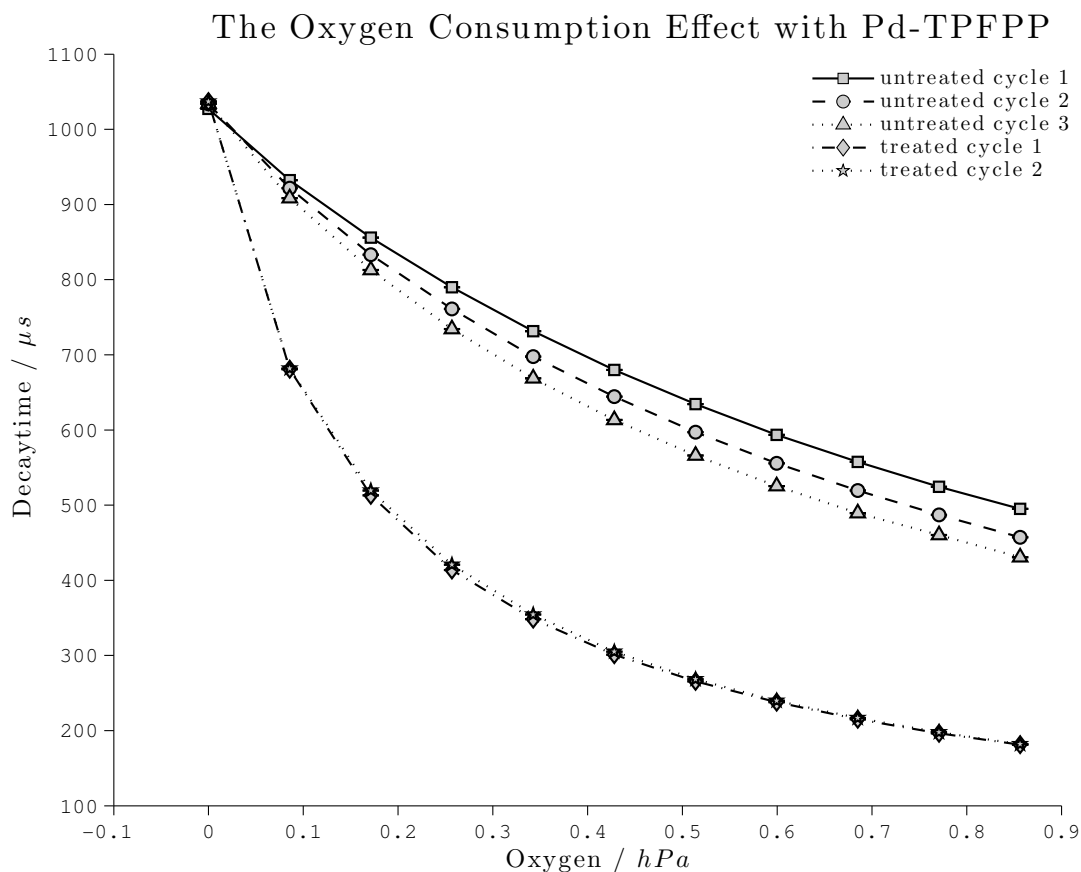
Figure 4.24: The influence of continued exposure on the apparent sensitivity of the end-capped Pd-TPFPP Silica Gel sensor.

This effect is most of the time barely noticeable due to the high excess of oxygen in direct vicinity of the dye molecules. It is merely perceived indirectly as oxidation alters matrix properties and dye functionality and is therefore a part of the normal sensor ageing process. However, if trace levels are reached the consumption of oxygen due to chemical reactions has a noticeable effect on the already low concentration of oxygen in dye vicinity. In this special case photochemical conversion of oxygen and subsequent removal quickly depletes oxygen in the matrix and oxygen concentration in the matrix is determined to an increasing part by diffusion rather than actual concentration in the medium. As more parts of the matrix have already reacted and are therefore not available for further oxidation, the likelihood of singlet

oxygen returning to its ground state increases and so does the concentration of oxygen in dye vicinity. This manifests itself in measurements as an observed "reverse bleaching", meaning the sensor appears to become more sensitive with each subsequent measurement cycle. This can be seen in figure 4.24 where an end-capped version of the Pd-TPFPP Silica Gel sensor was measured with and without vacuum treatment. Possibly due to an oxidizeable residue, that was pre-emptively removed in the preparation of the second sensor, the first untreated sensor showed the above mentioned increase in apparent sensitivity. Which, if left to condition under high light intensities, would probably have reached the sensitivity of the treated sensor.

Generally this effect can be avoided if the sensor matrix is completely stable in the presence of singlet oxygen. But even if this is not the case, the effect can be minimised by reducing light intensity and exposure times. This approach is of course limited by the need to achieve good signal to noise ratios.
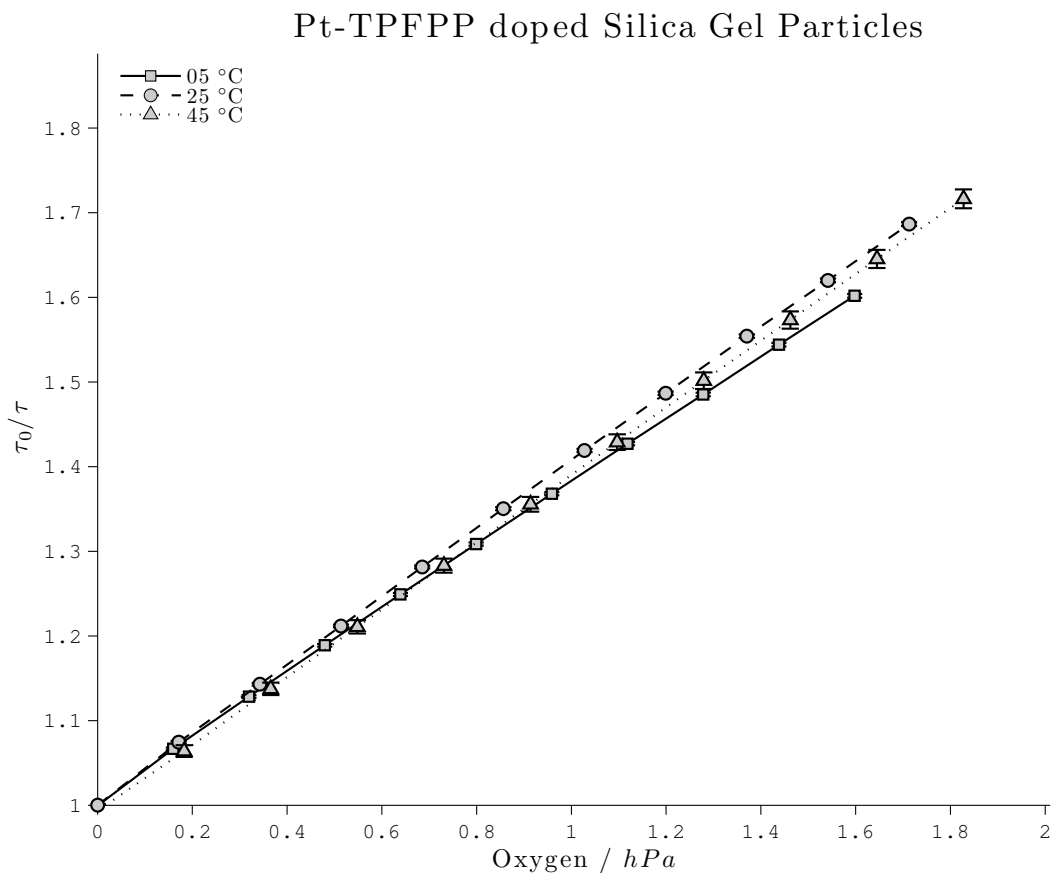
Figure 4.25: The Pt-TPFPP Silica Gel sensor calibrated at different temperatures

4.7.2 Properties

In figure 4.25 the calibration for the Pt-TPFPP Silica Gel sensor at various temperatures can be seen. The first obvious difference to sensors characterized in previous sections is the perfect linearity of these sensors. This enables the determination of K_{SV} values with a simple linear fit and more importantly sensor calibration with only two points of data. This linearity is in clear contrast to other polymer matrix based sensors where formation of multiple domains

and resulting non linearity is commonly observed. This special linearity is accredited to high homogeneity in dye environment in the Silica Gel sensor, which is a direct result of the covalent attachment of the dye to the particle surface. It is also easy to imagine how dye agglomeration is made impossible by the covalent attachment.

Furthermore if one compares the sensitivities of this sensor to previously discussed ones the sensitivity of this sensor is well above even that of Pd-TPTBP in *t*-butyl styrene (fig. 4.1). So, if instead of the platinum dye the palladium dye is used, the sensor is expected to further increase its sensitivity. This Pd-TPFPP Silica Gel sensor is characterized in figure 4.26.
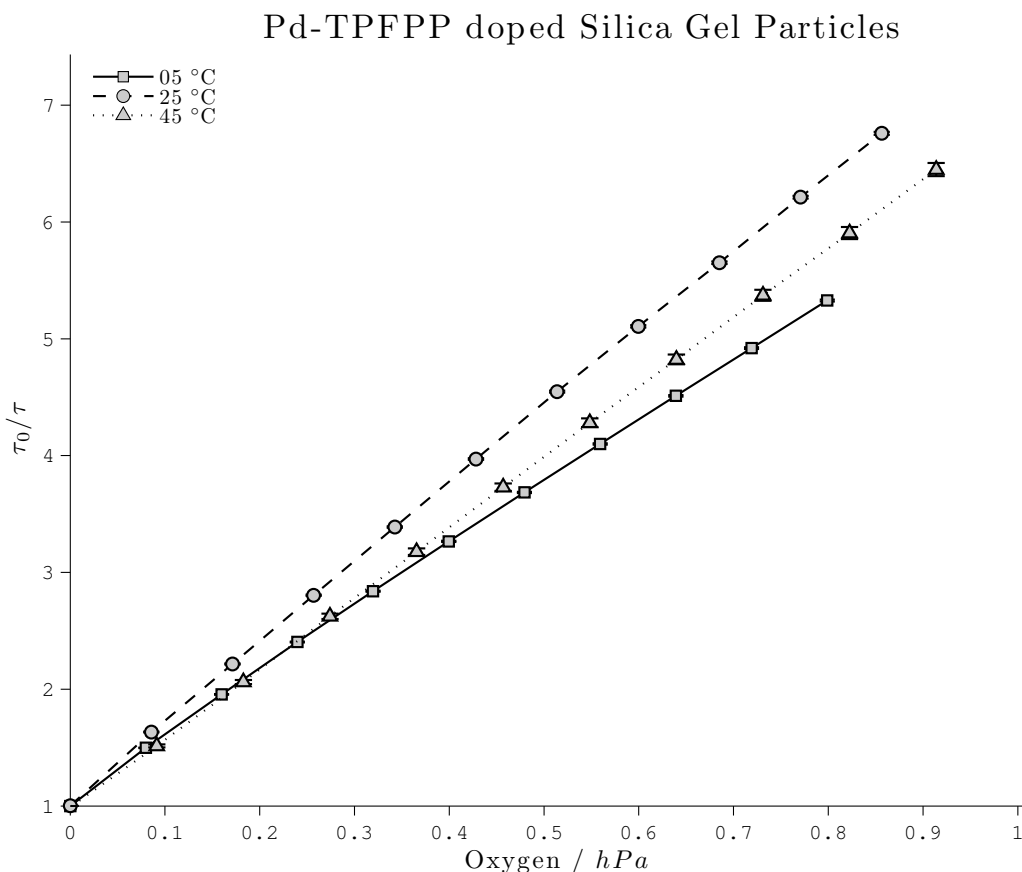
Figure 4.26: The Pd-TPFPP Silica Gel sensor calibrated at different temperatures

Interestingly the temperature dependence of this sensor behaves differently than other sensors. It is common for optical oxygen sensors to show thermal quenching. Still for most polymer sensors, sensitivity increases with increasing temperature despite thermal quenching of the dye, mostly due to increased oxygen diffusion. But permeability is determined not only by the oxygen diffusion coefficient, but also the solubility, which can decrease as oxygen desorption increases due to thermal activity. The combination of this variable contribution of thermal quenching, diffusion increase and solubility decrease can have the effect of reversed temperature dependence of K_{SV} and can evidently also lead to the situation in figure 4.26 where K_{SV} has a its maximum value at a certain temperature.

Another effect observed is the increased decay time under non quenching conditions, τ_0 of the dyes is perceptibly higher in silica gel than in polystyrene as seen in table 4.2. This is probably due to reduced probability of non luminescent exited state deactivation because of the covalent

link and resulting reduced mobility of the dye. Also with the high excess of amino linker on the surface it is likely that some dye molecules are attached to the surface by more than one linker, which would further increase this effect.

Dye	Decaytime / μs	
	polystyrene	silica gel
Pt-TPFPP	56	73
Pd-TPFPP	930	1023

Table 4.2: The increased dye decay times covalently bound to silica gel particles compared to immobilization in polystyrene.

4.7.3 Response Time
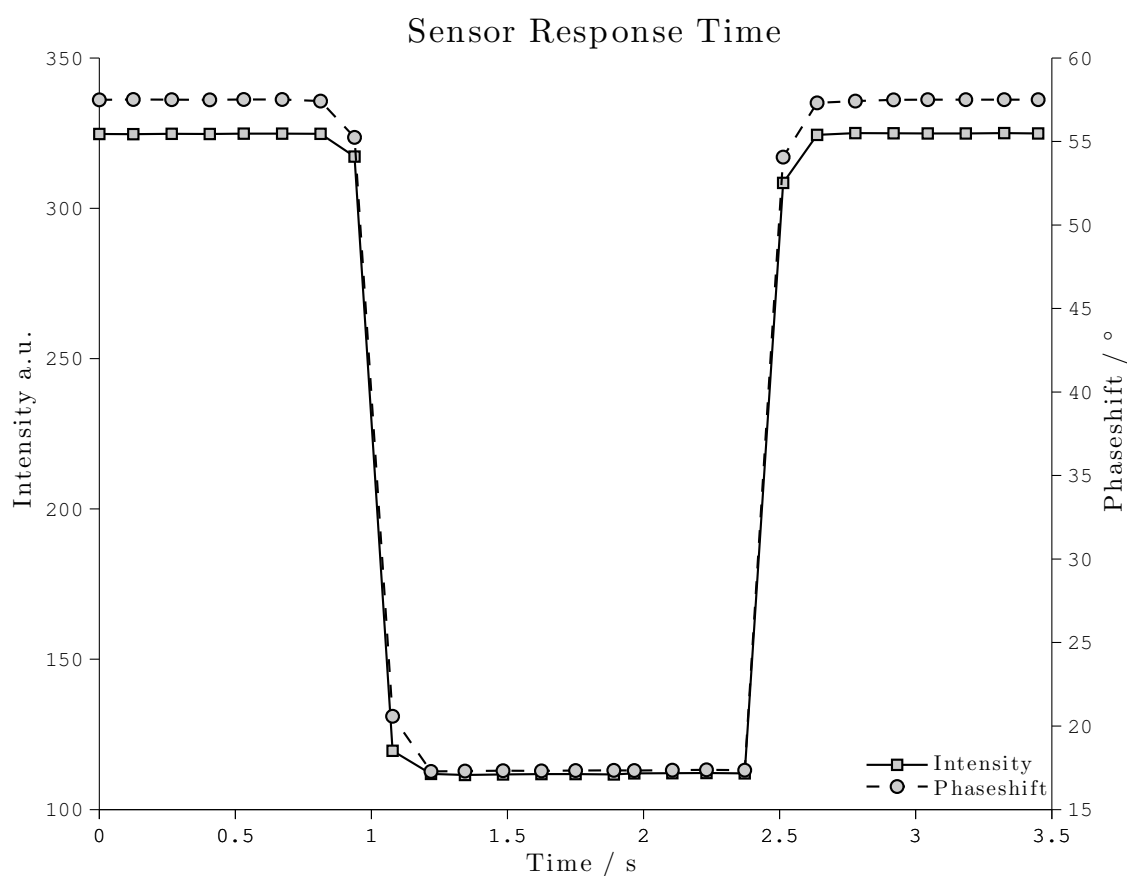
Figure 4.27: Real time measurement showing the response time of a silica gel based sensor.

In figure 4.27 the real time response can be seen for the change from $0\,\%$ to $1\,\%$ oxygen and vice versa. From these data a response time of 150 ms can be estimated. This is faster than other common oxygen sensors and means that the sensor responds virtually in real time. However, two things have to be considered. Firstly, the observed response time also includes

the amount of time it takes to reach a new equilibrium in the gas test chamber. Secondly, if the sensor is supplied for underwater measurement, response times will be much slower probably because of the slower equilibrium between liquid phase and the gas phase in the silica pores. It is, however, not trivial to directly measure response times under water since there is no reliable way to instantly oxygenate or deoxygenate a specific amount of water.
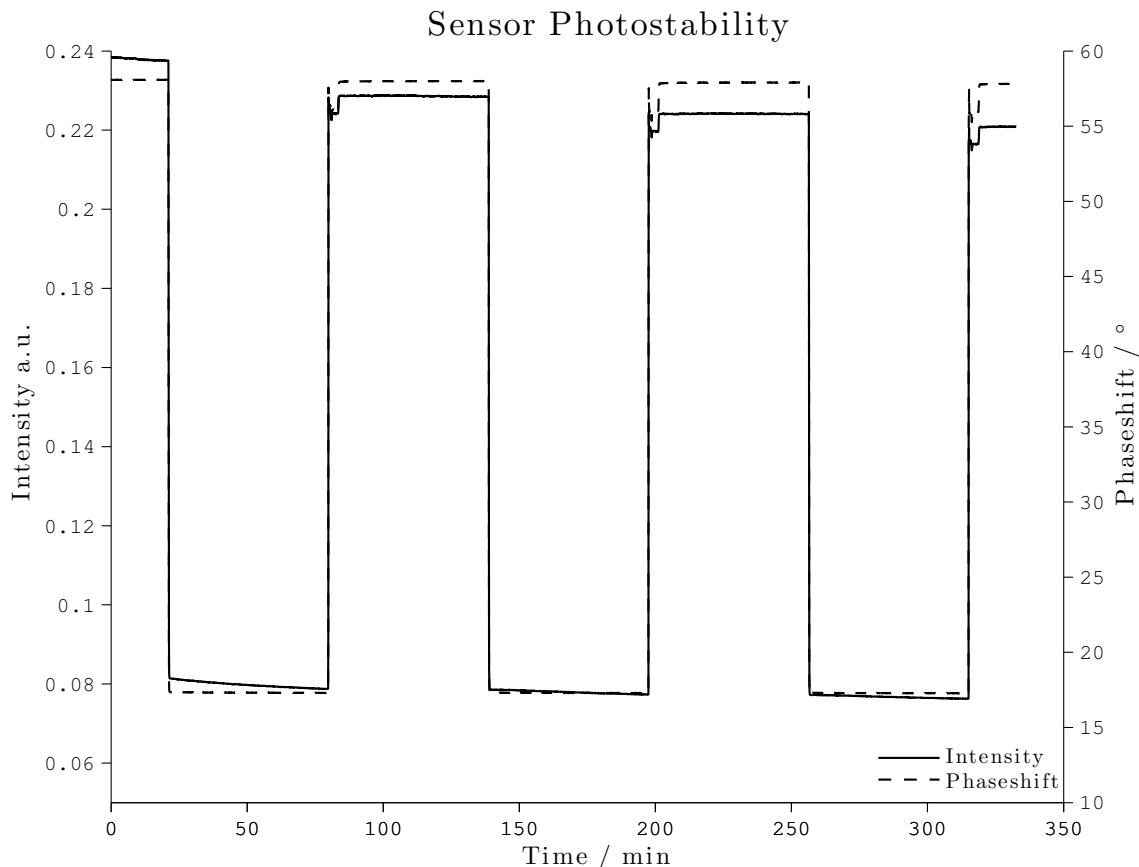
Figure 4.28: The stability of the Pd-TPFPP Silica Gel sensor under continuous irradiation of a 405 nmLED

4.7.4 Photo Stability

In the laboratory the sensors proved to be stable for at least two months when stored in the dark under ambient conditions, which is not surprising considering the high photostability of the used dye[32]. But equally if not more important than storage stability is stability under measurement conditions. Figure 4.28 shows how the sensor performs under continuous radiation of a 405nm LED. Under normal measurement conditions, 0.1 s of irradiation is in general enough to obtain a data point. This means that one hour of continuous irradiation equals the acquisition of 36000 data points, or 100 hours of data points every 10 seconds. As can be seen in the figure the intensity loss over one hour is as low as 2 % to 5 %, while the decay time is even more stable with only 0.1 % h^{-1}. This means that recalibration should not be necessary during normal use.
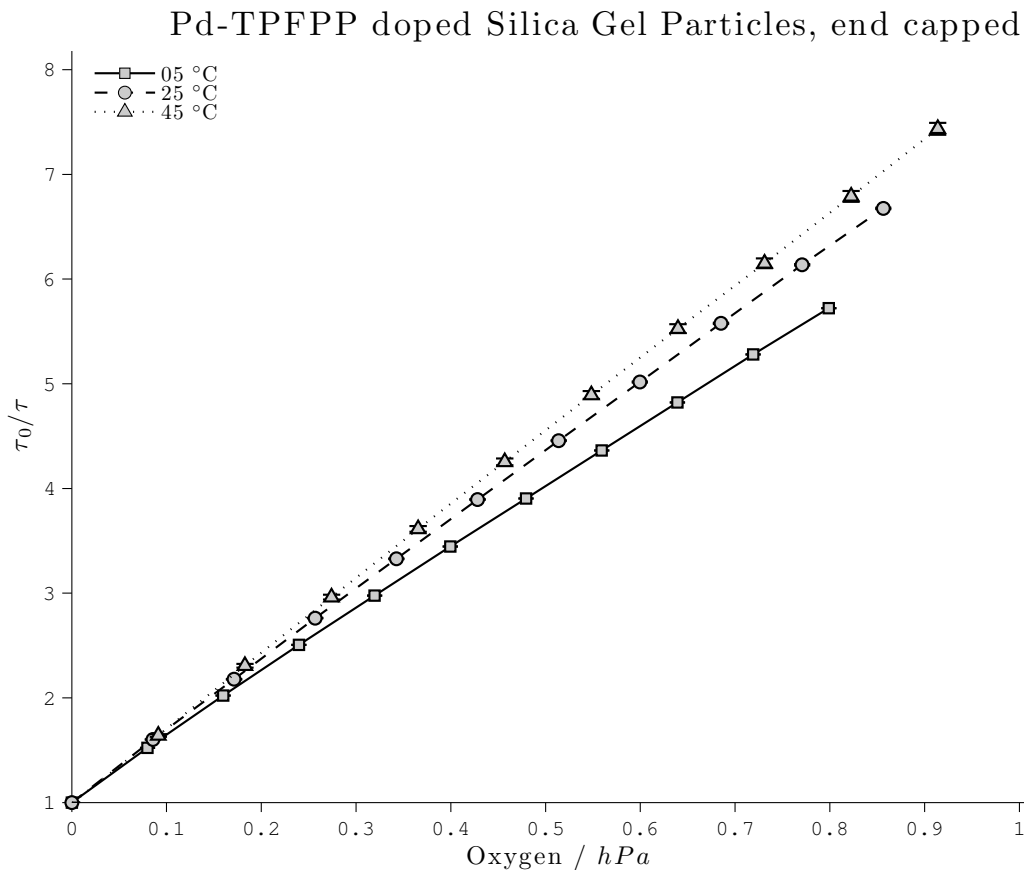
Figure 4.29: Characterization of the end capped Pd-TPFPP sensor.

4.7.5 Performance under Humidity

In figure 4.29 one can see the characterization at different temperatures for the end capped Pd-TPFPP sensor. Interestingly the temperature dependence anomaly is not observed with this end capped version. Possibly because the fluorinated particle surface reduces oxygen adsorption and reduces its influence on temperature dependence. The reason of performing this "end capping" was a different though. It was hoped that the cross sensitivity to humidity would be reduced if the surface was made more hydrophobic. End capping didn't alter the performance under humidity. In figure 4.30 it is clear that the sensor has around 5 % reduced sensitivity under 100 % humidity as compared to dry gas. In the insert a two point calibration under water is compared to the other two measurements showing no significant deviation. However, cross talk to humidity could maybe be further reduced by bigger substituents used for end-capping. It is important to note that even if this sensor is working in water under lab conditions, due to its intrinsic porosity it is unclear how the sensor performs under high pressure at deep sea levels. Pressure change of a possible gaseous phase inside the pores may have an unpredictable influence on the sensor calibration.
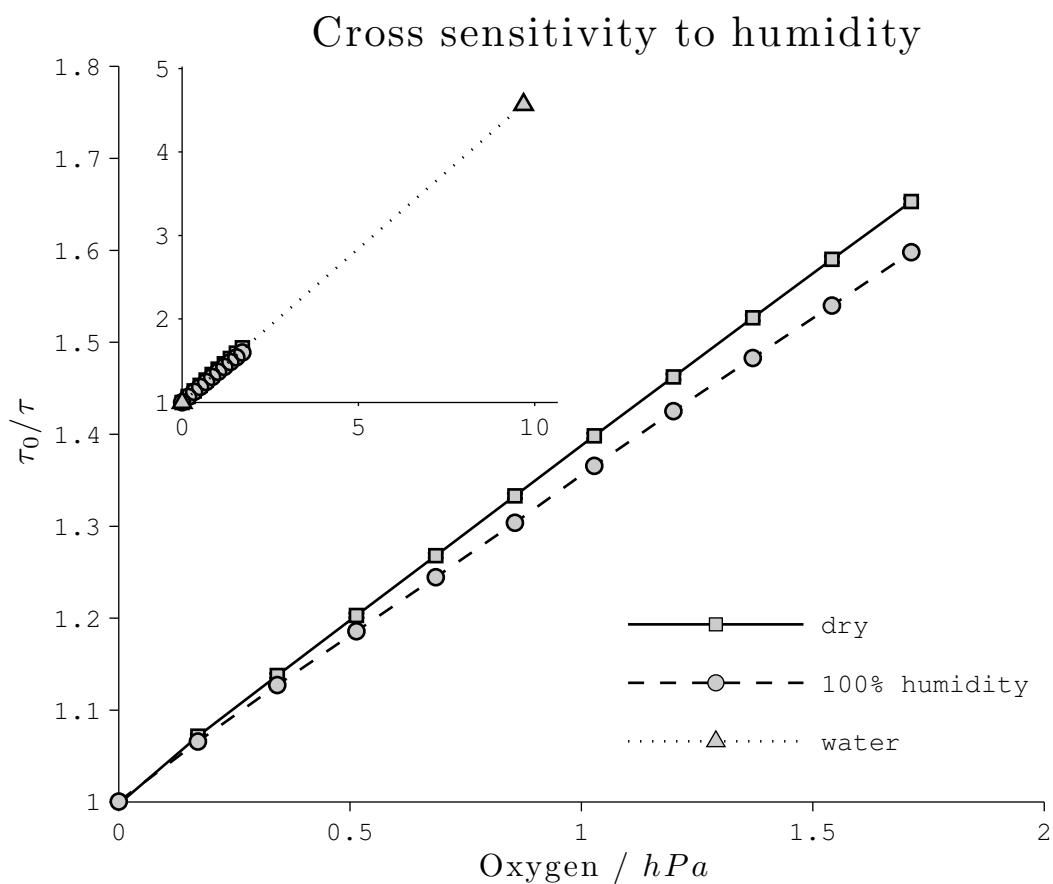
Figure 4.30: The cross sensitivity to humidity of the end-capped Pd-TPFPP Silica Gel sensor.

4.8 Comparing Results

In table 4.3 the characteristics for all measured sensors are compiled. Presented K_{SV} values were obtained either by a two site model fit (see section 1.1.5) or linear fit in the case of silica gel based sensors. Error values were only given for measurement with a statistically relevant data set size. R^2 values are not shown due to size constraints, but are higher than 0.98 for all fits.

Dye	Matrix	T / °C	K_{SV1} / hPa^{-1}	K_q / Pa^{-1}s^{-1}	f
		05	$0.0441 \pm 6.5 \cdot 10^{-5}$	7.1	0.95
Pt-TPTBP	EC	25	$0.0471 \pm 5.9 \cdot 10^{-5}$	9.1	0.91
		45	$0.0480 \pm 1.0 \cdot 10^{-4}$	7.8	0.94
Pt-TPTBP	F$_3$ EC	25	$0.0617 \pm 1.8 \cdot 10^{-4}$	13	0.96
		05	$0.0877 \pm 2.4 \cdot 10^{-4}$	19	0.88
Pt-TPTBP	Ormosil	25	$0.1296 \pm 3.9 \cdot 10^{-3}$	29	0.88
		45	$0.1898 \pm 6.1 \cdot 10^{-4}$	43	0.88
		05	$0.0167 \pm 1.2 \cdot 10^{-4}$	3.2	0.96
Pt-TPTBP	PS	25	$0.0173 \pm 2.0 \cdot 10^{-4}$	3.4	0.97
		45	$0.0204 \pm 5.8 \cdot 10^{-4}$	4.0	0.95
Pt-TPTBP	perfluoropropyl PS	25	0.0336	5.9	0.95
Pd-TPTBP	poly-t-butylstyrene	25	$0.2914 \pm 1.8 \cdot 10^{-3}$	8.0	0.65
		05	$0.0779 \pm 3.5 \cdot 10^{-4}$	15	0.95
Pt-TPTBP	PPO	25	$0.0764 \pm 7.7 \cdot 10^{-4}$	15	0.95
		45	$0.0752 \pm 9.4 \cdot 10^{-4}$	15	0.95
Pt-TPTBP	perfluorobutyl PPO 4x	25	0.0987	18	0.97
	trimethylsilyl PPO 2x	25	0.1416	25	0.98
		05	0.0325	5.4	0.84
Pt-TPTBP	PTFEMA	25	$0.0362 \pm 1.6 \cdot 10^{-4}$	6.2	0.84
		45	$0.0366 \pm 6.6 \cdot 10^{-4}$	6.3	0.85
Pt-TPTBP	polysulfone	25	0.1416	25	0.98
	(CH$_3$)$_3$Si polysulfone	25	0.1416	25	0.98
Pt-TPTBP	Teflon AF 1600	25	0.6904	141	0.80
	Teflon AF 2400	25	$0.5704 \pm 3.1 \cdot 10^{-2}$	167	0.81
Pd-TPTBP	Teflon AF 1600	25	$3.716 \pm 8.6 \cdot 10^{-2}$	91	0.83
	Teflon AF 2400	25	$5.109 \pm 1.4 \cdot 10^{-2}$	139	0.87
		05	$0.378 \pm 2 \cdot 10^{-3}$	52	-
Pt-TPFPP	silica gel	25	$0.423 \pm 1.9 \cdot 10^{-2}$	59	-
		45	$0.40 \pm 6 \cdot 10^{-2}$	62	-
		05	$0.380 \pm 6 \cdot 10^{-3}$	50	-
Pt-TPFPP	silica gel end-capped	25	$0.374 \pm 9 \cdot 10^{-3}$	53	-
		45	$0.386 \pm 4 \cdot 10^{-3}$	60	-
		05	5.34 ± 0.11	52	-
Pd-TPFPP	silica gel	25	6.82 ± 0.11	70	-
		45	5.92 ± 0.22	65	-
		05	5.95 ± 0.02	57	-
Pd-TPFPP	silica gel end-capped	25	6.71 ± 0.05	68	-
		45	7.18 ± 0.03	78	-

Table 4.3: A summary of characteristic properties of all sensors calibrated in the course of this thesis. The factor f is only applicable for sensors that were fitted using a two site model. If no error is given the dataset was not big enough to perform statistics. R^2 values are not shown, but are above 0.98 for all fits.

5 Conclusion and Outlook

In this thesis it has been shown that there are a number of promising polymer matrices for the development of trace oxygen sensors. A measurement device was also constructed to reliably calibrate oxygen concentrations in the range of 0.05 hPa to 5 hPa pO_2, with even lower concentrations achievable if 1 % test gas is used instead of air for metering. This device can be temperature controlled and is fully automated if connected to a PC.

It was also displayed that modification of polymer matrices is a viable way of increasing permeabilities and subsequently sensor sensitivity. For example PPO modification yielded some promising results and most other matrices also showed an increase in sensitivity due to modification. Further, Teflon AF Matrices displayed excellent oxygen permeabilities even if problems with dye solubility still remain to be solved. Still, Teflon AF is the polymer based matrix with the highest oxygen permeability in this thesis but the high cost might be restrictive for some applications.

The silica gel based sensors presented in this work have a high linearity, owing to the high homogeneity introduced through covalent dye coupling. They also display excellent sensitivity with a limit of detection as low as 0.3 Pa and 0.02 Pa in gas phase, for the platinum and palladium based sensors respectively. Therefore they are the most sensitive sensors in this thesis. Furthermore, their response times are comparably fast and they feature high photo stability. The photo stability is of course a characteristic largely attributed to the dyes and is conclusively also very good for all other sensors in this thesis (none of the presented matrices are known to suffer from fast photo degradation).

Silica gel sensors are highly suitable for different tasks and it has been shown that they are also usable for measuring dissolved oxygen, even without end-capping. Both silica gel and Teflon AF sensors are well suited for application in breweries, boilers and marine research. But, because of the porous nature of silica gel, a change in hydrostatic pressure might have undesired effects on the calibration because of compression of a gas phase inside the silica pores. So Teflon AF based sensors might be the better choice for deep sea measurements until the stability of silica gel based sensors is verified in a pressure chamber. But for other areas silica gel based sensors should be preferred because of their easier calibration and lower cost.

5.1 Outlook

There are multiple interesting angles for approaching future sensors that reach even lower concentrations of oxygen. Teflon AF matrices already provide excellent oxygen permeability and future use of dyes that are modified with fluorinated side chains will increase dye solubility and therefore also linearity and sensor brightness. The resulting sensors might even show slightly higher sensitivity. Especially Teflon AF 2400 is suspected to perform even better once a matching dye is incorporated.

Silica gel sensors have both excellent linearity and sensitivity. While further improvement of the matrix is unlikely to dramatically increase the sensitivity, the approach of covalently coupling dyes to a particle surface or matrix has been used in other fields and might also be interesting for

trace oxygen sensors, namely they decrease solubility and aggregation problems in conventional polymer matrices and therefore make calibration curves more linear and subsequently calibration easier and also help overcome dye solubility problems.

Sensors based on modified PPO matrices may never reach the highest sensitivities. But their low cost compared to sensor matrices with higher permeabilities like Teflon AF, can make them viable for sensors that do not require the extremely low detection limits of above mentioned Teflon AF based sensors. And, if modifying other polymers with rigid main chains, further increase in intrinsic free volume and consequently permeability might be possible.

There is still a lot of room for improvement in this field of research as the search for even more sensitive sensors continues and newer and better matrices and dyes are about to be developed.

6 References

[1] Kazuo Tanno. "An Automatic Recording Analyzer for the Determination of Dissolved Oxygen in Boiler Feed Water". In: *Bulletin of the Chemical Society of Japan* 37.6 (Feb. 1964), pp. 804–810.

[2] C Huber, TA Nguyen, C Krause, H Humele, and A Stangelmayer. "Oxygen Ingress Measurement into PET-bottles using Optical-Chemical Sensor Technology". In: *Brewing Science - Monatschrift für Brauwissenschaften* 60 (Nov. 2006), pp. 5–15.

[3] N P Revsbech, L H Larsen, J Gundersen, T Dalsgaard, O Ulloa, and B Thamdrup. "Determination of ultra-low oxygen concentrations in oxygen minimum zones by the STOX sensor". In: *Limnol Oceanogr Methods* 7 (2009), pp. 371–381.

[4] Elena Zaikova, David A Walsh, Claire P Stilwell, William W Mohn, Philippe D Tortell, and Steven J Hallam. "Microbial community dynamics in a seasonally anoxic fjord: Saanich Inlet, British Columbia". In: *Environmental Microbiology* 12.1 (Jan. 2010), pp. 172–191.

[5] S Nagl, C Baleizão, and SM Borisov. "Optical Sensing and Imaging of Trace Oxygen with Record Response". In: *Angewandte Chemie* 46 (2007), pp. 2317–2319.

[6] Carlos Baleizão, Stefan Nagl, Michael Schäferling, Mário N Berberan-Santos, and Otto S Wolfbeis. "Dual Fluorescence Sensor for Trace Oxygen and Temperature with Unmatched Range and Sensitivity". In: *Analytical Chemistry* 80.16 (Aug. 2008), pp. 6449–6457.

[7] Y Amao and T Miyashita. "Novel optical oxygen sensing material: platinum octaethylporphyrin immobilized in a copolymer film of isobutyl methacrylate and tetrafluoropropyl methacrylate". In: *Reactive and Functional Polymers* 47 (2001), pp. 49–54.

[8] Y Amao, K Asai, and T Miyashita. "Novel optical oxygen sensing material: platinum porphyrin–styrene–pentafluorostyrene copolymer film". In: *Analytical Communications* 36 (1999), pp. 367–369.

[9] Yutaka Amao, Keisuke Asai, Ichiro Okura, Hiromi Shinohara, and Hiroyuki Nishide. "Platinum porphyrin embedded in poly(1-trimethylsilyl-1-propyne) film as an optical sensor for trace analysis of oxygen". In: *The Analyst* 125.11 (2000), pp. 1911–1914.

[10] Haoran Zhang and Bin Li. "Preparation and oxygen sensing properties of a sol-gel derived thin film based on a covalently grafted ruthenium(II) complex". In: *Sensors and Actuators B* 123 (Mar. 2007), pp. 508–515.

[11] Ingo Klimant, Falk Ruckruh, Gregor Liebsch, Achim Stangelmayer, and Otto S Wolfbeis. "Fast Response Oxygen Micro-Optodes Based on Novel Soluble Ormosil Glasses". In: *Microchimica Acta* 131.1-2 (June 1999), pp. 35–46.

[12] Joseph R Lakowicz. *Principles of Fluorescence Spectroscopy*. 2nd ed. Second Edition. Kluwer Academic / Plenum Publshers, Jan. 1999.

[13] ER Carraway and JN Demas. "Photophysics and Photochemistry of Oxygen Sensors Based on Luminescent Transition-Metal Complexes". In: *Analytical Chemistry* 63 (1991), pp. 337–342.

[14]   J Crank and G S Park. *Diffusion in Polymers*. Ed. by P Neogi. Marcel Dekker Inc., Feb. 1996.

[15]   I Quijada-Garrido, J M Barrales-Rienda, and G Frutos. "Diffusion of Erucamide (13-cis-Docosenamide) in Isotactic Polypropylene †". In: *Macromolecules* 29.22 (Jan. 1996), pp. 7164–7176.

[16]   Enikő Földes. "Transport of small molecules in polyolefins. II. Diffusion and solubility of irganox 1076 in ethylene polymers". In: *Journal of Applied Polymer Science* 48.11 (June 1993), pp. 1905–1913.

[17]   J Klein and B J Briscoe. "Diffusion of long molecules through solid polyethylene. II. Measurements and results". In: *Journal of Polymer Science: Polymer Physics Edition* 15.12 (Dec. 1977), pp. 2065–2074.

[18]   P V Krishna Pant and Richard H Boyd. "Simulation of diffusion of small-molecule penetrants in polymers". In: *Macromolecules* 25.1 (Jan. 1992), pp. 494–495.

[19]   C H Klute. "Diffusion of small molecules in semicrystalline polymers. II. The permeability of unoriented polymer films". In: *Journal of polymer science* XLI (Jan. 1959), pp. 307–317.

[20]   Michael L Greenfield. "Simulation of small molecule diffusion using continuous space disordered networks". In: *Molecular Physics* 102.4 (Feb. 2004), pp. 421–430.

[21]   S M Borisov, A S Vasylevska, Ch Krause, and O S Wolfbeis. "Composite Luminescent Material for Dual Sensing of Oxygen and Temperature". In: *Advanced Functional Materials* 16.12 (Aug. 2006), pp. 1536–1542.

[22]   F Kimura, G Khalil, N Zettsu, and Y Xia. "Dual luminophore polystyrene microspheres for pressure-sensitive luminescent imaging". In: *Measurement . . .* 17 (2006), pp. 1254–1260.

[23]   Sang-Kyung Lee and Ichiro Okura. "Photostable Optical Oxygen Sensing Material: Platinum Tetrakis(pentafluorophenyl)porphyrin Immobilized in Polystyrene". In: *Analytical Communications* 34.6 (1997), pp. 185–188.

[24]   S M Borisov, G Nuss, and I Klimant. "Red Light-Excitable Oxygen Sensing Materials Based on Platinum(II) and Palladium(II) Benzoporphyrins". In: *Analytical Chemistry* 80.24 (Dec. 2008), pp. 9435–9442.

[25]   Fareha Zafar Khan, Toshikazu Sakaguchi, Masashi Shiotsuki, Yoshiyuki Nishio, and Toshio Masuda. "Perfluoroacylated Ethyl Cellulose: Synthesis, Characterization, and Gas Permeation Properties". In: *Macromolecules* 39.26 (Dec. 2006), pp. 9208–9214.

[26]   Anna Bravo, Bjørsvik Hans-René, Fontana Francesca, Liguori Lucia, Mele Andrea, and Minisci Francesco. "New Methods of Free-Radical Perfluoroalkylation of Aromatics and Alkenes. Absolute Rate Constants and Partial Rate Factors for the Homolytic Aromatic Substitution by n-Perfluorobutyl Radical". In: *The Journal of Organic Chemistry* 62 (June 1997), pp. 7128–7136.

[27]   Jian Zhang and Xiaohuai Hou. "The gas permeation propety in trimethylsilyl-substituted PPO and triphenylsilyl-substituted PPO". In: *Journal of Membrane Science* 97 (1994), pp. 275–282.

[28]   Otto S Wolfbeis. "Materials for flourescence-based optical chemical sensors". In: *Journal of Materials Chemistry* 15 (July 2005), pp. 2657–2669.

[29]   Reham Ali, Thomas Lang, Sayed M Saleh, Robert J Meier, and Otto S Wolfbeis. "Optical sensing scheme for carbon dioxide using a solvatochromic probe." In: *Analytical Chemistry* 83.8 (Apr. 2011), pp. 2846–2851.

[30] X Chen, Z Zhong, Z Li, Y Jiang, and X Wang. "Characterization of ormosil film for dissolved oxygen-sensing". In: *Sensors and Actuators B* 87 (2002), pp. 233–238.

[31] BJ Basu. "Optical oxygen sensing based on luminescence quenching of platinum porphyrin dyes doped in ormosil coatings". In: *Sensors and Actuators B: Chemical* 123 (2007), pp. 568–577.

[32] Y Amao and T Miyashita. "Platinum tetrakis(pentafluorophenyl)porphyrin immobilized in polytrifluoroethylmethacrylate film as a photostable optical oxygen detection material". In: *Journal of Fluorine Chemistry* 107 (2001), pp. 101–106.

[33] M Trinkel. "Optical sensors for trace oxygen analysis". PhD thesis. Karl Franzens University Graz: University of Graz, Jan. 1998.

[34] Sergey M Borisov, Philipp Lehner, and Ingo Klimant. "Novel optical trace oxygen sensors based on platinum(II) and palladium(II) complexes with 5,10,15,20-meso-tetrakis-(2,3,4,5,6-pentafluorphenyl)-porphyrin covalently immobilized on silica-gel particles." In: *Analytica Chimica Acta* 690.1 (Mar. 2011), pp. 108–115.

7 List of Figures

8 List of Tables

9 Appendix

9.1 Additional Data

Ethyl-Cellulose at different temperatures
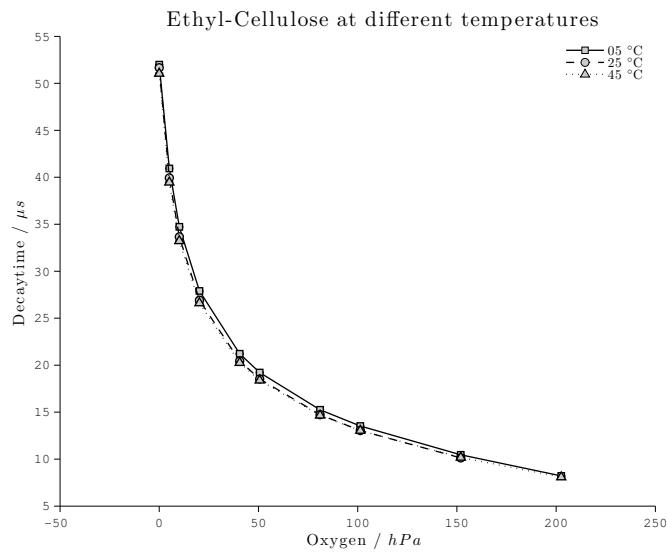
Figure 9.1: Decay time plot of a sensor with ethylcellulose matrix
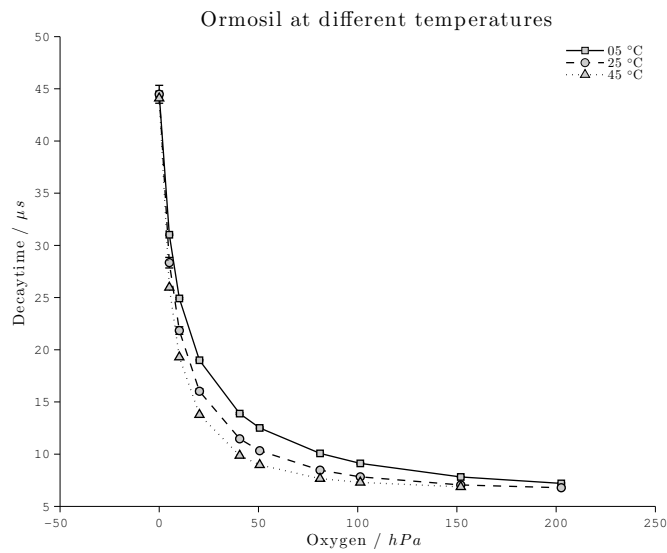
Ormosil at different temperatures

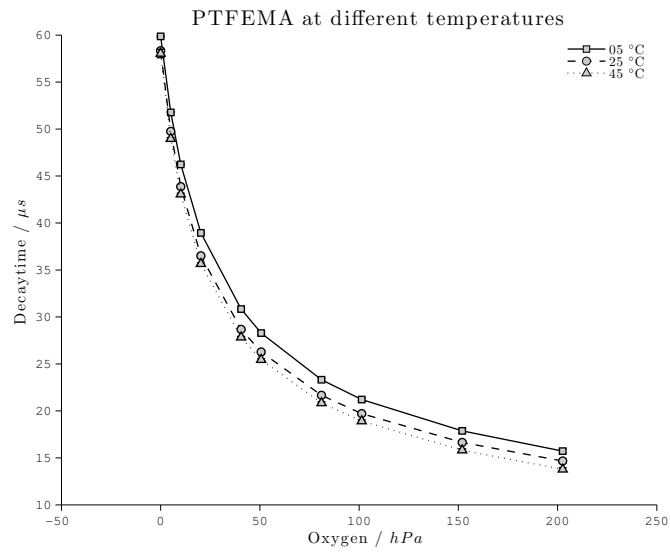**Figure 9.2:** Decay time plot of a sensor with ormosil matrix

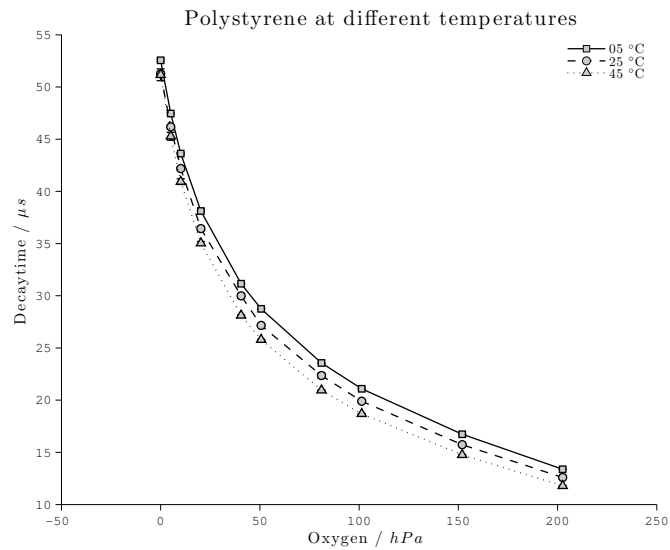**Figure 9.3:** Decay time plot of a sensor with PTFEMA matrix

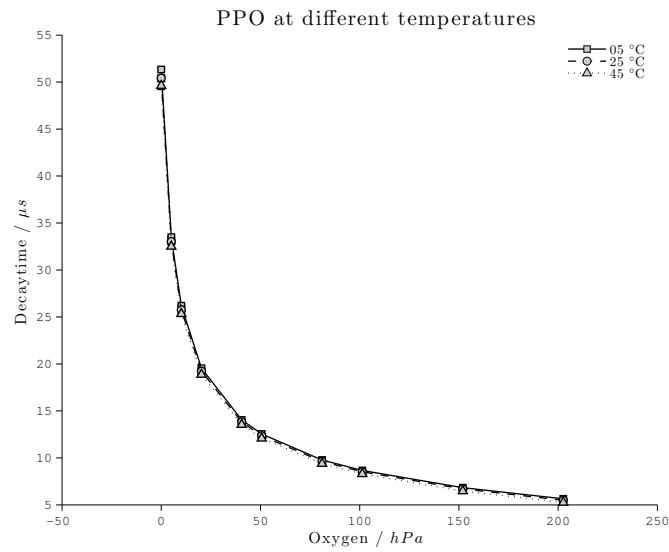**Figure 9.4:** Decay time plot of a sensor with polystyrene matrix

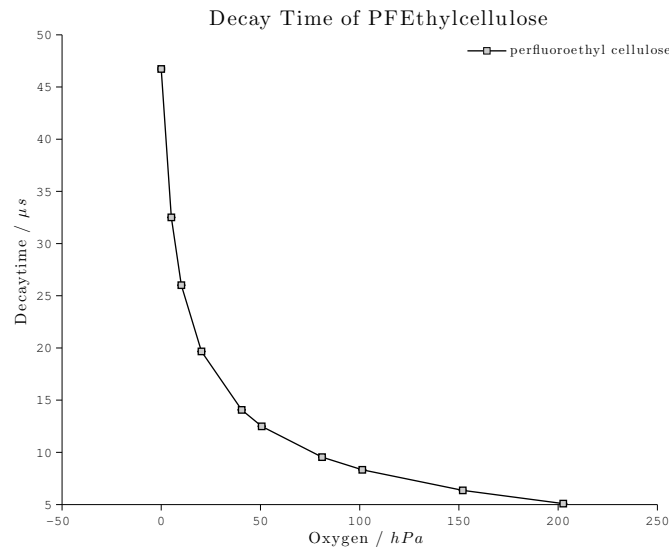**Figure 9.5:** Decay time plot of a sensor with PPO matrix

Figure 9.6: Decay time plot of a sensor with perfluoroethylcellulose matrix
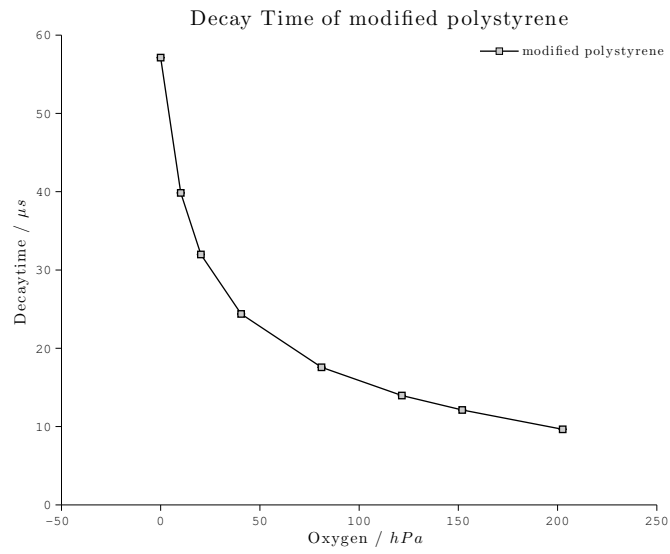
Figure 9.7: Decay time plot of a sensor with poly(perfluoroalkylstyrene) matrix

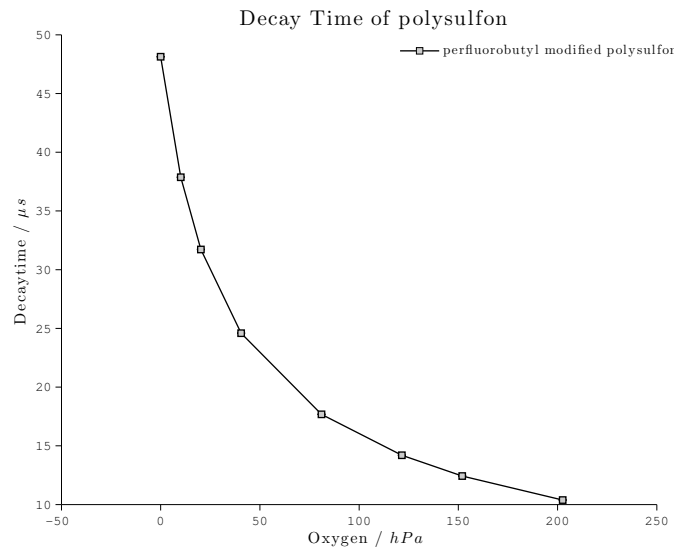

Figure 9.8: Decay time plot of a sensor with polysulfone matrix
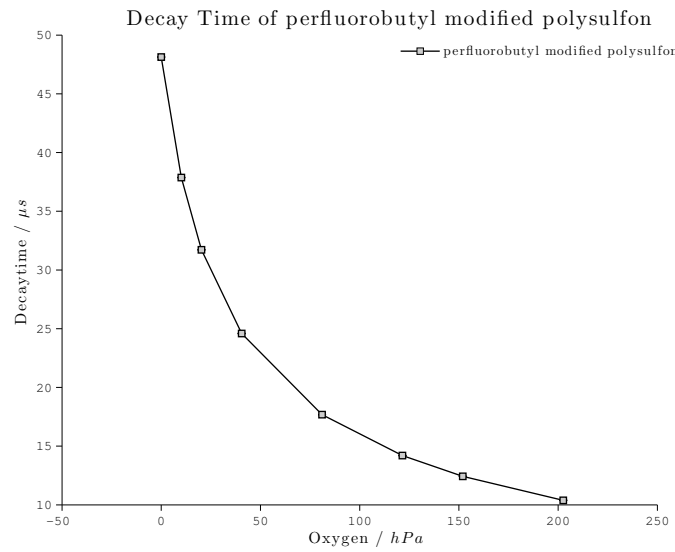
Figure 9.9: Decay time plot of a sensor with silanized polysulfone matrix
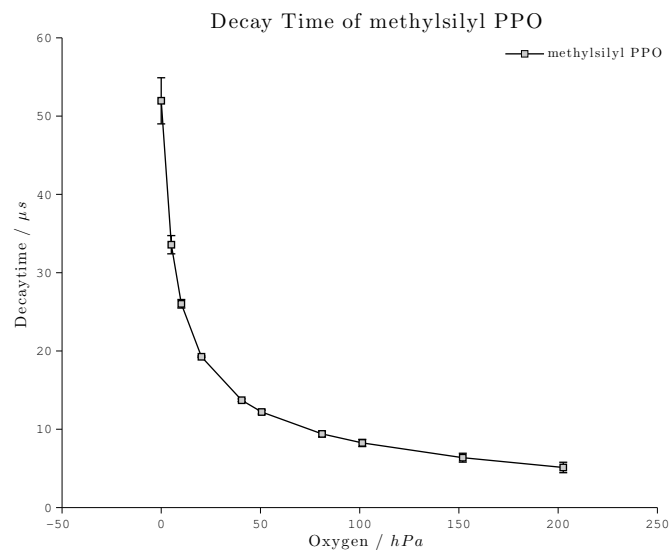
Figure 9.10: Decay time plot of a sensor with silanized PPO matrix
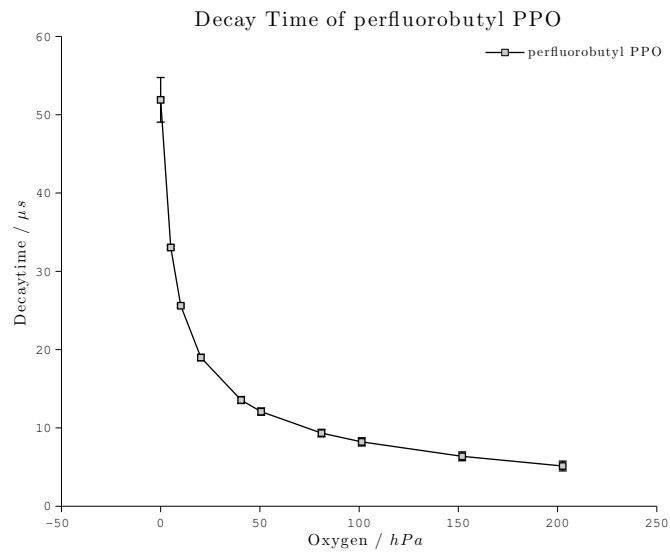
Figure 9.11: Decay time plot of a sensor with perfluoroalkylated PPO matrix
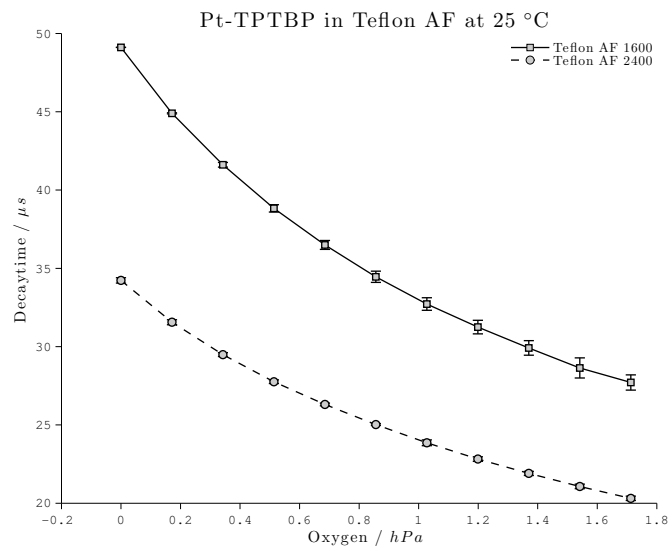
Figure 9.12: Decay time plot of a sensor with Pt-TPTBP in different Teflon AF matrices
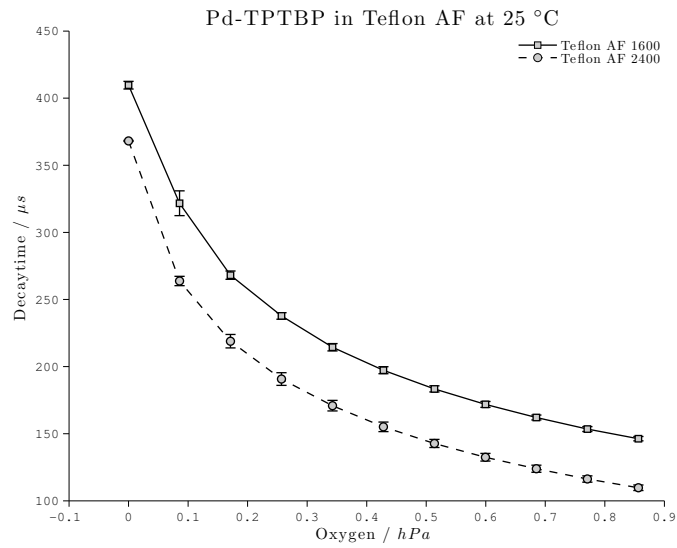
Figure 9.13: Decay time plot of a sensor with Pt-TPTBP in different Teflon AF matrices
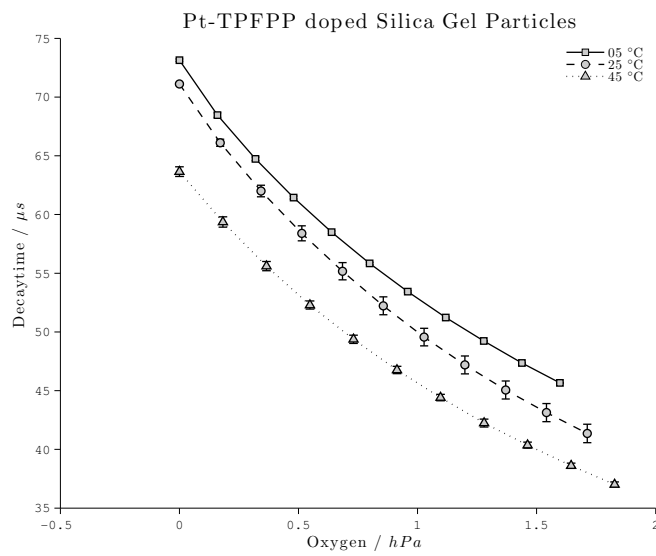
Figure 9.14: Decay time plot of a sensor with Pt-TPFPP in silica gel matrix at different temperatures
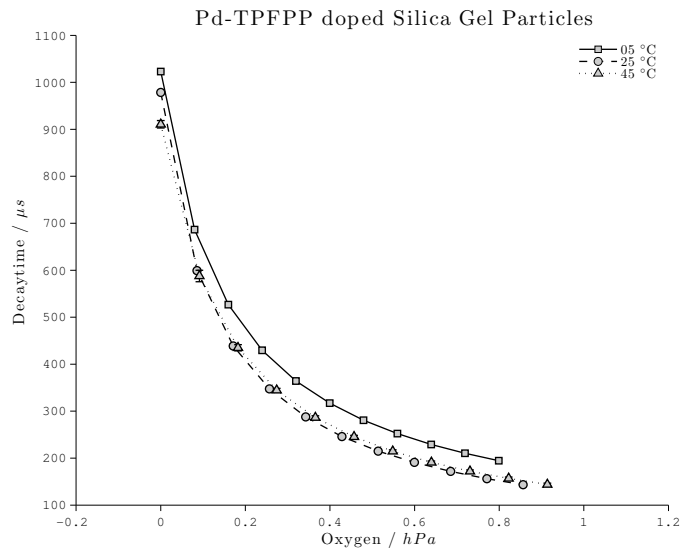
Figure 9.15: Decay time plot of a sensor with Pd-TPFPP in silica gel matrix at different temperatures
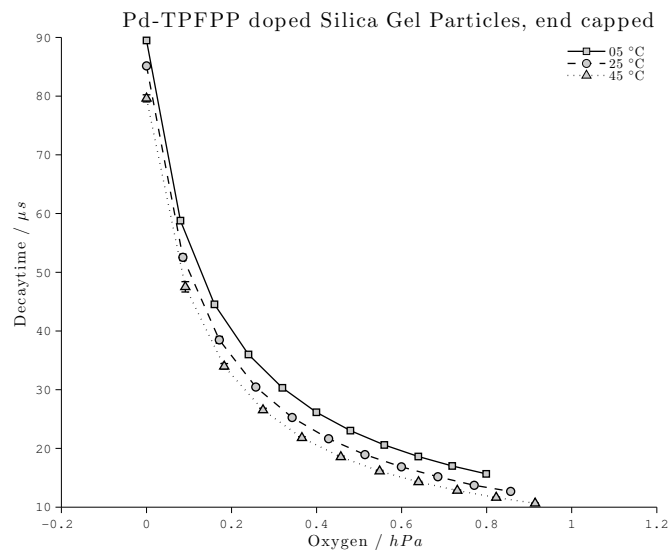
Figure 9.16: Decay time plot of a sensor with Pd-TPFPP in an end capped silica gel matrix at different temperatures

9.2 Measurement Cube Firmware Source Code

```
1  #include <WString.h>

   /*
   #--------------------------------------------------------------------------#
   |                                                                          |
6  |    MeassureBlock Control Programm written by Philipp Lehner in 2010      |
   |                                                                          |
   #--------------------------------------------------------------------------#

   This Program provides a serial interface via the USB connection to
11 control the valves, pump, tempsensor and fan of the Cube.

   The provided Interface will be as basic as possible, with Commands beeing accepted
   and either an OK or a readValue returned. Or ERR if something didn't work out right.

16 Also temperature calibration is now possible via COM through get and set functions for
   calibration variables.

   Sample input Commands:
   vex on                Open the valves to let gas flow through
21 vin on
   {delay}               delay for a while (that's not a command, the sending programm
         has to delay)
   vin off               Close the valves
   vex off
   rte                   Meassure temperature to see if everything is allright
26 {delay}
   pum 500               Pump specified Volume in Microliters

   Every command should be ended by a linefeed and more importantly has to be sent
         separately

31 */



   // Define connected Pins
36 const int tempInPin = 0;        //analog In for Temperature Sensor Value
   const int inletValvePin = 3;    //these 4 Pins are attatched to the MOSFETS
   const int outletValvePin = 4;   // and switch their respective load
   const int pumpPin = 5;
   const int fanPin = 6;
41 const int statusLedPin = 7;     //Eventually include Status LEDs

   //Define Commands accepted via Serial
   char commandString[21] = "";
   char testString[7] = "NOVal";
46 boolean readComplete = false; //only test readings after a terminate char arrives
   int i; //count incoming character position

   #define INPUT_VALVE "vin"
   #define EXHAUST_VALVE "vex"
51 #define SOLENOID_PUMP "pum"
   #define MIXING_FAN "fan"
   #define STATUS_LED "led"
   #define TEMPERATURE_READ "rte"
   #define TEMPERATURE_SLOPE_READ "tsr"
56 #define TEMPERATURE_SLOPE_WRITE "tsw"
   #define TEMPERATURE_DRIFT_READ "tdr"
   #define TEMPERATURE_DRIFT_WRITE "tdw"

   #define ACTIVATE "on"        //These Commands control Valve and Pump state
61 #define DEACTIVATE "off"

   const char SUCCESS[3] = "OK"; //The String returned if command was succesfully Executed
```

```
      const char ERROR[4] = "ERR";  //The String returned if something goes wrong

66 #define TERMINATECHAR 10 //defines the end Character this can be set to 13 (carriage
         return) or
   //10 (LF) depending on the software (arduino testsoftware insists on carriage return)

   //Define Pump Frequency
   const int pumpFrequency = 5;
71
   // Define Variables for Temperature Sensor Calibration
   float sensorValue = 0;         //initialize ReadValue
   float voltFactor = 0.004883;   //increment to Volt 5/1024
   float tempSlope = 23.339;       //The slope of the temperature calibration, is
         changeable via COM
76 float tempDrift = -14.560;       //y-intersect, the current values where obtained with a
         thermostat

   void setup() {

     // initialize serial communications at 9600 bps:
81   Serial.begin(9600);

     //initialize Pins and switch them LOW when Unit starts
     pinMode(inletValvePin, OUTPUT);
     pinMode(outletValvePin, OUTPUT);
86   pinMode(pumpPin, OUTPUT);
     pinMode(fanPin, OUTPUT);
     pinMode(statusLedPin, OUTPUT);
     digitalWrite(inletValvePin, LOW);
     digitalWrite(outletValvePin, LOW);
91   digitalWrite(pumpPin, LOW);
     digitalWrite(fanPin, LOW);
     digitalWrite(statusLedPin, LOW);
   }

96 void loop() { //Heres the Main Control Loop

       getIncomingChars();                                  //Read Data from Serial Port
           Buffer

       if (strstr(commandString,INPUT_VALVE) != NULL) {      // Decide what to do
101     operateActor(inletValvePin);
       }
       else if(strstr(commandString,EXHAUST_VALVE) != NULL) {
         operateActor(outletValvePin);
       }
106     else if(strstr(commandString,SOLENOID_PUMP) != NULL) {
         pumpVolume(commandStringValueToDouble(commandString));
       }
       else if(strstr(commandString,MIXING_FAN) != NULL) {
         operateActor(fanPin);
111     }
       else if(strstr(commandString,STATUS_LED) != NULL) {
         operateActor(statusLedPin);
       }
       else if(strstr(commandString,TEMPERATURE_READ) != NULL) {
116     returnTemperature();
       }
       else if(strstr(commandString,TEMPERATURE_SLOPE_READ) != NULL) {
         returnTempSlope();
       }
121     else if(strstr(commandString,TEMPERATURE_SLOPE_WRITE) != NULL) {
         setTempSlope(commandStringValueToDouble(commandString));
       }
       else if(strstr(commandString,TEMPERATURE_DRIFT_READ) != NULL) {
         returnTempDrift();
126     }
       else if(strstr(commandString,TEMPERATURE_DRIFT_WRITE) != NULL) {
```

```
          setTempDrift(commandStringValueToDouble(commandString));
        }
        else {
131       Serial.println(ERROR);
        }
        Serial.flush();
        memset(commandString, 0, sizeof commandString);    //Clear Read Memory

136   // wait 10 milliseconds before the next loop
      // for the analog-to-digital converter to settle
      // after the last reading and serial communication to happen
      delay(10);
    }
141
    void operateActor(int operatorPin) {              //Control on/off Actors
      if (strstr(commandString,ACTIVATE) != NULL) {
        digitalWrite(operatorPin, HIGH);
        Serial.println(SUCCESS);
146   }
      else if (strstr(commandString,DEACTIVATE) != NULL) {
        digitalWrite(operatorPin, LOW);
        Serial.println(SUCCESS);
      }
151   else {
        Serial.println(ERROR);
      }
    }

156 void pumpVolume(float Volume) {
      Volume = Volume / 20;
      if (Volume  == int(Volume)) {         //Check if Volume is a multiple of 20
        for (int i=0; i < Volume; i++) {    //Move the Pump for the required Number of
              Steps
          digitalWrite(pumpPin, HIGH);
161       delay(500/pumpFrequency);              // Delay for half the frequency in Milliseconds
          digitalWrite(pumpPin, LOW);
          delay(500/pumpFrequency);
        }
        Serial.println(SUCCESS);
166   }
      else {
        Serial.println(ERROR);
      }
    }
171
    void returnTemperature() {
      // read the analog in value:
      sensorValue = analogRead(tempInPin);
      sensorValue = sensorValue * voltFactor;           //convert Sensor increment to
            Volt
176   sensorValue = sensorValue * tempSlope + tempDrift;   //use linear Calibration to get
          Temperature
      //Sensor is linear form ~ -5C - ~ 70C

      // print the results to the serial monitor:
      Serial.print("Temp = " );
180   Serial.println(sensorValue, 1);
    }

    void returnTempSlope() {            //Setters and Getters for the Calibration variables
      Serial.println(tempSlope);
186 }

    void setTempSlope(float Slope) {
      tempSlope = Slope;
      Serial.println(SUCCESS);
191 }
```

```
      void returnTempDrift() {
        Serial.println(tempDrift);
      }
196
      void setTempDrift(float Drift) {
        tempDrift = Drift;
        Serial.println(SUCCESS);
      }
201
      void getIncomingChars() {

       /* char input;                        // DEPRECATED VERSION OF getIncomingChars()
        for (int i=0; i <= 11; i++) {       // Read the characters into an array
206       input = Serial.read();
          if (input == TERMINATECHAR) {
            commandString[i] = '\0';        // and terminate the String
            break;
          }
211       else {
            commandString[i] = input;
          }
        } */

216     i = 0;                // reset i
        while (!readComplete) {
          char input;
          if (Serial.available() > 0) {
          input = Serial.read();
221         if (input == TERMINATECHAR) { //read until terminatechar, then terminate String
              commandString[i] = '\0';
              readComplete = true;
            }
            else commandString[i] = input;
226       i++;
          }

        }
        readComplete = false;
231   }

      float commandStringValueToDouble(char *inString) {  // convert a Input Value to Float
        strncpy(testString, inString + 4, 8);
236     return atof(testString);
      }
```